
Everything should be made as simple as possible, but not simpler.

Albert Einstein

Acknowledgements

I would like to thank my supervisors for their own specific expertise throughout this project: Prof. Giampietro Alberti, Prof. Alberto Minetti, Prof. Jacques Van Hoecke, Prof. Nicolas Babault. I would also like to acknowledge the financial support of the University of Milan (Milano, Italy) and the University of Burgundy (Dijon, France). Special mention must also go to Professor Fred Yeadon who supervised my thesis in my last Ph.D. year at Loughborough University (United Kingdom). His experience in simulations combined with his mathematics genius were helpful to understand, develop and evaluate my model based on experimental data previously collected in the French Lab. I would like to acknowledge Matt Pain who has often acted as external adviser to improve my model. I would like to thank Martin Lewis for his support and advices. I would like to express my gratitude to Petar Bozadzhiev, Yves Ballay and Glen Bishop for their help during experimental sessions. I would like to say thanks to Dr. Davide Lorenzoli for implementing the simulated annealing algorithm in visual basic code language. Finally, I would like to thank everyone in the Centre d'Expertise de la Performance Gilles Cometti (STAPS, Dijon, France) and in the Sports Biomechanics and Motor Control Research Group (Loughborough University, United Kingdom).

...to my loving parents Domenico and Maria

Résumé

Un modèle du système musculo-squelettique humain composé de 3 moteurs basés sur le couple de force des articulations, a été créé à partir des caractéristiques individuelles d'un sujet. L'objectif était de simuler un exercice de force, à savoir le squat jump avec et sans la charge. Le moment net de la force de la hanche, du genou et de la cheville a été modélisée à partir des données expérimentales. La composante élastique n'a pas été considérée. Deux modèles ont été créés pour chaque articulation. Les deux modèles ont été comparé l'un avec l'autre pour établir lequel était le plus proche de la performance réelle. En analysant les données de cinétique et cinématique au moment du décollage, il a été montré qu'un modèle simple et rigoureux basé sur le couple de force pourrait être employé dans une simulation pour reproduire un saut vertical. Le modèle le plus précis a été utilisé pour optimiser la performance en détente verticale avec et sans charge. Une diminution linéaire a été trouvée avec l'augmentation de la charge. La charge avec laquelle le modèle ne serait plus capable de décoller a été estimée. Les résultats de la puissance des sauts montrent une probable imprécision de la simulation des forces de réaction au sol. Il a été conclu qu'une approche informatique combiné avec des données expérimentales, est une manière originale de faire des recherches dans le domaine de l'entraînement de la force. Cela aide les entraîneurs, les athlètes et les scientifiques à mieux comprendre la performance humaine. Cette thèse est une première étape d'un plus grand projet qui a comme but l'évaluation des avantages d'une approche informatique pour comprendre les exercices de force musculaire.

Abstract

A subject specific forward dynamic 3-actuator torque-driven model of the human musculoskeletal system was created, based on measurements of individual subject characteristics. The goal was to simulate a common strength exercise: squat jump with and without extra load. Hip, knee and ankle resultant net torques were modeled from experimental data. Elastic components were not considered. Two models were created for each joint, and then implemented into simulations. Subsequently they were compared to each other to establish which one best matched actual performances. By analyzing kinematic and kinetic experimental data at the instant of the toe-off, it was shown that accurate joint torque models implemented in a simple computer simulation could reproduce squat jumps. The model that best matched actual jumps was used to optimize jump height performance with and without extra load. A linear decreasing of the jump height was found as the load increased. The load at which the model would not be able to take-off was predicted. In addition, joint and global power outputs for different extra load conditions were estimated. It seemed that global power output probably suffered from a slight inaccuracy of simulated vertical ground reaction forces. It was concluded that a computational approach combined with experimental data, is an original way to conduct research in strength and conditioning training. It would help coaches, athletes and scientists to better understand human performances. This investigation is the first step in a wider project aiming to evaluate the advantages of the individual subject approach for understanding strength exercise tasks.

Riassunto

Basato su misure sperimentali effettuate su un solo soggetto, è stato creato un modello del sistema muscolo-scheletrico umano animato da 3 generatori di momento di anca, ginocchio e caviglia. Lo scopo era di simulare un comune esercizio muscolare: lo squat jump con e senza carichi aggiuntivi. La componente elastica del muscolo non è stata considerata. Due modelli per ogni articolazione sono stati comparati per stabilire quello più idoneo a simulare la performance reale. Analizzando i dati sperimentali di cinematica e cinetica, è stato dimostrato che modelli accurati di produzione di momento articolare possono riprodurre fedelmente uno squat jump reale. Il modello più accurato è stato usato per verificare se fosse in grado di simulare dei salti con aggiunta di carico, risultando in un lineare decremento dell'altezza di salto all'aumentare del carico. Anche il carico che non permetteva più al modello di saltare è stato predetto. La potenza globale e di ogni singola articolazione è stata ottenuta per le diverse condizioni di carico. I risultati della potenza sembrarono influenzati da una leggera imprecisione di simulazione delle forze di reazione al suolo. È stato concluso che un approccio informatico, combinato con dei dati sperimentali, può essere una strada originale da percorrere nelle ricerche sull'allenamento muscolare, aumentando la consapevolezza e la comprensione di allenatori, atleti e ricercatori della performance umana. Questo studio è il primo passo di un progetto che ha come scopo la valutazione dei vantaggi che un approccio modellistico, basato sui dati sperimentali di un singolo soggetto, può avere nella comprensione degli esercizi di forza muscolare.

Contents

Contents	x
List of Figures	xv
List of Tables	xxvi
1 Introduction	1
1.1 Computational approach in sport science	1
1.2 Literature review	2
1.2.1 Skeletal muscle force exertion	2
1.2.2 Neuromuscular interaction	4
1.2.3 Structure of the muscle-tendon complex	5
1.2.3.1 Muscle-tendon complex mechanics and modelling	5
1.2.3.2 Tension-length relationship	7
1.2.3.3 Tension-velocity relationship	9
1.2.4 Isokinetic dynamometry	11
1.2.5 State of the art in computational research	12
1.2.5.1 Modelling and simulations in vertical jumping .	12
1.2.5.2 Modelling and simulations in strength and condi- tioning training	14
1.3 Algorithms	15
1.3.1 Brute-force algorithm	16
1.3.2 Simulated annealing algorithm	16
1.4 Thesis statement purpose	17
1.5 Summary	20

2	Experimental measurements	21
2.1	Dynamometer testing session	21
2.1.1	Hip joint testing	23
2.1.2	Knee joint testing	25
2.1.3	Ankle joint testing	27
2.1.4	Dynamometer data processing	29
2.1.4.1	Correction of crank joint angle	29
2.1.4.2	Correction of torque-measuring dynamometer	30
2.2	Results of torque-measuring dynamometer	32
2.2.1	Hip joint results	32
2.2.2	Knee joint results	33
2.2.3	Ankle joint results	33
2.2.4	Ankle joint correction	36
2.3	Kinematic, kinetic and EMG assessments during jumping experiments	37
2.3.1	Procedures: squat jump and 1RM experimental trials	40
2.3.2	Experimental squat jump results	41
2.4	Summary	48
3	Development of the jumping model	49
3.1	Whole-body 4 link rigid segment model	49
3.1.1	Foot-ground interface	50
3.1.2	Determination of subject-specific mass and centre of mass segments	52
3.1.3	Subject-specific inertial data determination	55
3.1.4	Barbell and plates inertial data determination	57
3.2	Human muscle force modelling	59
3.2.1	Tension-velocity modelling (concentric-isometric)	59
3.2.2	Tension-velocity modelling (eccentric-isometric)	60
3.2.3	Tension-length modelling	60
3.2.4	Differential activation	62
3.2.5	Subject-specific hip, knee, ankle joint modelling	63
3.2.5.1	Model-based on 5-parameter function	63

3.2.5.2	Model-based on 9-parameter function	67
3.3	The active state of skeletal muscle model	72
3.4	Summary of joint torque generation	76
3.5	Summary	76
4	Torque-driven model evaluations: results and discussion	77
4.1	Vertical jumping modelling evaluations	77
4.2	Cost functions	79
4.3	Squat jump matching performance	80
4.3.1	Squat jump Model A: 5-parameter function, trust region algorithm for fitting input data and, brute-force search method for matching simulations.	80
4.3.2	Squat jump Model B: 9-parameter function, Simulated Annealing (SA) algorithm for fitting input data and, SA method for matching simulations.	81
4.3.3	Model A <i>vs.</i> Model B <i>vs.</i> actual performance	82
4.3.3.1	Jump height	82
4.3.3.2	Kinetic	82
4.3.3.3	Torque output	84
4.3.3.4	Kinematic	85
4.3.3.5	Activation pattern profiles	89
4.3.3.6	Joint power output	91
4.4	Matching simulations for SJ with extra load	92
4.4.1	Jump height evaluation	93
4.4.2	Kinetic evaluation	94
4.4.3	Torque output	96
4.4.4	Joint power output	98
4.4.5	Kinematic evaluation	100
4.4.6	Activation patterns for SJ extra load matching simulations	105
4.5	Summary	107
5	Validation of a subject 3-actuator torque-driven model in human vertical jumping	109

5.1	Abstract	109
5.2	Introduction	110
5.3	Methods	110
5.3.1	Forward Simulation Model	110
5.3.2	Experimental Data	111
5.3.3	Muscle Model	112
5.3.4	Model Input Data	113
5.4	Results	114
5.4.1	Squat Jump bw	116
5.4.2	Squat Jump +40%	116
5.4.3	Squat Jump +80%	116
5.5	Discussion	116
5.6	Acknowledgment	118
5.7	Appendix	118
6	Comparison between squat jump <i>vs.</i> weighted squat jump: simulation study	120
6.1	Introduction	120
6.2	Methods	121
6.3	Results and discussion	122
6.4	Conclusions	124
7	Model optimization - predictions: results and discussion	125
7.1	Squat jump optimization	125
7.1.1	Jump height performance optimized for SJ, SJ+25kg and SJ+50kg	127
7.1.2	Activation patterns optimized	129
7.1.3	Torque output	131
7.1.4	Joint power output	132
7.1.5	Global power output	136
7.2	Predictions	137
7.2.1	Impact of extra loads on jump height in squat jump	137
7.2.2	1RM prediction	141

7.3 Summary	143
8 Conclusions	144
8.1 General discussion	144
8.1.1 Simulated Performances	144
8.1.2 Electromechanical delay	145
8.1.3 Selection of cost function	146
8.2 Research questions	146
8.3 Simulation model strength	149
8.4 Simulation model weakness	150
8.5 Future developments	150
8.6 Conclusion	152
References	154
Appendix A	165
Appendix B	187

List of Figures

1.1	Hill's elastic muscle model. F: Force; CE: Contractile Element; SE: Series Element; PE: Parallel Element.	6
1.2	The relation between tension and sarcomere length. The drawn line is the relation obtained by Gordon et al. [34]. A plateau is visible at the top of the graphic and tension decrease at both sides.	8
1.3	Hyperbolic relation between load and speed of shortening. From Hill [38]	10
1.4	A comprehensive diagram to summarize how the simulation model was created is shown. The simulation model needs input data in numerical form (e.g. functions obtained from experimental data). Indeed, experimental measurements (dynamometer assessments for each joint with kinematic, kinetic and sEMG measures during squat jumping) were performed in order to describe muscle force and movement characteristics. Inertial and anthropometric data came from estimations based on regression equations available in the scientific literature (e.g. see Chandler's report [20]). Actually, simulations were run by the means of inputs which describe as closely as possible all considered characteristics. Subsequently, results were used to make sure that the model could represent the reality then able to make some prediction.	19
2.1	Torque (τ) and angle (θ) data acquisition procedures.	21
2.2	Dynamic test procedure (e.g. knee joint). A maximal isometric contraction was followed by a dynamic contraction.	22

LIST OF FIGURES

2.3	Hip joint Biodex test angle definition. The subject position is shown in the left side. The right side highlighted muscle groups involved.	23
2.4	Hip joint example data from the dynamometer during testing. Concentric and eccentric sample data are shown in the left and in the right side, respectively. Shaded aereas represent the isove- locity portion. Light lines are the first and the second derivate of the position in time.	24
2.5	Knee joint Biodex test angle definition. The subject position is shown in the left side. The right side highlighted muscle groups involved.	25
2.6	Knee joint example data from the dynamometer during testing. Concentric and eccentric sample data are shown in the left and in the right side, respectively. Shaded aereas represent the isovelocity portion. Light lines are the first and the second derivate of the position in time.	26
2.7	Ankle joint Biodex test angle definition. The subject position is shown in the left side. The right side highlighted muscle groups involved. Since the knee was fully extended, the gastrocnemius was strongly involved.	27
2.8	Ankle joint example data from the dynamometer during testing. Concentric and eccentric sample data are shown in the left and in the right side, respectively. Shaded aereas represent the isovelocity portion. Light lines are the first and the second derivate of the position in time.	28
2.9	Correction of crank joint angle considering goniometer data vs. biodex angle.	30
2.10	Biodex© signal processing (e.g. concentric knee joint test). The central chart helps to identify the isovelocity portion. The chart at the bottom of the figure shows the gravity and leg weight torque corrections.	31

LIST OF FIGURES

2.11	Red points are experimental data obtained from the hip joint dynamometer test. Only the isovelocity portion throughout the ROM was considered. The image at top right side helps to read the chart axes.	32
2.12	Knee extensor experimental data. Green points are experimental data obtained from the knee extension dynamometer test. Only the isovelocity portion throughout the ROM was considered. The image at top right side helps to read the chart axes.	34
2.13	Ankle plantar flexors experimental data. Here, blue points are experimental data obtained from the ankle joint dynamometer test. Only the isovelocity portion throughout the ROM was considered. The image at top right side helps to read the chart axes.	35
2.14	Marker positions, framework of the model obtained from the marker coordinates and example of Vicon© cameras used during the experiment.	38
2.15	A comprehensive illustration of the experimental setup is shown. The participant wore a belt which contained the electronic wireless device to send to the computer sEMG signals coming from each electrode. The right side was chosen to be assessed and the subject was allowed to wear shoes. The right hand side of the figure shows the experiment configuration. This example shows the athlete ready to perform trials with extra load before to setting himself in the squat jump start position. In the left side and centre of the figure, the muscle art design of the right leg help the understanding of the electrode locations for assessing the surface electromyography signals.	39
2.16	Maximal achievement in terms of COM toe-off velocity for each experimental condition.	41
2.17	Vertical ground reaction forces recorder for the best jump (jump height) for each condition (SJ, SJ+25kg, SJ+50kg), synchronized at the toe-off. Peak GRF was reached at 0.109s, 0.098s, 0.089s fro SJ+50kg, SJ+25kg, SJ, respectively. Value 0 for the abscissa represents the instant of the toe-off.	42

2.18 Squat Jump bandpass (10-400Hz) rectified sEMG data example. Charts show the last 600ms before the instant of the toe-off. The start of the propulsive phase occurred at -0.334s from the toe-off (0s). Main monoarticular and biarticular muscles were investigated.	43
2.19 Peak EMG (rms) with respect to time expressed as percentage of the propulsive phase. The toe-off instant is 100%. This simple analysis suggests that if one wants to model the active state of muscles, it has to be considered to allow to reach the maximal activation by the half propulsive phase of the jump for all conditions. Otherwise, a simulation model could give as result a low jump height performance, since the magnitude of the activation would not be enough to reproduce a jump. Further, it seems there is a tendency which show that squat jumps with extra load need a shorter the time to reach the activation peak.	44
2.20 Surface EMG (rms). Signal was sampled at 960Hz and Band-Pass filtered (10-400Hz). RMS was calculated over a window of 50ms. Signals are synchronized at the toe-off. Abscissa represent time to toe-off. Solid line=SJ; shaded line=SJ+25kg; dotted line=SJ+50kg. Monoarticular muscles are on the left side, whilst biarticular muscles are in the right side.	45
2.21 Squat jump joint angles and angular velocities time history. In the left side, angles time history of three squat jump trials are reported. Trial 3 is the best squat jump in terms of jump height and it was used as reference for the matching simulation. The right side of the figure shows angular velocities of the best trial for each joint.	47
3.1 Technical model definition of the angles and segment lengths. . . .	52

LIST OF FIGURES

3.2	Detailed foot-ground interface of the model, which represent the feet of the subject. The five final segments linked by using springs allowed to better reproduce the natural movement of the foot during plantar flexion movement. The length of the foot segment was calculated measuring the length of the shoe used during the experiment. The vertical slot constraint attached at the toe was created to avoid sliding during the push-off phase of the jump.	53
3.3	Olympic bar and plates measures used during the experiment. . .	58
3.4	Representation of the parameters of the function that describe the torque-angular velocity relationship. From [95], <i>mod.</i>	61
3.5	Graphic illustration of the tension-length relationship. k_2 is the width of the curve, θ_{opt} is optimal the angle.	61
3.6	Graphic representation of the differential activation modelling. . .	62
3.7	Hip extensors joint model obtained by the means of the trust region algorithm minimizing the difference between the model and the experimental data. Red points represent hip joint torque measured by using the dynamometer. The checkerboard surface represents the original fitting, whilst the uniform gray surface is the corrected model.	64
3.8	Knee extensors joint model obtained by the means of the trust region algorithm minimizing the difference between the model and the experimental data. Green points represent knee joint torque measured by using the dynamometer.	65
3.9	Ankle plantar flexors joint model obtained by the means of the trust region algorithm minimizing the difference between the model and the experimental data. Blue points represent ankle joint torque measured by using the dynamometer.	66
3.10	Hip joint modelling surface of the 9-parameter function. Eccentric and concentric phases are included. Red points are the experimental data.	68
3.11	Knee joint modelling surface of the 9-parameter function. Eccentric and concentric phases are included. Green points are the experimental data.	69

LIST OF FIGURES

3.12	Ankle joint modelling surface of the 9-parameter function. Eccentric and concentric phases are included. Blue points are the experimental data. The 4 dark red points collected during the functional isometric ankle test were used to scale the torque starting from parameters showed in Table 3.13.	70
3.13	Quintic function $f(x)$ and its derivatives $f'(x)$ and $f''(x)$	73
3.14	The way the human body activate muscles is simply represented by using a quintic function that is equivalent to the neuromuscular activation pattern.	74
3.15	Example of the ankle joint activation profiles time history. The solid line is the activation modeling which is compared with the sEMG linear envelope and the rectified sEMG. GA and SOL are the gastrocnemius laterals and the soleus, respectively. The graphic sequence at the bottom of the figure help to understand the activation phenomena during the push-off phase of the squat jump.	75
4.1	Diagram of the two squat jump model (A-B). They are compared to each other for the matching performance simulation purpose.	78
4.2	In the left side: Model A vs. Model B vs. actual performance (SJ GRF). In the right side: Model A vs. Model B (global power output). The abscissa 0 value correspond to the instant of the toe-off.	83
4.3	Torque exerted by the Model A and B . Charts show a comparison between the two models for matching performance. Dashed line = Model B; solid line = Model A.	84
4.4	Ankle displacement. Comparison between Model A (dashed line), Model B (dotted line) and actual performance (solid line). These two models showed very similar results in relation to the knee joint displacement.	85
4.5	Knee displacement. Comparison between Model A (dashed line), Model B (dotted line) and actual performance (solid line).	86
4.6	Hip displacement. Comparison between Model A (dashed line), Model B (dotted line) and actual performance (solid line).	86

LIST OF FIGURES

4.7	Hip angular velocity. Solid thick line=actual performance; solid thin line= Model B ; Dashed line= Model A	88
4.8	Knee angular velocity. Solid thick line=actual performance; solid thin line= Model B ; Dashed line= Model A	88
4.9	Ankle angular velocity. Solid thick line=actual performance; solid thin line= Model B ; Dashed line= Model A	89
4.10	Squat jump activation profiles: Model (A) vs. Model (B) vs. sEMG. sEMG linear envelope: gluteus (GL), biceps femoris (BF), vastus lateralis (VL), rectus femoris (RF), gastrocnemius lateralis (GL), soleus (SOL). Hip joint (left, red): solid line= B, dashed line=A, dotted line=GL, dotted dashed line=BF. Knee joint (centre, green): solid line= B, dashed line=A, dotted line=RF, dotted dashed line=VL. Ankle joint (right, blue): solid line= B, dashed line=A, dotted line=GA, dotted dashed line=SOL.	90
4.11	sEMG linear envelope. The signal was first Band-Pass filtered (10Hz-400Hz) then Low-Pass filtered at 7Hz. The chart shows the sEMG path of the monoarticular muscle recorded: dashed red line = gluteus; dotted green line = vastus lateralis; blue line = soleus.	90
4.12	Joint power production during simulated squat jump (matching performance). Solid line = Model A , dashed line = Model B	92
4.13	GRF for the squat jump matching simulation. Model B vs. actual performance. The matching simulation is represented by the solid line.	95
4.14	GRF for the squat jump +25kg matching simulation. Model B vs. actual performance. The matching simulation is represented by the solid line.	95
4.15	GRF for the squat jump +50kg matching simulation. Model B vs. actual performance. The matching simulation is represented by the solid line.	96
4.16	Torque output obtained from matching simulations. Thin solid line = SJ; dashed line = SJ+25kg; thick solid line = SJ+50kg.	98
4.17	Hip displacement (SJ+25kg). Comparison between actual performance (dashed line) and simulation (solid line).	100

LIST OF FIGURES

4.18	Knee displacement (SJ+25kg). Comparison between actual performance (dashed line) and simulation (solid line).	100
4.19	Ankle displacement (SJ+25kg). Comparison between actual performance (dashed line) and simulation (solid line).	101
4.20	Hip displacement (SJ+50kg). Comparison between actual performance (dashed line) and simulation (solid line).	102
4.21	Knee displacement (SJ+50kg). Comparison between actual performance (dashed line) and simulation (solid line).	102
4.22	Ankle displacement (SJ+50kg). Comparison between actual performance (dashed line) and simulation (solid line).	103
4.23	SJ+25kg activation profiles for matching simulation. Dashed lines are matching activation results, solid lines represent the jump height optimization. Thin lines are sEMG envelopes of gluteus, vastus lateralis, soleus for hip, knee and ankle joint, respectively.	105
4.24	SJ+50kg activation profiles for matching simulation. Dashed lines are matching activation results, solid lines represent the jump height optimization. Thin lines are sEMG envelopes of gluteus, vastus lateralis, soleus for hip, knee and ankle joint, respectively.	106
4.25	SJ+50kg activation profiles for matching simulation. Dashed lines are matching activation results, solid lines represent the jump height optimization. Thin lines are sEMG envelopes of gluteus, vastus lateralis, soleus for hip, knee and ankle joint, respectively.	106
5.1	a) Subject position and markers location, b) four linked rigid segments model, c) foot details: the part from the ball to the end of tips was modeled using the flexbeam WM2D script.	111
5.2	Vertical ground reaction force curves. Black line is the actual performance, gray line is the SIM. a) SJbw, b) SJ+40%, c) SJ+80%. Subject picture and stick diagram, in the a panel, show the starting position for actual and SIM performance, respectively. The subject picture and the stick diagram are synchronized with the instant of the propulsive phase start. 0 = instant at the toe-off. .	117

LIST OF FIGURES

5.3	Activation profiles example (SJbw). Bold lines represent SIM results. Activations are shown as function of percentage jump push-off phase. Toe-off = 100%. (GL, BF, RF, VL, GA, SOL = sEMG envelopes low-pass filtered at 7Hz).	119
6.1	a) SJbw start position; b) Subject performing SJ+40%; c) and d) stick models, SJbwstart position and SJ+40% fly phase.	121
6.2	Vertical component of the ground reaction force: SJbw <i>vs.</i> SIM SJbw, RMS error=6.5%; SJ+40% <i>vs.</i> SIM SJ+40%, RMS error=9.8%. Solid lines=actual jumps; dashed lines=SIM. Shaded area represents difference in relation to the net impulse.	122
6.3	Activation function compared with normalized rectified sEMG. A) SJbw chart; B) SJ+40%. 0=Toe-off.	123
7.1	Jump height differences between matching and optimized simulations for SJ, SJ+25kg and SJ+50kg. Large points represent optimized jump heights, whilst small points represent jump height output in matching simulations. These data suggest that the jump height was not maximal in matching simulations.	127
7.2	Activation profiles time history of the squat jump. The dotted line is the matching performance whilst the continuous line is the optimized performance. This condition shows slightly differences between the matching and the optimized performance.	129
7.3	Activation profiles time history of the squat jump with 25kg extra load. The dotted line is the matching performance whilst the continuous line is the optimized performance. This condition shows slightly differences between the matching and the optimized performance.	130
7.4	Activation profiles time history of the squat jump with 50kg extra load. The dotted line is the matching performance whilst the continuous line is the optimized performance. For each joint the ramp time obtained from the optimized performance is slower than in the matching performance profiles.	130

LIST OF FIGURES

7.5	Theoretical hip joint power model (considering 2 legs). The maximal value is 820.9 W.	133
7.6	Theoretical knee joint power model (considering 2 legs). The maximal value is 1193.0 W.	133
7.7	Theoretical ankle joint power model (considering 2 legs). The maximal value is 1153.9 W.	134
7.8	Global power meant as jump power for optimized simulations. SJ (solid line), SJ+25kg (dashed line) and SJ+50kg (dotted line).	136
7.9	Jump height prediction model. A linear decrease in jump height was found simulating different squat jump extra loaded. Jump height decreased as extra load increased.	138
7.10	Standardized residuals of the jump height model.	138
7.11	Vertical ground reaction force for the simulated half squat 1RM. The 0 in the abscissa axis represent the beginning of the propulsive phase.	142
7.12	Activation profile time history of the simulated 1RM half squat.	143
8.1	The cycle of theory-prediction-experiment theory, from Yeadon [93].	153
2	Kistler force plate output schema.	187
3	Kistler force plate coordinates.	188
4	Calculations.	189
5	Biodex specification.	190
6	Vicon specification.	191

LIST OF FIGURES

List of Tables

2.1	Hip joint torque experimental data for each isovelocity test.	33
2.2	Knee joint torque experimental data for each isovelocity test.	34
2.3	Ankle joint torque experimental data for each isovelocity test.	35
2.4	Data obtained from the experiment used to scale the original (dynamometer data) ankle joint torque model.	36
2.5	sEMG (rms) peak values. RMS was calculated over a window of 50ms. GL=gluteus; BF=biceps femoris; RF=rectus femoris; VL=vastus lateralis; GA=gastrocnemius medialis; SOL= soleus.	44
2.6	Kinetic and jump height characteristics of the best jump for each given condition (SJ,SJ+25kg,SJ+50kg).	46
2.7	Kinematic characteristics of the best jump for each given condition (SJ,SJ+25kg,SJ+50kg) at the start and at the toe-off instant of the jump.	46
3.1	Subject characteristics.	49
3.2	Parameter definitions of the planar model.	51
3.3	Segment weight regression equations from Chandler et al. [20].	54
3.4	Weight and mass of each model component. FB = flexbeam	55
3.5	Segmental moment of inertia considering the somersault axis.	56
3.6	Whole-body 4 link rigid segment model parameters.	56
3.7	Barbell and plates moment of inertia parameters.	58
3.8	Parameter of the hip joint torque model obtained from the statistical fitting.	64
3.9	Parameter of the knee joint torque model obtained from the statistical fitting.	65

LIST OF TABLES

3.10	Parameter of the ankle joint torque model obtained from the statistical fitting.	66
3.11	Description, values and bounds of the 9 parameters used to fit the experimental data of the torque produced by the hip extensor muscle group.	69
3.12	Description, values and bounds of the 9 parameters used to fit the experimental data of the torque produced by the knee extensor muscle group.	70
3.13	Description, values and bounds of the 9 parameters used to fit the experimental data of the torque produced by the ankle plantar flexor muscle group.	71
3.14	Summary of the parameters obtained using two different models. For the hip and ankle joint the calculated isometric torque was lower in the 5-parameter function than in the 9-parameter one. Similar calculated optimal angle occurred for the hip and the knee joint. Maximal shortening velocity parameter (ω_{max}) was very different comparing the two different knee models.	71
4.1	Kinematic data: SJ conditions compared for starting and toe-off angles. RMSE is calculated over the whole jump, whilst the column <i>difference</i> (deg) is about the instant of the toe-off.	87
4.2	Activation timing set for the squat jump matching simulation. Model A (A), Model B (B). Graphical representation is presented in Figure 4.10. <i>Ramp time</i> represents the time that the torque generator needs to reach the full activation. A proximal-to-distal activation pattern could be noticed (from the hip to the ankle).	91
4.3	Result of the jump height for actual performance and relative COM velocity at toe-off. Model A and Model B are shown. Differences (diff.) between the Model A against the Model B and, between the Model B vs. the actual (act) performance are reported. COM (centre of mass).	93

LIST OF TABLES

4.4 Data of the GRF are reported in this table for matching simulations. Result of the GRF for actual performance, **Model A** and **Model B** are shown. The RMSE was calculated over the propulsive phase of the jump in relation to the actual performance of the given condition. 94

4.5 Torque (τ), velocity (ω) values for matching simulations (match). Angles (θ) at which the maximal torque occurred are reported for each conditions and each joint. 97

4.6 Matching simulation peak torque (τ , 2 legs) expressed as the percentage of the predicted maximum isometric torque (T_0). 98

4.7 Power (P) , velocity (ω) values for matching simulations (match). Angles (θ) at which the maximal torque occurred are reported for each conditions and each joint. 99

4.8 Angle values (matching simulation) for each joint at the instant of the toe-off for SJ, SJ+25kg, SJ+50kg. The RMSE error refers to the whole propulsive phase comparing actual performances against the models. 104

4.9 Activation and onset timing obtained from matching simulations for SJ, SJ+25kg and SJ+50kg. 107

5.1 Data set obtained from matching simulation at 60Hz for SJbw , SJ+40% and SJ+80%. Hr, Kr and Ar are the rise time for building torque of hip, knee and ankle joints respectively. Kd and Ad are the onset delay of the knee and the ankle joints with regard to the hip joint. 115

5.2 Jump height was calculated using the flight time method; * the start of the propulsive phase was located when the force value was greater than three time the deviation standard of the average value of the start equilibrium position before to jump. 115

5.3 Jump height was calculated using the flight time method. RMSE % is calculated with respect to the average vertical GRF. 115

LIST OF TABLES

5.4	Data set obtained from matching simulation at 60Hz for SJbw, SJ+40% and SJ+80%. Hr, Kr and Ar are the rise time for building torque of hip, knee and ankle joints respectively. Kd and Ad are the onset delay of the knee and the ankle joints with regard to the hip joint.	119
6.1	Data set obtained from matching simulation at 60Hz for SJbw and SJ+40%	123
6.2	Parameters at the instant of the toe-off for both SJbw and SJ+40%.123	123
7.1	Parameter boundaries used to optimize squat jump conditions by using the simulated annealing algorithm.	126
7.2	Optimized activation patterns for SJ, SJ+25kg and SJ+50kg. Match = matching simulation; Opt = Optimized simulation.	128
7.3	Peak torque (τ) for matching and optimized simulations (match, opt). Angles (θ) and velocity (ω) at which the maximal torque occurred. Match = matching simulation; opt = optimized simulation.	131
7.4	Peak torque (τ) for matching and optimized simulations expressed as percentage of the predicted maximum isometric torque at each joint (T_0). Match = matching simulation, Opt = optimized simulation.	132
7.5	Power (P) of hip, knee and ankle joint expressed as percentage of the maximal power of the theoretical model.	134
7.6	Power (P) , velocity (ω) values for matching simulations (match). Angles (θ) at which the maximal torque occurred are reported for each conditions and each joint.	135
7.7	Jump Height results for matching and optimized simulations. . . .	137
7.8	Jump height vs. load predictions: estimated parameters. $R^2 = 0.99$	139
7.9	Activation parameters set for each given optimized squat jump condition. Onset time is always in relation to the hip joint that showed to be the first joint activated for each condition.	140

LIST OF TABLES

Chapter 1

Introduction

1.1 Computational approach in sport science

Applied research in Sport Science is a relatively new field that studies the application of scientific principles and techniques with the goal of improving sport performance. Sport is a context related to the scientific disciplines of the human movement. However, Sport Science can be focused on different areas: physiology, psychology, motor control, biomechanics, neuromechanics, etc. All of these areas can also include many topics such as nutrition and diet, sports technology, performance analysis, technique optimization, exercise physiology, coaching and strength and conditioning training.

Generally, applied scientific research is developed by the means of several approaches depending on epistemology. These methods could include interviews, analysis of video recordings, clinical studies, mathematical modelling, simulations and measurements (or estimations) from different experimental conditions. Descriptive research is often used in exercise physiology and strength and conditioning research. However, in research experiments variability during testing could be a limitation. In addition, in order to have an accurate statistical analysis, a group of subject with average characteristics has to be considered. Therefore, availability of many participants might be difficult. These limitations could be reduced using a computational approach based on a subject-specific model developed using experimental data. Indeed, if we model a theory based on ex-

perimental finding, then many details can be disclosed. For these reasons in this thesis a computational approach was chosen to create a human vertical jumping model. In addition, recently scientists have taken up the challenge to create subject-specific musculoskeletal models by using individual subject characteristics [28; 48]. Therefore, simulations may subsequently optimized to give results as close as possible to the measured data. Subject-specific model has yielded successful matching simulations for various athletic performances, for example: running jumps for height, step and jump phase win triple jumping [5; 90].

Generally, in modelling and simulation a simple rule should be followed: the simpler, the better. Alexander for example argued that simple models are particularly useful in identifying basic principles because the simpler the model, the easier it is to discover which of its features gives rise to the observed effect [3].

This work wanted to be the first part of a large project aiming to apply simulations to strength and conditioning training research. However, in spite of the fact that a simple strength ability was considered, the model requires accurate description of neuromuscular (e.g. muscle activation in time, differential activation \rightarrow neural inhibition during eccentric contractions), anthropometric and inertial characteristics. Therefore, in this introductory Chapter previous literature on neuromechanics, modelling, simulations and computational methods is reviewed. The purpose of the thesis is outlined (see section 1.4). Research questions are posed and, lastly an overview of the thesis is given with brief descriptions of the content of each Chapter.

1.2 Literature review

1.2.1 Skeletal muscle force exertion

Human skeletal muscles are crucial in movement, they are composed of specialized contracting fibers supported by a connective tissue framework situated in different deep levels (fascia, epimysium, perimysium, endomysium). These connective tissue layers are at some point combined, generating tendons that attach muscles to the bones allowing force transmission produced by neuromuscular contraction. Basically, this is the way of human bodies to generate movements around joints.

Generally speaking the process used by muscles to contract was firstly described by Andrew F. Huxley and it is known as sliding filament theory [40]. This theory remains a work in progress for scientists. In fact, it is still unable to explain a number of features of muscle, for example: the origin of the elastic forces in the sarcomere and the specific action of adenosine triphosphate (ATP) [41]. However, human muscle force production requires to consider at least four main key points: nervous signals, chemical events, muscle fiber types and its architecture.

Indeed, muscle contraction involves the interaction between the nervous system and the muscles. The nervous system generates the signals responsible of the muscle activation in order that the muscles provide tension (see section 1.2.2 for details).

Once the nervous system signals have reached myofibrils the main role is played by the release of intracellular Ca^{++} causing a chemical phenomena referred to as excitation-contraction coupling in the presence of adenosine triphosphate (ATP) [73]. This chemical process allows mechanical movement by the means of two main structural proteins in the basic unit of a muscle (sarcomere): myosin and actin. Consequently, more or less tension can be produced in relation to the characteristics of four pure fiber types: slow type I, fast type IIA, fast type IIX and fast type IID [71; 78].

Finally, the fourth factor above mentioned is about the arrangement of muscle fibres in relation to their aponeurosis or tendons (architecture). This finite geometry will determine the amount of tension that can be exerted by the whole muscle-tendon unit at its origin or insertion. Aagaard et al. [2] were able to show that pennation angle was a property of the human muscle. Pennation angle is sensitive to strength training changing into an optimal geometry which give improvement in terms of force. Therefore, in human pennate muscle, changes in the total area of the cross-sections parallel to the muscle fibers (anatomical cross-sectional area: CSA) [60], fascicle length or volume caused by training or inactivity may not necessarily reflect the change in physiological CSA (cross-sections perpendicular to the muscle fibers), and thereby in maximal contractile force, since a simultaneous change in muscle fibre pennation angle could also occur [2].

However, in a mechanical point of view, a joint torque is always produced

thanks to the sum of tensions produced by different muscle groups which act around joints via microscopic events above described. Therefore, torque exertion represent a key factor in modeling and simulation research approach. Indeed, researchers have to create an equivalent mechanical system to accurately describe the human skeletal muscle. Once a mechanical model is developed they are able to investigate by using a computational approach. A torque-driven model is used in this thesis to represent human muscle force.

1.2.2 Neuromuscular interaction

Muscles generally need an electrical input to produce tension. Consequently, in humans the nervous system manages the process which allow muscles to contract their self taking advantage from its own biological features. This suggests that the final result in terms of tension exerted depends on muscle and nervous system characteristics.

Muscle fibers are divided into functional units: the motor units. A single motor unit is the smallest subunit that can be controlled because it is innervated separately by a motor axon allocated in the spinal cord that innervate a muscle fibers group. Actually, the motor unit consist of a synaptic junction in the ventral root of the spinal cord, a motor axon, and a motor end plate in the muscle fibers. A single motor unit can control few muscle fibers up to as many as 2000, this depend on the fineness of the control required [26]. Each muscle has several number of motor units, each motor unit is controlled by a separate nerve ending. When a motor unit is activated an all-or-nothing event occurs. The electrical signal produced by the nervous system (motor unit action potentials) gives as mechanical result a twitch tension. In particular, the contralateral motor cortex drives muscle discharge to generate tensions by the means of events above described. If a given muscle requires much tension, then two ways are possible to achieve this goal: 1) increasing the stimulation rate; 2) additional motor units recruitment. Indeed, mathematical models describing recruitment have been reported in the literature to investigate the relationship between force and firing rate [25; 87]. As previously mentioned muscle fibers can be of different type and consequently motor units could be slow-twitch (fibers type I) and fast-twitch (fibers type II).

In a mechanic point of view, tonic units produce twitches with a low peak tension and a long time to peak (60-120ms), whilst phasic units reach a larger tension in a shorter time (10-50ms) [1; 18; 87]. Wani and Guha stated that considering 60 ms contraction time as the dividing margin between fast and slow motor units, it is seen that the muscle as a whole is a fast one [87]. Rainoldi and Gazzoni [1] stressed that the motor unit scheme described above could not appear to be appropriate for human muscles on the basis of three considerations: 1) difficulty to distinguish motor unit types in human muscles; 2) the first motor units activated in a voluntary contraction can be either slow-twitch or fast-twitch; 3) the cross-sectional area of human muscle fibers often does not increase from type I to type II. However, this consideration does not affect modeling of muscle force.

Despite the fact that the nervous system is the most important characteristic of the muscle contraction process, in modelling this is a simple feature which is often described by using a simple ramping function [14; 68; 94; 95]. Magnitude of the contraction, time to peak and onset of muscle activity become parameters of the given function in order to govern delays, activation and sometime deactivation timing [14; 49; 94]. Indeed, in this thesis a quintic function used in previous works by Yeadon [94] was used to model the active state of the human muscle. In addition a differential activation (see differential activation in Chapter 3 section 3.2.4) was considered to model the neural inhibition which occur at slow velocities during concentric and eccentric contractions [95]. In summary, the force that a muscle exerts during a contraction depends on the excitation provided by the nervous system, the mechanical property of the muscle and the muscle architecture.

1.2.3 Structure of the muscle-tendon complex

1.2.3.1 Muscle-tendon complex mechanics and modelling

The skeletal muscle-tendon complex (Fig. 1.1) is generally categorised into a three components assembly: contractile element (CE), series elastic element (SE) and parallel elastic element (PE) [11].

The Contractile Element also referred to as the Contractile Component (CC) forms the primary active force producing part of the muscle. The sarcomere

composed of actin and myosin filaments displaying a cyclic cross-bridging action to generate force and enable the muscle fibres to change length [41]. The force exerted by muscle fibres has been shown to be the function of both its length and its velocity of shortening or lengthening [34; 38]. It is now generally accepted that the force produced by the CC is due to the interaction, via so-called cross-bridges, of the myosin and actin filaments of the muscle fibre. The contractive force produced by a muscle fibre is thus equal to the sum of the forces produced by all the cross bridges in one half-sarcomere of the fibre, at any instant of time. Here, CC was modeled using joint torque generators based on experimental dynamometer data.

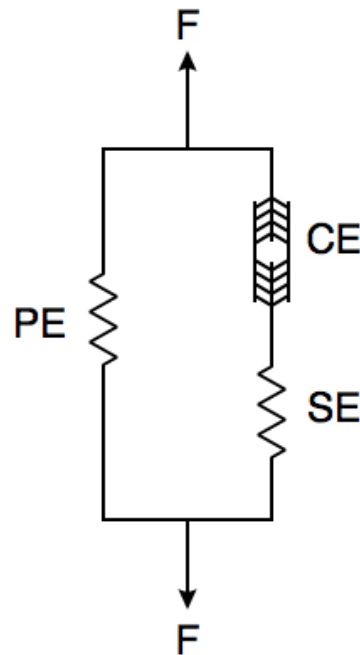


Figure 1.1: Hill's elastic muscle model. F: Force; CE: Contractile Element; SE: Series Element; PE: Parallel Element.

The SE is the broad term given for the constituent parts of the muscle-tendon complex which are in series with the CC. They exert elastic properties which are associated with the magnitude of stretching and are responsible for transferring the force generated in the contractile element to the skeleton [39]. Lewis [49] cited different works to explain that the magnitude of the elastic energy delivered dur-

ing jumping has been calculated using simulation models and measures in-vivo. He reported a work of Bobbert et al. [13] who calculated that the elastic properties of the plantar flexors delivered 40% of the energy produced by these muscle-tendon units during a squat jump. Anderson and Pandy [7] calculated a similar value of 35% for all the elastic structures included in their model. Bohm et al. [19] calculated 32% on average across all muscle-tendon units. Fukashiro et al. [31] implanted a buckle transducer around the Achilles tendon of living participants and measured the energy storage in the tendon during squat, counter-movement jumps and hopping. Their measurements agree well with the simulation model calculations where energy storage for the three activities totaled 23%, 17% and 34% respectively. Generally, SE is included in modelling simulations. However, here it was decided to make a challenge: attempting to model the muscle considering only CC. This in order to understand if a very simple actuator could be enough to represent the muscle behaviour for a pure concentric movement (e.g. squat jumps).

The Parallel Elastic Element (PE) constitutes the various connective tissues which surround the contractile component and include the sarcolemma, perimysium, epimysium and endomysium. The PE exerts an elastic force independent of the series elastic element but in parallel with the contractile element. The forces exerted by the PE are directly related to CC length but are independent of the CC activation [91]. The PE has often been disregarded in several computer simulation studies [5; 48; 49] since its effect is minimal within the normal functional range of a joint [21]. For the same reasons, the PE was not included in the model presented in this work.

1.2.3.2 Tension-length relationship

Ramsey and Street published one of the first works which identify a tension-length relationship in vitro muscle [72]. Indeed, they found that for a fibre stretched to different starting lengths, then electrically stimulated, fibre tension was maximal near its slack length and decreased at lengths either side of this optima fibre length.

More precisely, when an isolated muscle fiber is stretched to the point of

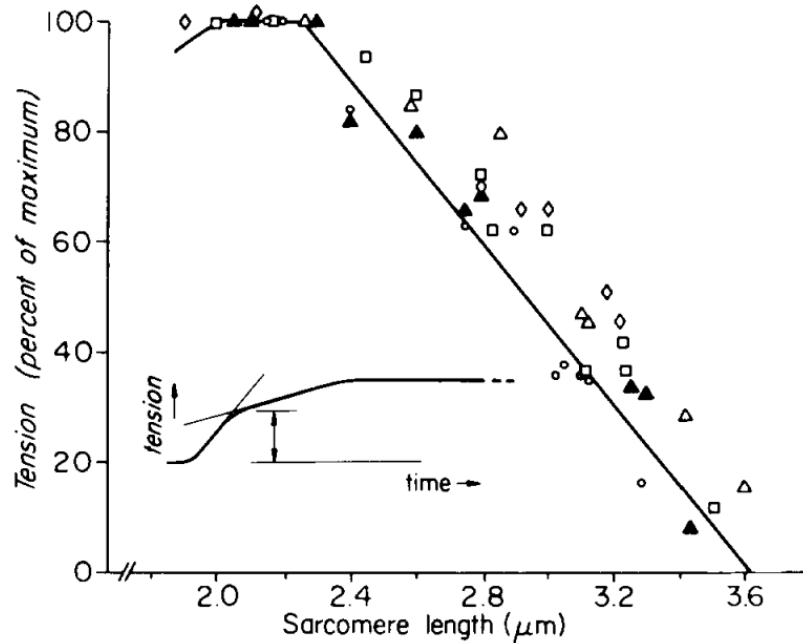


Figure 1.2: The relation between tension and sarcomere length. The drawn line is the relation obtained by Gordon et al. [34]. A plateau is visible at the top of the graphic and tension decrease at both sides.

minimal overlap of actin and myosin and then stimulated by an electrode to contract, the force of contraction measured is minimal. When an isolated muscle fiber is stimulated to contract when there is optimal overlap of actin and myosin the force produced is maximal. When an isolated muscle fiber is stimulated to contract when there is maximal overlap of actin and myosin the force produced is minimal. The result is a graph that has a parabolic shape (Fig. 1.2).

It has to be mentioned a work of Gordon et al. published in 1966 [34]. They re-investigated the tension-length relationship in vitro with special precautions to ensure uniformity of sarcomere length within the part of the fibre being studied (Fig. 1.2). In most respects the results of Ramsey and Street [72] were confirmed. However, three different features were described: 1) the peak of the curve was found to consist of a plateau between sarcomere lengths of $2.05\mu\text{m}$ and $2.2\mu\text{m}$; 2) the decline of tension above this plateau is steeper than found by Ramsey and Street; 3) the decline of tension below the plateau becomes suddenly steeper

at a sarcomere length of about $1.67\mu\text{m}$. However, humans operate on either the ascending or descending limbs of the whole muscle force-length relationship, rather than across the full ascending-descending range of the single fibers.

Actually, *in vivo* conditions have to be considered. A torque-angle relationship was found to be equivalent to the tension-length *in vivo* relationship. Normally, by using a dynamometer (see Section 1.2.4) one can test the torque-angle relationship finding similar results with the *in vitro* condition. However, in modelling a general assumption about the joint torque generator is necessary: the torque exerted at the joint is a function of only the angle and velocity of that joint (see next section for tension-velocity relationship). This assumption is widely used throughout the literature for forward-dynamic torque-driven models [8; 49; 76]. Therefore, the model presented in this thesis was based on the same assumption. Generally, modelling the force length relationship of muscle is often approximated by a quadratic function since it provides a reasonable fit of experimental data. However, this relationship might also be approximated by a bell shaped function similar to the normal distribution. These functions assume symmetry of the data. For this work a quadratic function was chosen and it is described in Chapter 3 in section 3.2.2.

1.2.3.3 Tension-velocity relationship

A second relationship was described in relation to the tension a muscle can exert and its velocity of shortening (concentric contraction) or lengthening (eccentric contraction). Theoretically, in 1935 Fenn and Marsh [27] and successively in 1938 Hill [38], studied the tension-velocity characteristics of *in vitro* muscle fibres. Experiments were performed using cat and frog muscle fibres. As result, they identified how muscle tension decreased as the velocity of shortening increased. Similarly to the tension-length relationship, mathematical models were created in order to approximate this second relationship.

Undoubtedly the most popular representation across the muscle modelling literature is the Hill's rectangular hyperbola [38]:

$$(P + a) \cdot v = b \cdot (P_0 - P) \tag{1.1}$$

Where \mathbf{P} is the force, \mathbf{V} is the velocity and, \mathbf{a} , \mathbf{b} , $\mathbf{P0}$ are constants. Equation (3.11) is a rectangular hyperbola with asymptote at $\mathbf{P} = -\mathbf{a}$ and $\mathbf{V} = -\mathbf{b}$. It relates speed and load in an isotonic shortening (Fig. 1.3).

Successively, an attempt was made by Edman [24] to extend the use of Hill's (1938) hyperbolic equation to also cover the high-force region of the force-velocity relation. Therefore, a biphasic function was proposed (Eq. 1.2) [24]:

$$V = \frac{(P_0^* - P)^b}{P + a} \cdot \left(1 - \frac{1}{1 + e^{-k_1(P - k_2 P_0)}}\right) \quad (1.2)$$

Where the first term expresses the tension-velocity curve at low and intermediate loads. The constants \mathbf{a} and \mathbf{b} represent the asymptotes of this rectangular hyperbola and have dimensions of tension and velocity, respectively. \mathbf{P}^* is the isometric force. The second term with in brackets reduces \mathbf{V} in the high-force range. \mathbf{k} is a constant, it has the dimension of 1/tension whereas \mathbf{k}_2 is dimensionless.

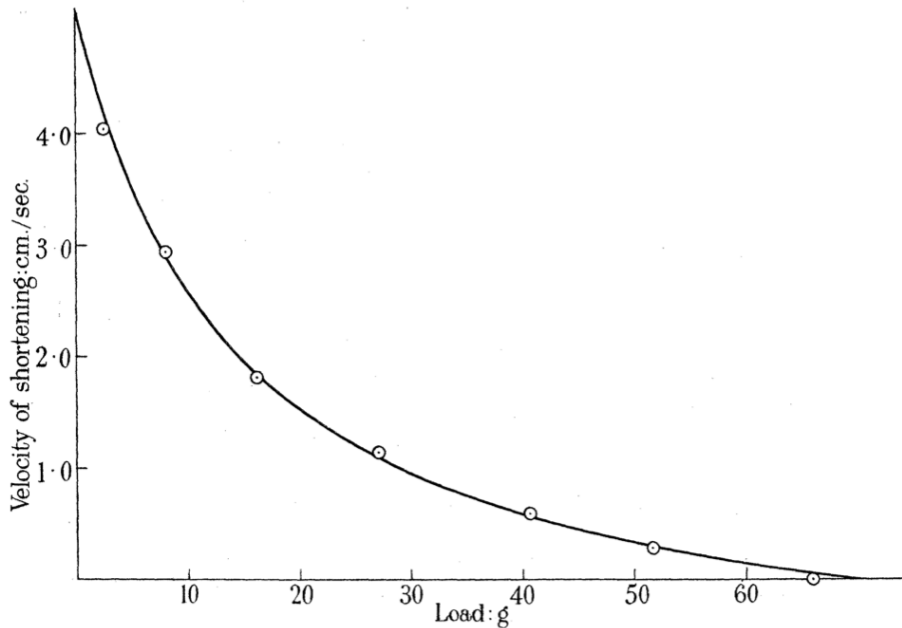


Figure 1.3: Hyperbolic relation between load and speed of shortening. From Hill [38]

As mentioned for the tension-length relationship, in vivo conditions are slight

different because a whole group muscle is considered instead of a single muscle fiber. However, if one collect dynamometer data for different given angular velocities, a similar shape can be found [10; 60; 64]. Therefore, mathematically the tension-velocity relationship has to be translated in torque-angular velocity relationship. Anderson [6] and Yeadon [95] proposed equivalent functions to describe this relationship in order to create model that might be implemented in simulations of human movement. The first author proposed a 4-parameter function to fit torque experimental data with regard to the torque-angular velocity, whilst the second author proposed an other similar 4-parameter function and successively a more complex 7-parameter function. The latter differed from the Anderson one because it took into account 3 additional parameters which described a differential activation (neural inhibition) in the slow part of the eccentric phase.

In this thesis, two models which we will call **A** and **B** were created (Chapter 3, sections 3.2.5.1 - 3.2.5.2): the first one fitted data by using the Yeadon's 4-parameter function, the second one the Yeadon's 7-parameter function [95] (tension-velocity relationship modelling).

1.2.4 Isokinetic dynamometry

The expression of in vivo whole muscle force production is poorly established compared to the in vitro equivalent first described by Hill [38]. However, in vivo description are based on maximum torque expressed at the joint level by the means of isokinetic dynamometer measurements. Isokinetic contraction is the muscular contraction that accompanies constant velocity limb movements around a joint [10]. Therefore, maximum torque is a complex integration of the muscle fibre contractile properties with the in vivo architecture of multiple muscle fibres, connective tissue and neural input [28]. This method has been extensively used in clinical research and, for assessing human muscle force characteristics [60; 61]. The velocity of movement is maintained constant by a special dynamometer (e.g. Biodex© [96]) . The resistance of the dynamometer is equal to the muscular forces applied throughout the range of movement. This method allows the measurement of the muscular forces in dynamic conditions and provides optimal loading of the muscles [37]. However, during movements in the vertical plane, the

torque registered by the dynamometer is the resultant torque produced by the muscular and gravitational forces [46], this is an error source. Errors that depend on the angular position of the tested muscle group should also be considered. Several methods have been developed for the correction of gravitational errors in isokinetic data [10; 37]. Other errors has been reported, for example issues about torque overshoot [74] and oscillation can occur before constant angular velocity is attained and deceleration occurs towards the end of the contraction [65]. The errors associated with measurements obtained on dynamometers can be kept small by ensuring the appropriate protocols are followed and that data is corrected for a number of phenomenon. Indeed, Allen [5] reported Chow [44] who stated that despite these concerns it should be emphasized that recognizing the limitations of these machines does not detract from the valuable contribution they make to the understanding of muscular function. Indeed, Forrester [28] explained that this approach has the advantage of allowing subject-specific torque functions to be readily obtained from maximum torque measurements on an isovelocity dynamometer [95] and hence model evaluation is more robust. Forrester [28] also reviewed that models of dynamic human movement are based on either individual muscle models, in which each muscle is represented by parameters describing its active, passive and architectural properties, or joint torque generators where all the muscles crossing a joint are lumped together to form a single torque generator. Regardless, the success of joint torque generators using measured torque functions has been demonstrated for many different activities [5; 32; 49].

In light of these facts and considering the topic which requires subject-specific data, in this thesis it was decided to mathematically represent human muscle force based on maximum torque measurements using a dynamometer and considering error corrections. Comprehensive methodology, procedures and results are presented in Chapter 2, section 2.1.

1.2.5 State of the art in computational research

1.2.5.1 Modelling and simulations in vertical jumping

Vertical jumping is often considered by biomechanists because it is simple to model and simulate this movement. Indeed, a planar 2D model would be enough

to answer several questions about activation patterns, optimization problems, coordination [14]. Sometime vertical jumping is represented considering only lower limbs [14; 32] or sometime arms are incorporated in the model to simulate specific kind of jump [49].

In 1992 van Soest published a paper about a simulation software (SPACAR). He used it in following years to investigate vertical jumping features [85]. Muscle properties, the role of biarticular muscles and a control strategy in human vertical jump height performance were investigate by van Soest in the decade between 1990 to 2000 [83; 84; 86]. For example he investigated the role of gastrocnemius (GAS) in vertical jumping found that jump height decreased by 10 mm when GAS was changed into a monoarticular muscle.

Bobbert studied vertical jumping using a simulation approach to investigate mechanic features of this specific movement [12; 14; 16].

Muscle coordination, jump height optimization were also studied by Pandy with his model. He used complex 3D models to establish that a proximal-to-distal joint activation sequence is a typical feature of vertical jumping ability [67; 68].

Selbie and Caldwell investigated how initial jumping posture affected vertical jump performance using a four-segment planar model driven by three torque actuators and, differently from Pandy they did not find a proximal-to-distal activation patterns. They argued that this sequence occurred because the model did not include biarticular muscles [76].

Yet, effects of muscle strengthening on vertical jump height was studied using simulations by Bobbert. This was one among his first papers focused on the impact of joint strengthness. Results disclosed that in order to take full benefit of an increase in muscle strength, activation patterns control needs to be adapted. Therefore, a force improvement requires an adaptation in terms of muscle coordination [15]. However, no study have investigated the effect of extra load in vertical jumping to add scientific informations in strength and conditioning training. Therefore, a first attempt to simulate vertical squat jumping with extra load was one of the goals of this work.

1.2.5.2 Modelling and simulations in strength and conditioning training

Computational approach can be considered a completely new approach in strength and conditioning training. Actually, no study has attempted to study strength exercises using simulations. This is why here it is not possible to review works but considerations can be done about how research could be structured to investigate strength exercise tasks.

Indeed, most of the time investigations are based on descriptive research. Fairly, it does not matter too much how sophisticated and accurate is the methodology used in descriptive research, in relation to the resulting analysis. In fact, this approach means that we want to measure a phenomena before and after a determined event, followed by an analyse attempting to explain what happened in time. Therefore, a fundamental limitation of the descriptive method is that findings indicate norms, not standards [43]. *The investigator learns what is being done, not what could be done or should bone.* He determines usual practices, rather than causes, reasons, meanings or possibilities.

In sport science, coaches and strength and conditioning trainer are “*playmakers outside the game*”. This suggests that research in sport should be performance-related to answer questions like: What is done? How is it done? Why does it work?. Therefore, the answers to What? How? and Why? are important to the athlete, coach and scientist, respectively. In 1994 Yeadon [93] suggested that sport biomechanics research should be structured in order to gain objective understanding about a phenomena: initially, a scientific investigation will probably take the form of a descriptive study which provides a record of what happens. The data may suggest a possible theory. Such a theory may be used to predict the outcome in a given situation. An experiment can then be conducted to determine the actual outcome. A comparison of theoretical and experimental outcomes can then establish the accuracy with which the theory models the activity. This will indicate the level of confidence that can be given to theoretical predictions and may suggest how the theory can be modified. He also argued that research in sports biomechanics should be a balanced mix of experimental data and theoretical modelling if a realistic understanding is to be achieved.

Similar suggestions about the structure of scientific method are given by Beck [75], Heath [66] and Davies [23]. In the light of this suggestions, strength exercises would be better understood if a mixed between experimental data, modeling and simulations would be considered for investigations. This thesis, is a first attempt to understand the impact of extra loads on human vertical jumping performance using experimental data, theoretical models and simulations.

1.3 Algorithms

Algorithms are often a key in computational approach. An algorithm is a procedure for solving mathematical problems in a finite number of steps that frequently involves repetition of an operation. Basically, an algorithm is a resolute procedure.

Yanenko described algorithms explaining that a computational algorithm processes the numerical and the symbolic information and usually involves a loss of information and of accuracy [92]. The loss of accuracy is the result of several errors which appear at the various stages in the computation: erroneous models, approximations, input data, and rounding-off operations. Erroneous models are the result of the approximate nature of a mathematical description of a real process. The errors in the input data may originate from errors in the observation, in the measurements, etc., as well as from the rounding off of the input information. The overall error originating from the model employed and from the input data is sometimes referred to as the inevitable error [92].

However, when an optimization problem needs to be solved the choice of the algorithm and the objective function employed are crucial. They can affect both the time taken to determine the optimal given parameters and the likelihood that the given set of parameters are indeed a global optimum and not some local phenomena. These issues can be of particular importance when determining the optimal solution. For human performance computational based research, the functions controlling human movement are complex and can have many local minima and maxima that can create problems for convergence [62]. Next two sections are about two algorithms used in this thesis: brute-force algorithm and simulated annealing.

1.3.1 Brute-force algorithm

The brute force algorithm consists in checking, at all positions in the text between 0 and $n - m$, whether an occurrence of the pattern starts there or not. Then, after each attempt, it shifts the pattern by exactly one position to the right. The brute force algorithm requires no preprocessing phase, and a constant extra space in addition to the pattern and the text. During the searching phase the text character comparisons can be done in any order. The time complexity of this searching phase is $O(mn)$ (when searching for $a^{m-1}b$ in a^n for instance). The expected number of text character comparisons is $2n$. Basically, the exhaustive search brute-force solution is based on listing all potential solutions to the problem in a systematic manner. Solutions are evaluated one by one keeping track of the best one found so far, when search ends, it gives the best solution. Due to its nature the weakness of this algorithm is its time cost. Generally, it is effective when the problem have few parameters in a small search space. In this thesis the Brute-force algorithm was used for some simulation.

1.3.2 Simulated annealing algorithm

Simulated annealing (SA) is a probabilistic method for finding the global minimum of a cost function that may possess several local minima [22; 57]. SA is motivated by an analogy to annealing in solids. The idea of SA comes from a paper published by Metropolis et. al in 1953 inspired by the Monte Carlo integration over configuration space [57]. The algorithm in this paper simulated the cooling of material in a heat bath. This is a process known as annealing. The metal is heated to a temperature typically below the *austenizing* temperature, and held there long enough to relieve stresses in the metal. The piece is then furnace cooled. It is then ready again for additional cold working. This can also be used to ensure there is reduced risk of distortion of the work piece during machining, welding, or further heat treatment cycles. Metropolis algorithm simulated the material as a system of particles [57]. The algorithm simulates the cooling process by gradually lowering the temperature of the system until it converges to a steady, frozen state. Geman and Geman provided a proof that SA, if annealed sufficiently slowly, converges to the global optimum [33]. Indeed, also

Corana et. al [22] stated that SA is able to search the optimal solution by learning from past solutions probabilistically, but without falling into local optima. Moreover, SA has been used to successfully determine the global optimum visco-elastic and activation properties of both angle-driven and torque-driven forward dynamics simulation models of dynamic human movements [5; 49]. However, for more complex solutions with many local optima a genetic algorithm approach might offers a fast and robust alternative to obtaining global optima.

This thesis succesfully used the SA to fitting dynamometer experimental data and to run simulations (see elsewhere for details → Chapter 4, Section 4.3.2).

1.4 Thesis statement purpose

Most of the studies about strength and conditioning performance use experimental data to describe kinematic, kinetic, physiological and hormonal features in subjects ranging from young novices to elite performers. This investigation approach is useful for providing information about what currently is happening during experiments to compare data in time. However, a huge number of subjects and tests should be performed to obtain a reasonable statistical result which is often the limit of this approach. In addition, predictions based on experimental results could be difficult to be theorized.

In light of this fact, a pragmatic research attitude could suggest to combine experimental data with mathematical modelling which can generate a complementary research method. Actually, this way allows predictions and improves the control of observed variables which describe models implemented into simulations, making research a quantitative deterministic system taking advantage of the computational power today available. A slight stochastic feature could be present if some randomized algorithm which employs a degree of randomness as part of its logic is used during computations. However, research examining simulated vertical jumping has continued to employ a simple squat jump to investigate coordination, activation patterns and mechanic features of the movement [12; 14; 16; 68; 76; 81]. Moreover, when some performance was investigated, nobody considered common strength exercises by using simulations [5; 42; 47; 49].

Therefore, the purpose of this thesis was to develop a subject specific 3-actuator

torque driven 2D forward-dynamic model to answer about biomechanics and practical strength training questions. A simulation approach was then chosen for that purpose and common squat jump exercises performed in different conditions (with and without extra load) were simulated. Indeed, extra load conditions were chosen to represent common strength exercises aiming to investigate the impact of load on squat jump task. Figure 1.4 illustrates how the model has been developed and why particular measurements or estimations were necessary to set-up the simulator, then run the models implemented into simulations.

Before a model can be used to make predictions, one should verify if the model reproduces accurately the actual performance. In order to achieve this goal 2 torque generators models were created (named A and B) to established which one better matched the actual performance, then using the better one for all other simulations.

Consequently, the first step was to determine parameters of the main features of the human jumping performance to give inputs to the model simulator. Combined experimental data and theoretical estimations were used to underpin the framework of the model and its working state.

Subsequently, the second goal was about jump height optimization starting from matching simulations results of the squat jump with and without extra load. This is the heart of modelling, optimized performances give information about what a system would do working in optimal conditions unless simulations disclose the model was already working in optimal way.

Further, the model was applied to make predictions as accurate as possible in order gain understanding and insight into human strategy movement and to avoid lengthy sessions in laboratory with subjects to collect many data. In summary, this thesis wanted to answer several questions here reported in details:

1. *Is a subject-specific 3-actuator torque driven model based on a monoarticularity assumption able to match human vertical jumping performances?*
2. *How accurately can the model reproduce the actual performance in squat jumps with and without extra load?*
3. *Is the model able to estimate the maximal load that a subject is able to lift in a half squat exercise?*

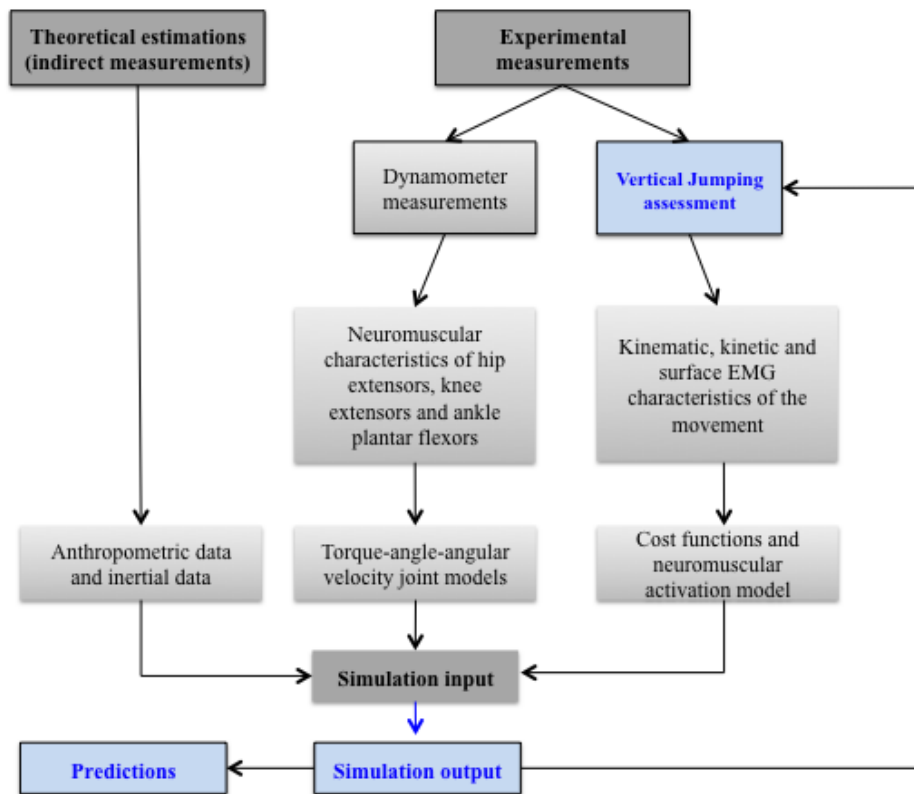


Figure 1.4: A comprehensive diagram to summarize how the simulation model was created is shown. The simulation model needs input data in numerical form (e.g. functions obtained from experimental data). Indeed, experimental measurements (dynamometer assessments for each joint with kinematic, kinetic and sEMG measures during squat jumping) were performed in order to describe muscle force and movement characteristics. Inertial and anthropometric data came from estimations based on regression equations available in the scientific literature (e.g. see Chandler’s report [20]). Actually, simulations were run by the means of inputs which describe as closely as possible all considered characteristics. Subsequently, results were used to make sure that the model could represent the reality then able to make some prediction.

4. *What is the impact of adding extra load during squat jump on jump height and power output?*

A model can be more or less complex depending on the questions we want to answer, but even the simplest model would require a clear explanation about its framework to understand how the model works and what we need to know to create it. In this thesis, Chapter 2 and Chapter 3 describe experimental and estimation methods used to measure or calculate data inputs for simulations. A crucial phase of modeling is the model evaluation to establish the accuracy of the model. This is analyzed and discussed from the Chapter 4 to the Chapter 6. The optimization phase and prediction part are discussed in Chapter 7. This thesis is concluded by the Chapter 8 with a general discussion and conclusions, including potential areas for improvement in future studies.

1.5 Summary

This Chapter introduced the purpose of this thesis. The main goal is to create a tailored model simulator based on one specific subject measurements (force, anthropometric data, inertial data, etc.). This model want to be evaluated by comparing it with experimental data, then optimized to understand whether the subject was operating sub-maximally (jump height parameter) during experimental tests. Subsequently, the model will make predictions about different squat jump (extra load) conditions and the maximum load achievable. A computational approach mixed with experimental data can be a new way to conduct research in strength and conditioning training exercises.

Chapter 2

Experimental measurements

The aim of this study was to create a subject-specific model. Thus, a male healthy subject (29yrs, 63kg, 1.74m) took part at experimental sessions. The right side of the subject was used for all measurements assuming bilateral symmetry.

2.1 Dynamometer testing session

A Biodex© dynamometer (Biodex Medical Systems, 840-000 System 4 Quick-Set, Inc. USA) was used to collect joint torque data throughout a joint range of motion (ROM) in time domain. This dynamometer (Fig. 2.1) operated on a three phase power supply and signals were recorded using a data acquisition system (Biopac© MP150CE, System, Inc. USA) operating on a software package (AcqKnowledge® 3.8.2). Data were sampled at 100 Hz.

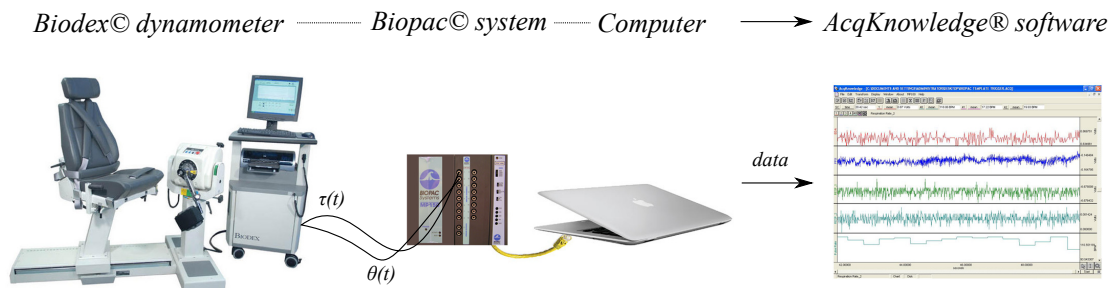


Figure 2.1: Torque (τ) and angle (θ) data acquisition procedures.

2. Experimental measurements

A series of isometric, concentric and eccentric isovelocitity joint torques were measured for a variety of joint actions: hip joint extension, knee joint extension and ankle joint plantar-flexion. Generally, the subject was strapped firmly to the dynamometer to reduce freeplay in the system which can change the alignment of the joint and crank axis. Otherwise, this could give effects on the crank-joint torque relationship. Therefore, the crank and joint centres of the selected joint were aligned in order to reduce the difference between the crank angle and joint angle.

Dynamometer measurement does not generally provokes learning effect [51], especially for the knee joint [51; 54; 55]. Despite this fact, the participant was asked to become familiar with different dynamometer velocities and procedure instructions [51]. Thus, the subject performed randomized muscle voluntary contractions (MVC) in isovelocitity and isometric conditions freely over 15 days for hip, knee and ankle joints. Any session number constraint was planned. Further, these data were recorded to improve subject motivation, one assistant or an audio file was always provided to prompt him to perform MVC at his best [79]. However, any data set collected from familiarization sessions was included in the final processing.

A general instruction was given for dynamic testing: the subject started to perform a MVC 1s before the dynamometer was turned on. This procedure (Fig. 2.2) allowed to obtain higher reliable torque values by reducing as much as possible submaximal neuromuscular activation through the ROM [61].

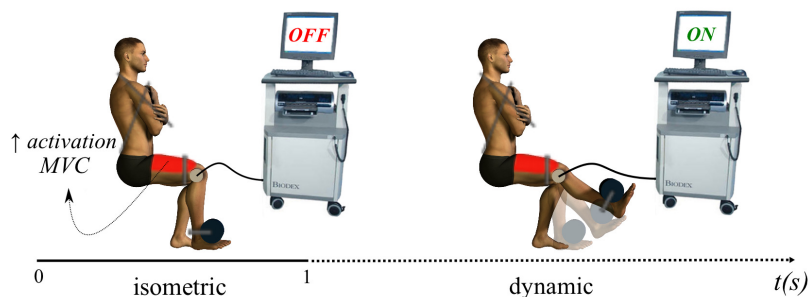


Figure 2.2: Dynamic test procedure (e.g. knee joint). A maximal isometric contraction was followed by a dynamic contraction.

2.1.1 Hip joint testing

The participant was lying supine on the dynamometer with his right leg flexed on the crank support. In order to avoid unwanted movements, the left leg was kept on a flat surface at the same level of the hip. Figure 2.3 shows a comprehensive description of the subject position and muscle involved during this test. The subject performed 3 different sessions separated by at least 1 week, all sessions required 3 trials for each isovelocity and 3 trials for each isometric selected angle condition. The protocol involved hip joint extension torque measurements over a ROM of 130° for concentric MVC at 0; 60; 120; 180; 240; 300 ($deg \cdot s^{-1}$) velocities and, for eccentric MVC at -60; -120; -180; -240 ($deg \cdot s^{-1}$) velocities. Isometric MVC was measured over the ROM of 90deg at each 10deg. The subject was asked to push (concentric) or to make an opposite effort (eccentric) maximally against the crank for each selected isovelocity. Isometric measurements required 3 trials of 6 seconds, with a rest of 30 seconds between trials for each given angle. The participant was encouraged to exert a MVC by ramping up from a relaxed state to maximal effort. The isovelocity portions of the central eccentric-concentric phase of each trial were identified by manually inspecting the joint velocity time history. Subsequently the data files of the time histories of the crank torque and the joint angle data were edited to leave just these portions (Fig. 2.4). Further, the velocity was corrected by analyzing the first derivate of the positional signal. For each trial the maximal value point by point was considered.

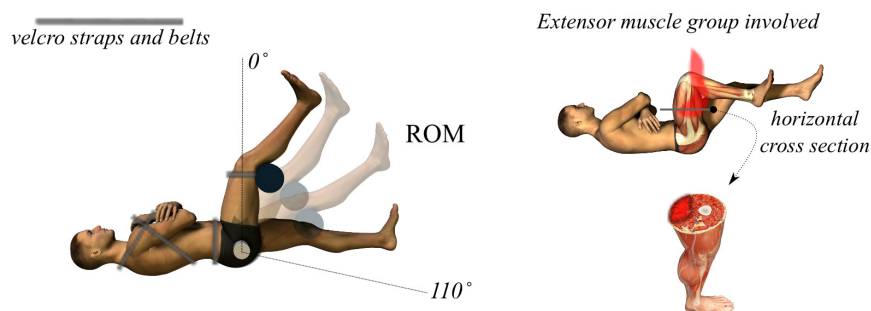


Figure 2.3: Hip joint Biodex test angle definition. The subject position is shown in the left side. The right side highlighted muscle groups involved.

2. Experimental measurements

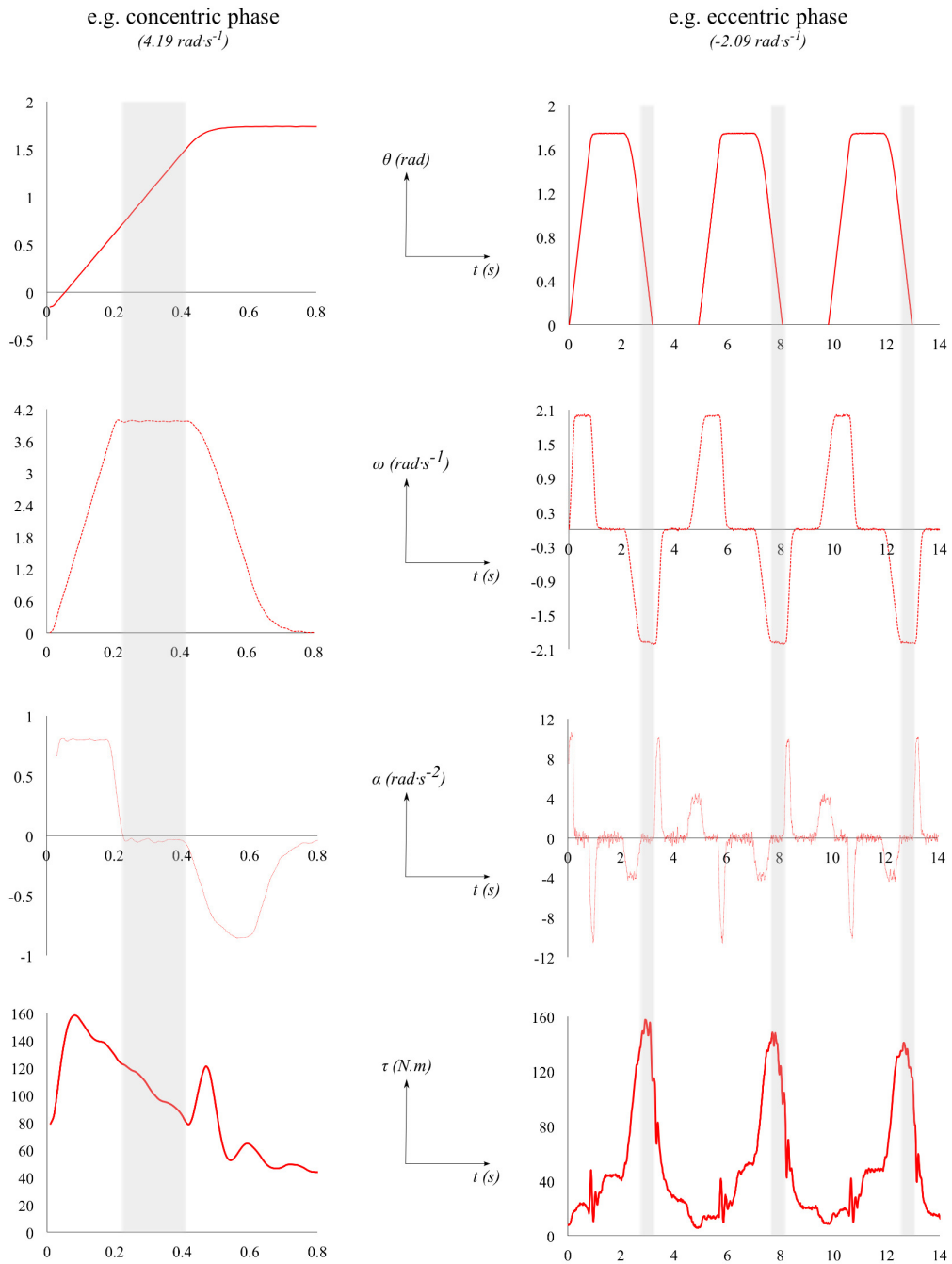


Figure 2.4: Hip joint example data from the dynamometer during testing. Concentric and eccentric sample data are shown in the left and in the right side, respectively. Shaded areas represent the isovelocity portion. Light lines are the first and the second derivate of the position in time.

2.1.2 Knee joint testing

The Subject was seated on the dynamometer with the trunk vertical and thigh fixed at a 90° hip angle, velcro straps were applied tightly across the thorax, pelvis, and distal thigh. Hands were placed on the shoulders. Details of the subject position are shown in Figure 2.5 in the left side, whilst muscle groups involved are shown in the right side. The protocol involved knee joint extension torque measurements over a range of 110° for concentric MVC at 0; 60; 120; 180; 240; 300 ($deg \cdot s^{-1}$) and, for eccentric MVC at -60; -120; -180; -240 ($deg \cdot s^{-1}$) velocities. Isometric MVC was measured over the ROM of 90deg at each 10deg. The subject was asked to push (concentric) or to make an opposite effort (eccentric) maximally against the crank for each selected isovelocity. Isometric measurements required 3 trials of 6 seconds, with a rest of 30 seconds between trials for each given angle. During the isometric trials, the participant was encouraged to exert a MVC by ramping up from a relaxed state to maximal effort. A visual feedback was available on-line in front of the subject. The isovelocity portions of the central eccentric-concentric phase of each trial were identified by manually inspecting the joint velocity time history. Subsequently the data files of the time histories of the crank torque and the joint angle data were edited to leave just these portions (Fig. 2.6). For each trial the maximal value point by point was considered.

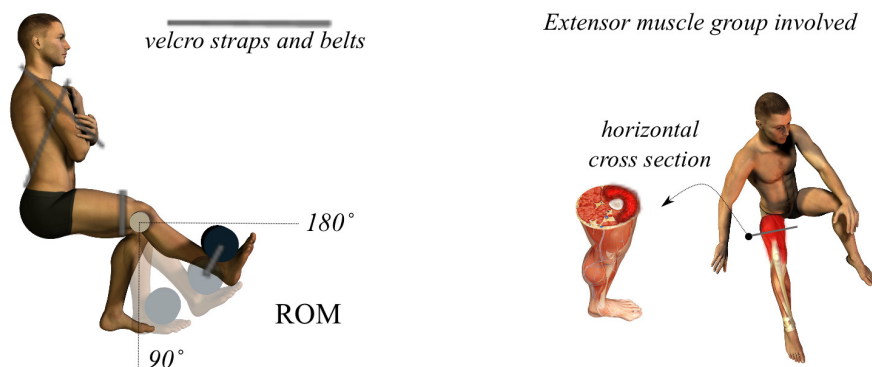


Figure 2.5: Knee joint Biodex test angle definition. The subject position is shown in the left side. The right side highlighted muscle groups involved.

2. Experimental measurements

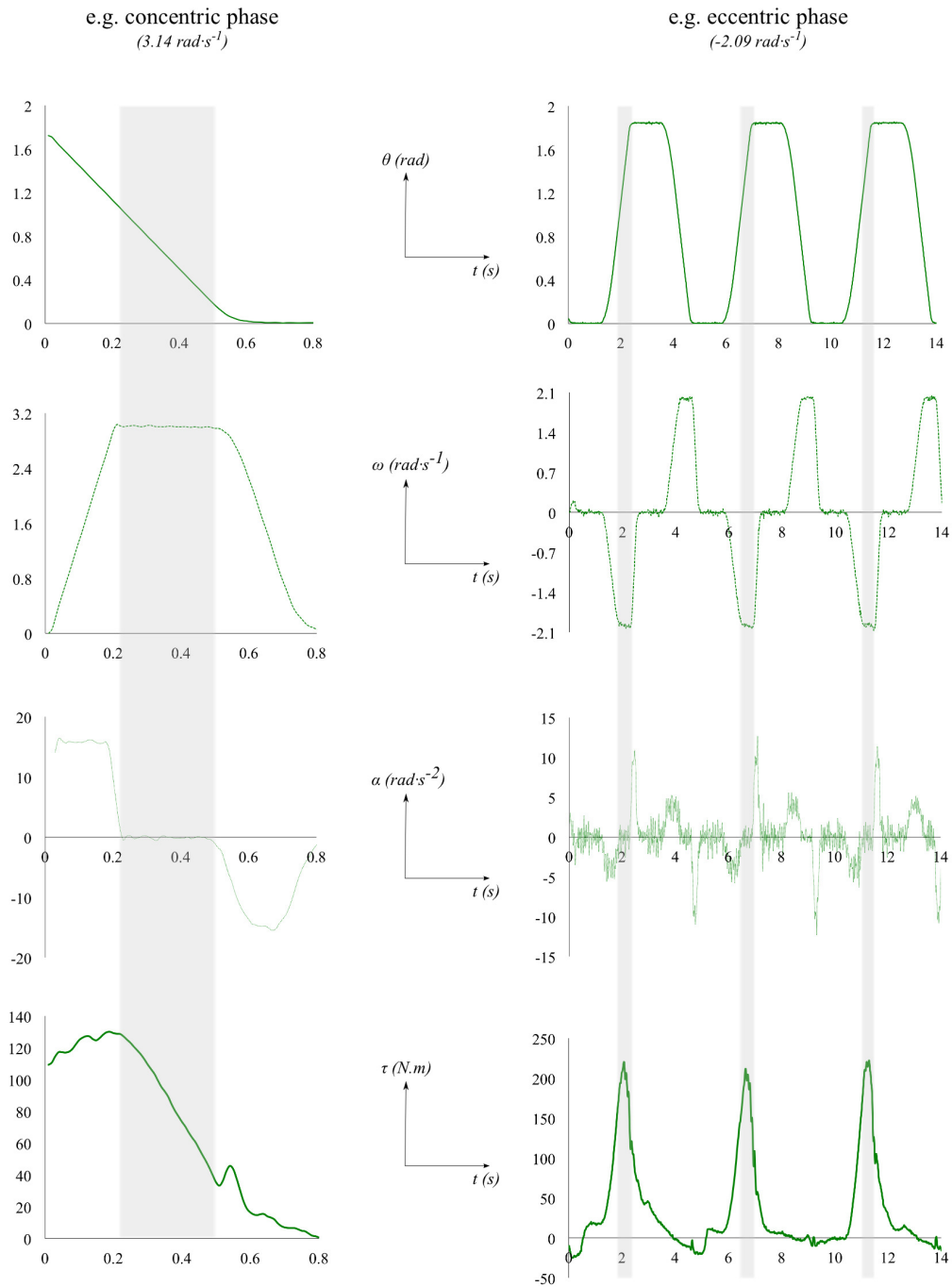


Figure 2.6: Knee joint example data from the dynamometer during testing. Concentric and eccentric sample data are shown in the left and in the right side, respectively. Shaded areas represent the isovelocity portion. Light lines are the first and the second derivate of the position in time.

2.1.3 Ankle joint testing

Standing upright, the foot flat on the floor and perpendicular to the shank the anterior ankle joint angle was 90° which represented the 0° angle during testing. The participant was seated on the dynamometer with the trunk free to move, but he was strapped firmly to the dynamometer at the feet, to reduce unwanted movements. The knee joint was extended for each trial, with full knee extension represented by an angle of 180° (Fig. 2.7). The protocol involved maximal isometric trials at six knee angles spanning the full range of motion (70°), and maximal isovelocity trials for concentric MVC at 0; 30; 60; 120; 150 ($deg \cdot s^{-1}$) and, for eccentric MVC at at -60; -120; -150 ($deg \cdot s^{-1}$) velocities. During the isometric trials, the participant was encouraged to exert a MVC by ramping up from a relaxed state to maximal effort. As consequence of hard velcro straps applied around the foot, the subject was allowed to stop the session and have a rest if the foot was too painful during trials. The isovelocity portions of the central eccentric-concentric phase of each trial were identified by manually inspecting the joint velocity time history as for the hip and knee joints. Data files were edited to leave just these portions (Fig. 2.8). For each trial the maximal value point by point was considered.

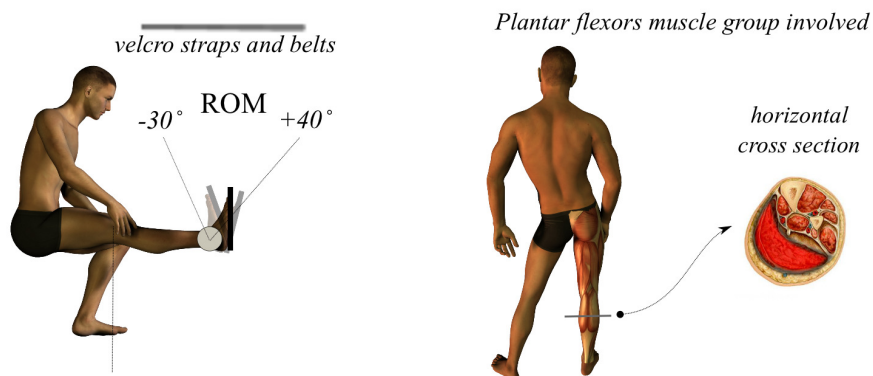


Figure 2.7: Ankle joint Biodex test angle definition. The subject position is shown in the left side. The right side highlighted muscle groups involved. Since the knee was fully extended, the gastrocnemius was strongly involved.

2. Experimental measurements

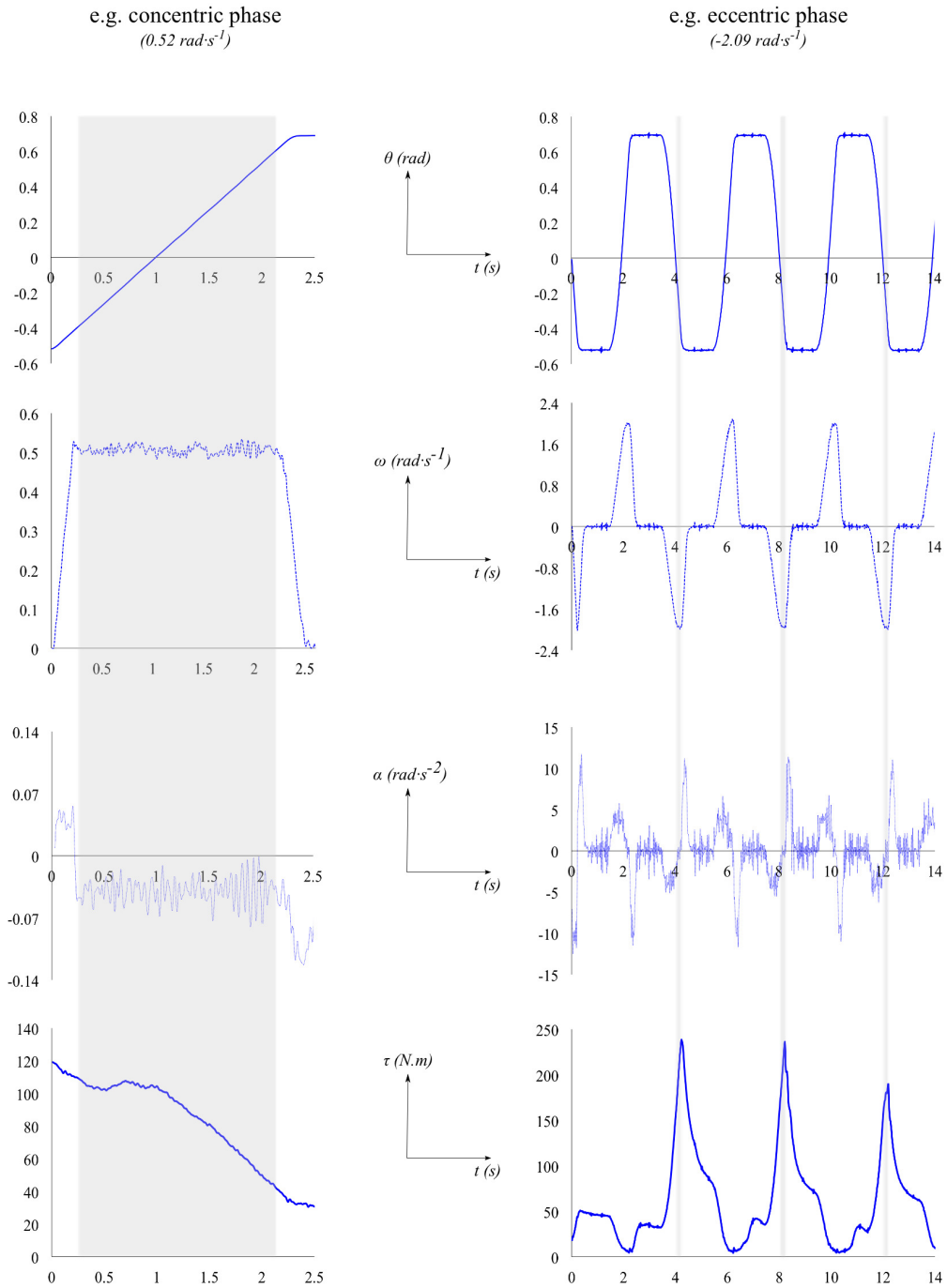


Figure 2.8: Ankle joint example data from the dynamometer during testing. Concentric and eccentric sample data are shown in the left and in the right side, respectively. Shaded areas represent the isovelocity portion. Light lines are the first and the second derivate of the position in time.

2.1.4 Dynamometer data processing

Analog torque signals were processed by using Biopac© system and then on-line filtering with a 30Hz low-pass Butterworth 4th filter by the means of AcqKnowledge software®. Angle signals were filtered on-line by using a 35Hz low-pass butter worth 4th filter. Subsequently, Excel® and Matlab® softwares were used for the final processing.

2.1.4.1 Correction of crank joint angle

As explained in the Chapter 1, section 1.2.4 the crank dynamometer-recorded angle and the actual joint angle differences are due to the way subject's limb is attached to the crank arm, to different percentage levels of the maximum actual joint moment, to dynamometer seat materials, etc. [10; 80]. In order to reduce these errors, an electronic goniometer was used to measure hip and knee joint angles during maximal MVC isometric test sessions for each given angle. The mean value of all trials for each given angle was then considered and, a suitable quadratic polynomial regression line (Eq: 2.1 - 2.2) was used to fit the data relating joint angles to crank angles (Fig. 2.9). Subsequently, it was assumed angle differences were similar for any isovelocity maximal MVC, eccentric and concentric data were scaled based on this linear regression analysis.

$$y_h = -0.0031x^2 + 1.5604x - 9.3697 \quad (2.1)$$

$$y_k = -0.0071x^2 + 2.7996x - 89.267 \quad (2.2)$$

Where x is the crank dynamometer-measured angle, y_h is the calculated hip joint angle and y_k is the calculated knee joint angle.

For technical reasons, it was not possible to attach the electronic goniometer at the ankle joint during testing, thus any angle correction was calculated to the ankle joint. However, the ankle support of the dynamometer was rigid and the foot firmly attached. Thus, similarity between the measured crank joint angle and the joint angle was assumed.

2. Experimental measurements

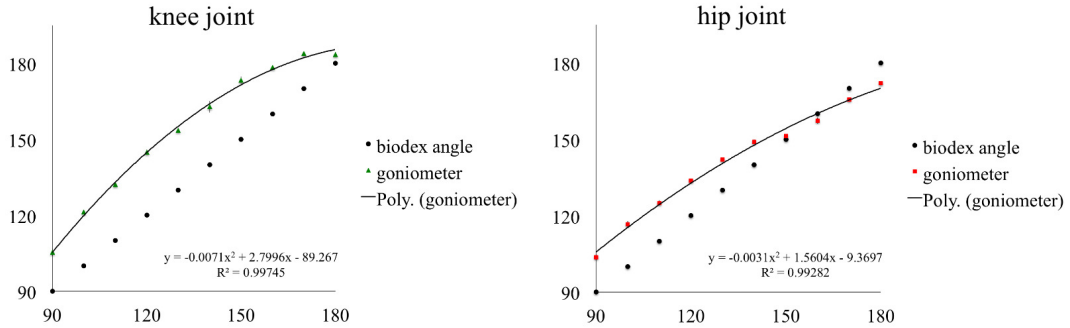


Figure 2.9: Correction of crank joint angle considering goniometer data vs. biodes angle.

2.1.4.2 Correction of torque-measuring dynamometer

As reviewed in the Chapter 1, a number of potential sources of error should be taken into account when we measure joint strength characteristics using a dynamometer. Errors include passive, active and inertial components [10].

Passive torques including the effect of gravity should be correctly identified, as well as passive torques related to the elastic properties of the soft tissues which may change throughout the range according to the configuration of the joint. Passive torques can be simply removed from torque measurements by taking measurements of the passive torques throughout the joint range and subsequently removing them (Fig. 2.10) to leave only the torques related to the active torque exerting contractile components [70]. For this, measurement the subject is asked to be passive and relaxed on the dynamometer.

Further, by selecting data only during isovelocity periods (Fig. 2.10 the middle chart), torques associated with the acceleration of the crank arm, its attachments and the limbs can be avoided [10] and also reduce the errors associated when the crank arm typically overshoots (Fig. 2.10 right side of the bottom chart) the preset velocity at the end of the acceleration phase of crank arm motion [64]. In summary, final resulting net torques are taken into account with errors reduced as much as possible for position, gravity and isovelocity components.

2. Experimental measurements

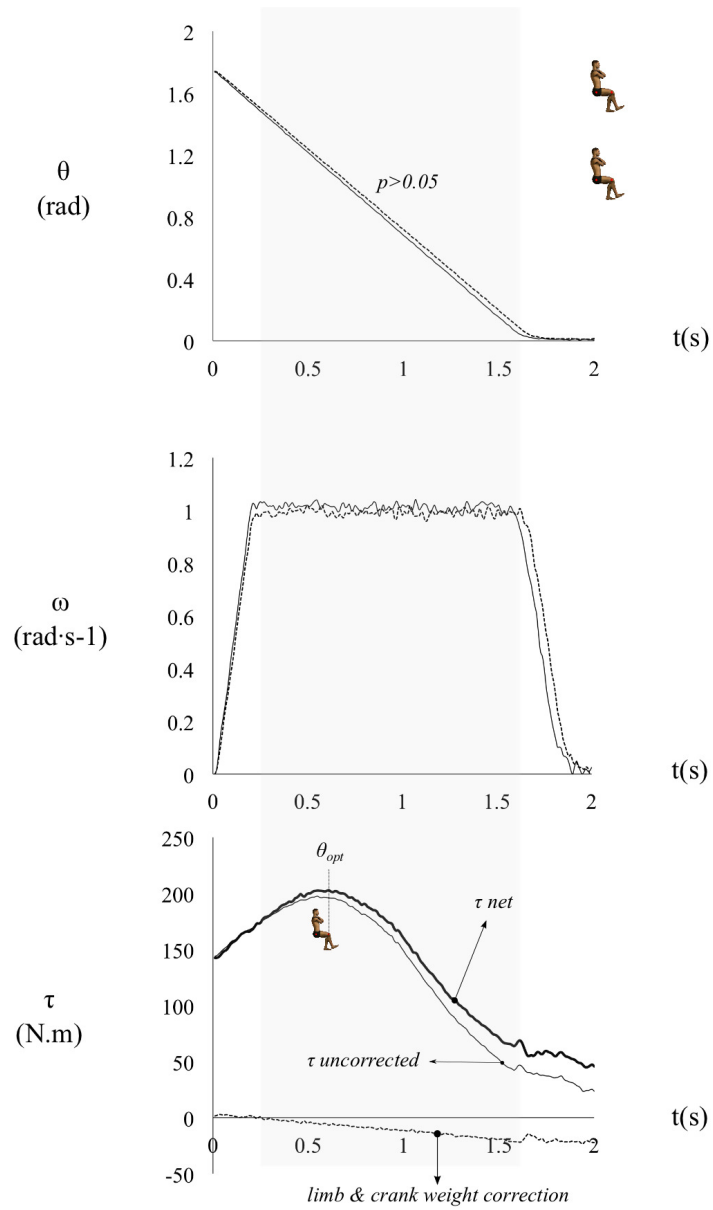


Figure 2.10: Biodex© signal processing (e.g. concentric knee joint test). The central chart helps to identify the isovelocity portion. The chart at the bottom of the figure shows the gravity and leg weight torque corrections.

2.2 Results of torque-measuring dynamometer

A common result for all joint measurements, a parabolic shape curve was obtained for each isometric concentric tested isovelocity. Probably, because of a natural and comfortable position, the knee joint data gave the best shape in relation to the tension-length theoretical model.

2.2.1 Hip joint results

Hip joint isometric peak torque was 195.2N.m and the ratio between the maximal eccentric value and the maximal isometric value measured at 1.74rad was 1.15. The concentric part showed similarity with the tension-velocity relationship theoretical model. A plateau was found for the eccentric velocities and isometric values well represented the tension-length theoretical model. Complete data are shown in Table 2.1, whilst a spatial 3D representation of the hip joint torque model is presented in Figure 2.11.

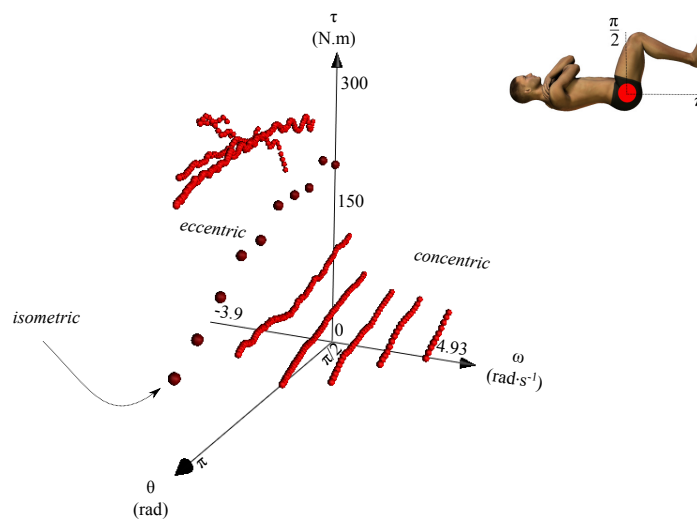


Figure 2.11: Red points are experimental data obtained from the hip joint dynamometer test. Only the isovelocity portion throughout the ROM was considered. The image at top right side helps to read the chart axes.

2. Experimental measurements

Table 2.1: Hip joint torque experimental data for each isovelocity test.

Isovelocity		max τ (N.m)	mean $\pm\sigma$ τ (N.m)	min τ (N.m)
$deg \cdot s^{-1}$	$rad \cdot s^{-1}$			
-225.3	-3.93	234.6	226.0 ± 12.7	193.2
-170.4	-2.97	238.8	220.5 ± 11.7	202.2
-113.6	-1.98	218.4	207.2 ± 8.8	180.0
-56.6	-0.99	236.4	212.2 ± 15.4	180.0
0	0	195.2	143.9 ± 42.5	70.3
57.8	1.01	123.8	96.9 ± 13.2	79.7
114.8	2.00	172.6	78.4 ± 11.4	57.9
171.5	2.99	170.2	72.0 ± 7.6	56.3
227.6	3.97	85.8	77.2 ± 6.1	65.8
282.7	4.93	81.1	73.7 ± 4.7	66.7

2.2.2 Knee joint results

Experimental data of the knee joint showed the higher isometric value between all joints tested (227.3N.m). The factor of 1.36 was the ratio between the maximal eccentric and the maximal isometric torques measured at 1.93rad. Tension-length and tension-velocity relationships were well represented by experimental data. Table 2.2 presents all data and Figure 2.12 shows data over three axes x, y, z.

2.2.3 Ankle joint results

An isometric peak torque of 84.3N.m was found for the right plantar flexors muscle group. The concentric part showed similarity with the tension-velocity relationship of the theoretical model (Fig. 2.13). A plateau was found for the eccentric velocities and isometric values well represented the tension-length theoretical model. However, a high ratio value of 2.14 set the ratio between the max eccentric torque and max isometric torque measured at -0.17rad. Data are shown in Table 2.3.

2. Experimental measurements

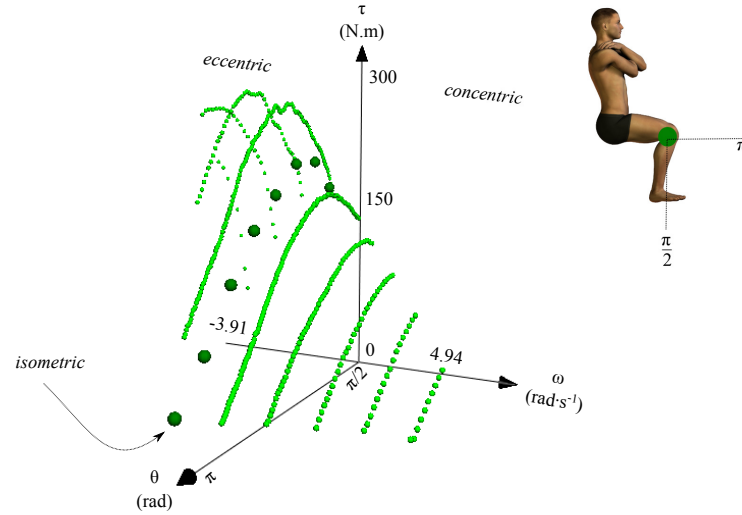


Figure 2.12: Knee extensor experimental data. Green points are experimental data obtained from the knee extension dynamometer test. Only the isovelocity portion throughout the ROM was considered. The image at top right side helps to read the chart axes.

Table 2.2: Knee joint torque experimental data for each isovelocity test.

Isovelocity		max τ (N.m)	mean $\pm\sigma$ τ (N.m)	min τ (N.m)
$\text{deg}\cdot\text{s}^{-1}$	$\text{rad}\cdot\text{s}^{-1}$			
-224.3	-3.91	224.4	165.0 ± 55.0	76.3
-169.6	-2.96	279.5	243.7 ± 43.4	137.2
-113.3	-1.98	294.9	255.4 ± 32.2	186.4
-56.6	-0.99	283.4	216.3 ± 58.0	92.2
0	0	227.3	162.1 ± 66.3	50.2
57.9	1.01	200.3	147.0 ± 48.9	49.8
115.2	2.01	159.8	118.5 ± 34.3	53.3
172.1	3.00	134.9	101.0 ± 26.3	52.5
228.4	3.99	111.6	84.2 ± 19.0	54.6
283.1	4.94	109.6	75.9 ± 17.6	51.3

2. Experimental measurements

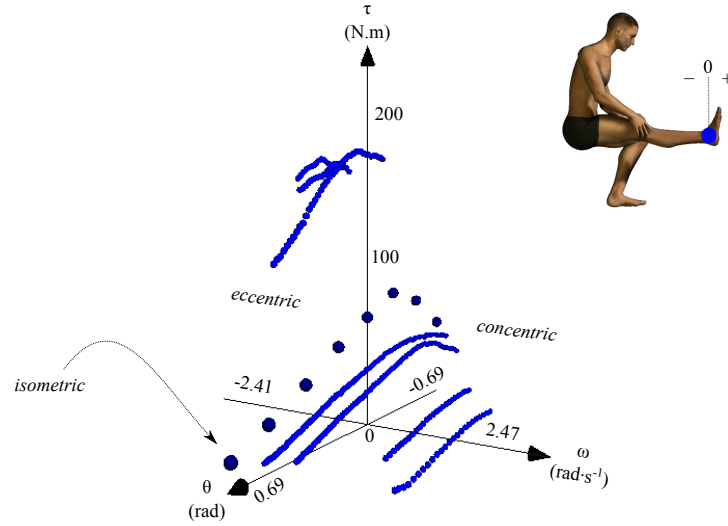


Figure 2.13: Ankle plantar flexors experimental data. Here, blue points are experimental data obtained from the ankle joint dynamometer test. Only the isovelocity portion throughout the ROM was considered. The image at top right side helps to read the chart axes.

Table 2.3: Ankle joint torque experimental data for each isovelocity test.

Isovelocity		max τ (N.m)	mean $\pm \sigma$ τ (N.m)	min τ (N.m)
$deg \cdot s^{-1}$	$rad \cdot s^{-1}$			
-138	-2.41	181.1	175.1 ± 4.9	165.1
-111	-1.94	176.8	168.6 ± 6.5	156.4
-60	-1.04	184.8	159.2 ± 25.3	109.6
-30	-0.52	155.1	109.6 ± 28.7	60.4
0	0	84.3	53.4 ± 24.0	15.6
30.6	0.53	55.1	41.4 ± 12.7	17.7
57.4	1.00	56.0	42.7 ± 10.5	20.5
114.4	2.00	32.8	27.9 ± 4.1	20.3
141.5	2.47	23.6	19.14.0	12.8

2.2.4 Ankle joint correction

The participant performed the ankle test using the dynamometer at his best effort. However, results suggest that the exerted torque could be much more than the measured one. Actually, data from literature about mean maximum isometric ankle torque are greater [29; 30; 81]. Probably, the position assumed during testing or the unusual movement of the ankle joint against a resistance were responsible for a lower torque production. In order to test this hypothesis another functional test was performed. A force plate was used for this purpose, the subject was asked to perform a maximal isometric contraction against a fixed bar in standing position. This test was performed at 4 different angles and three trials for each given angle were recorded (Table 2.4). The best value for each angle was then considered. A ratio of 3.58 between these four points and values obtained from the isometric dynamometer measurements at the same angles was used to scale the ankle joint original torque. The maximum torque at 10 deg became 208N.m for one leg.

Angle (deg)	GRF (N)	Lever arm (m)	Torque (N.m)	Torque (Biodex©) (N.m)	Ratio (N.m)
-15	1406	0.127	178.6	84.3	2.1
0	2206	0.131	289	72	4.0
20	1550	0.123	190.7	41.8	4.6
40	1525	0.100	152.5	27.2	5.6

Table 2.4: Data obtained from the experiment used to scale the original (dynamometer data) ankle joint torque model.

Another practical experiment was performed to be sure the subject was really able to produce a greater torque than the measured one at the dynamometer and the one calculated via force plate. Thus, the participant was asked to lift as much weight as possible by performing a calf exercise using an olympic barbell positioned on the shoulders. The subject was able to lift his heels with an extended knee (180 degrees) up to 210kg. Considering 63kg the mass of the subject, a lever arm of 0.14m (from the heel to the ball of the foot) a torque of 374.9N.m exerted for both legs was estimated at about 0 -10 degrees plantar flexion. This suggests

that results obtained from the force plate measurements were quite accurate and reliable.

In summary, the subsequent models of the ankle joint torque in this thesis were scaled by using a factor of 3.58 to best represent the strength capacity of the subject.

2.3 Kinematic, kinetic and EMG assessments during jumping experiments

A set of common strength exercises were chosen and analyzed. Therefore, the participant performed body weight squat jumps (SJbw), squat jumps with 25kg-50kg extra load which means the 40% and the 80% of the body weight (SJ25kg, SJ50kg).

Six Vicon© Cameras were used for motion tracking of five 25 mm retroreflective markers (Fig. 2.14). Vicon© cameras provide real-time and offline digital-optical motion capture data. Each camera has a strobe unit that emits flashes of near infrared light, illuminating retroreflective markers located at key locations on the subject (right temple, right great trochanter eminence, right side of the knee joint centre, right lateral malleolus, right ball of the foot). The camera then captures and electronically converts the pattern of reflected light from the markers into data that represents the position and radius of each marker in the image. Cameras were situated around the experimental area in order to cover 0.5m x 0.5m x 2.5m volume where vertical jumps were performed. Data were sampled at 120Hz. A static calibration was performed in order to define the global coordinate system in the capture volume using a calibration frame. Vicon© cameras were calibrated identifying focal length and orientation by the means of a dynamic calibration procedure.

Ground reaction force (GRF) measurements have been a valuable source of information in the study of human motion. Therefore, kinetic measurements were obtained by using a force platform (Kistler©), data were sampled at 960Hz. The force plate is a piece of equipment which has been used in jumping studies either on its own or in combination with other recording equipment. Here, the force

2. Experimental measurements

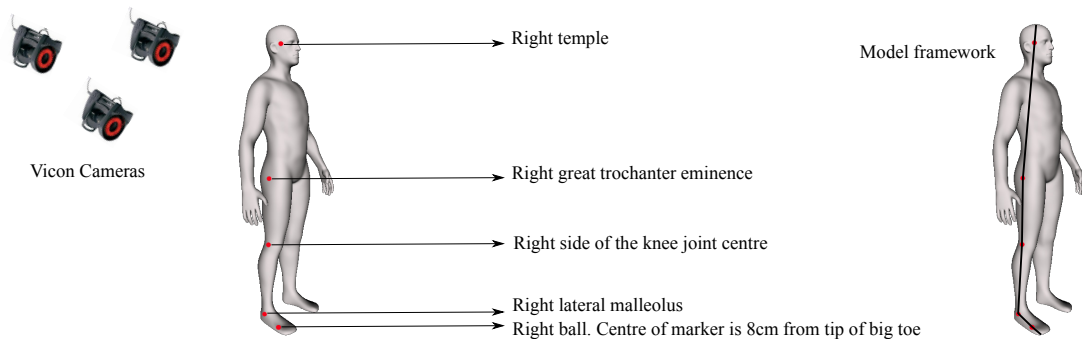


Figure 2.14: Marker positions, framework of the model obtained from the marker coordinates and example of Vicon© cameras used during the experiment.

plate was set to be synchronized with the other recording equipment: kinematic and surface EMG acquisition systems. Actually, if a subject makes a standing jump from a force plate, the data from the plate alone is sufficient to calculate acceleration, work, power output, jump angle, and jump distance using basic physics. However, simultaneous video measurements of leg joint angles and force plate output can allow the determination of torque, work and power at each joint using a method called inverse dynamics.

Surface EMG activity (SMART-BTS©, Milan, Italy) of the rectus femurs (RF), vastus lateralis (VL), Gluteus (GL), Biceps femurs long head (BF), tibialis anterior (TA), gastrocnemius medialis (GM) and soleus (SOL) was registered (Fig. 2.15). Data were sampled at 960Hz. The skin was shaved and cleaned with alcohol to ensure low resistance. The distance between each electrode was two centimeters and electrodes were placed over the muscle bellies. Figure 2.15 clarifies the position of sEMG electrodes as well the way that equipment was set on the body of the participant. The art design make visible muscle groups of the subject's right leg tested and an example of the standing position before performing an extra load squat jump trial.

Kinematic, kinetic and sEMG signals were synchronized and registered in order to obtain detailed information for each selected exercise to allow the whole analysis of the movement.

2. Experimental measurements

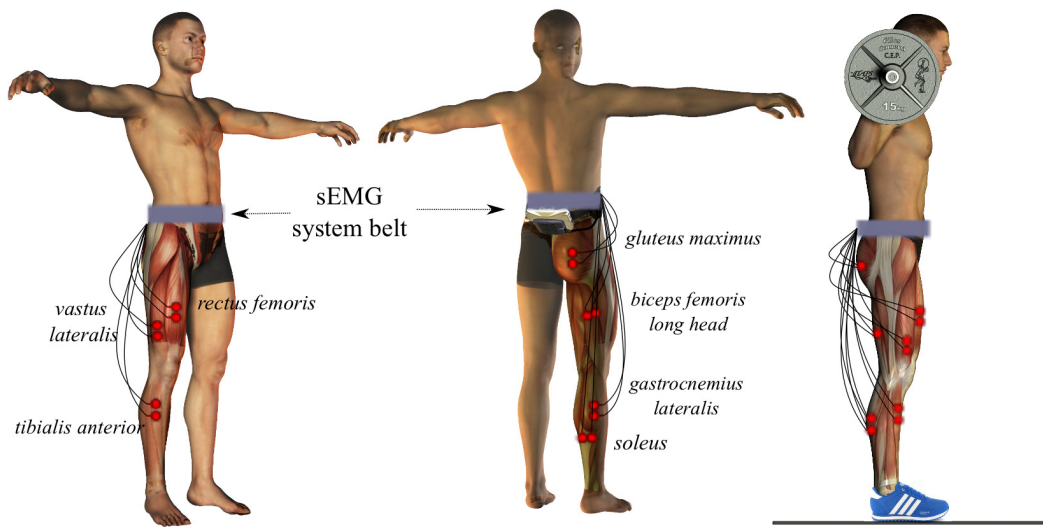


Figure 2.15: A comprehensive illustration of the experimental setup is shown. The participant wore a belt which contained the electronic wireless device to send to the computer sEMG signals coming from each electrode. The right side was chosen to be assessed and the subject was allowed to wear shoes. The right hand side of the figure shows the experiment configuration. This example shows the athlete ready to perform trials with extra load before to setting himself in the squat jump start position. In the left side and centre of the figure, the muscle art design of the right leg help the understanding of the electrode locations for assessing the surface electromyography signals.

2.3.1 Procedures: squat jump and 1RM experimental trials

The subject was asked to perform 10 vertical SJbw, 6 vertical SJ25kg and 6 vertical SJ50kg (no guide bar). The aim was to reach the maximal vertical jump height in each trial for each condition. It was decided to exclude the intervention of the arms during the jump because the goal was to focus only on the neuromuscular capacity of the subject without involving arm coordination assistance. Yet, attempting to focus all the activity in lower limbs was a priority for this thesis. Thus, hands placed at the hip and knee angle flexed at about 90 degrees were the given instructions for the start position. From that posture a purely concentric action was asked to be performed by the subject. However, if the trial required extra load, tests began with the shoulders in contact with the barbell from a full knee extended position. Subsequently, the participant lowered down under control to the position (knee flexed at about 90 degrees) hands still firmly kept the barbell on the shoulders and a maximal jump effort was required to make the test close to the real half squat jump exercise performed during training workouts.

A total of 22 trials randomized (including all conditions) was performed. After each trial the subject had at least 1 minute rest, or if he felt affected by fatigue a rest up to 3 minutes was allowed to recover neuromuscular capacities. The whole experiment was then performed on the same day in about 2 hours including instructions, setting up of equipment and mock trials.

For any condition, if the subject clearly jumped submaximally or lost equilibrium during the jump, the trial was not considered, then it was repeated. Before starting the experiment a few submaximal jumps were performed to ensure that any devices set on the body of the participant (EMG electrodes, markers, etc.) did not make the subject uncomfortable during the experiment.

Finally, a general rule was applied for analyzing data, all squat jump trials that showed a slightly countermovement at the beginning of the movement were not considered. Therefore, if at the beginning of the propulsive phase, vertical GRF decreased by more than 10% of the GRF peak of the jump, then the trial was not considered. Subsequently, from 22 SJ trials including all conditions valid jumps were taken into account and only the best jump for each condition in relation

2. Experimental measurements

to the jump height output was selected and fully analyzed.

Finally, 1 Repetition Maximal (RM) half squat test was also performed without recording data, except the maximal load successfully lift. The participant was able to lift up to 145kg extra load, whilst the trial with 150kg failed. Trials started from 125kg to be increased by 10kg each attempt taking advantage from a 7 minutes rest between attempts. Thus, an estimated 1RM ranging between 145kg - 155kg was considered to be the load that the subject could lift for only one repetition.

2.3.2 Experimental squat jump results

A total of three jumps were analyzed which meant the best jump for each condition: SJbw, SJ+25kg, SJ+50kg. As expected the heavier the total mass, the lower the jump height, 2.164m/s, 1.791m/s and 1.433m/s were the COM velocity at instant of the toe-off reached for SJbw, SJ+25kg and SJ+50kg, respectively (Fig. 2.16). This gave a calculated jump height of 23.9cm (SJbw), 16.3cm (SJ25kg) and 10.4cm (SJ+50kg). Thus, the jump performed with 50kg extra load produced a height jump of 43.5% of the jump height reached without any extra load. This, suggests that a small load in relation to the half squat 1RM of the subject (145kg-150kg) has a crucial impact on the capacity to accelerate the COM of the body.

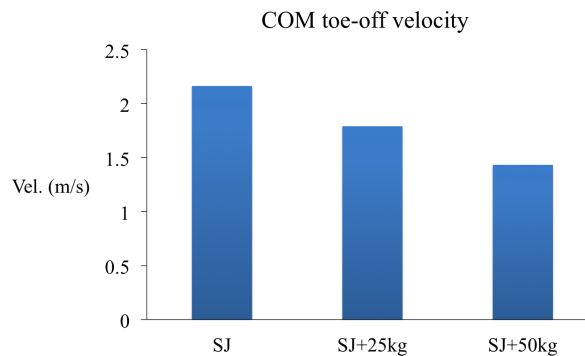


Figure 2.16: Maximal achievement in terms of COM toe-off velocity for each experimental condition.

2. Experimental measurements

Considering the nature of these three different jump conditions, the higher peak GRF was recorded for SJ+50kg (1797 N), followed by the SJ+25kg (1674 N) and the SJbw (1450 N). In addition, the lower the load, the shorter the time to reach the GRF peak (Fig. 2.17). GRF and velocity of the COM of the body are quite important if we are interested on the global peak power of the jump. Neuromuscular capacity to produce muscle tension as fast as possible determine the power output. Electromyography assessment gave data useful to obtain quali-

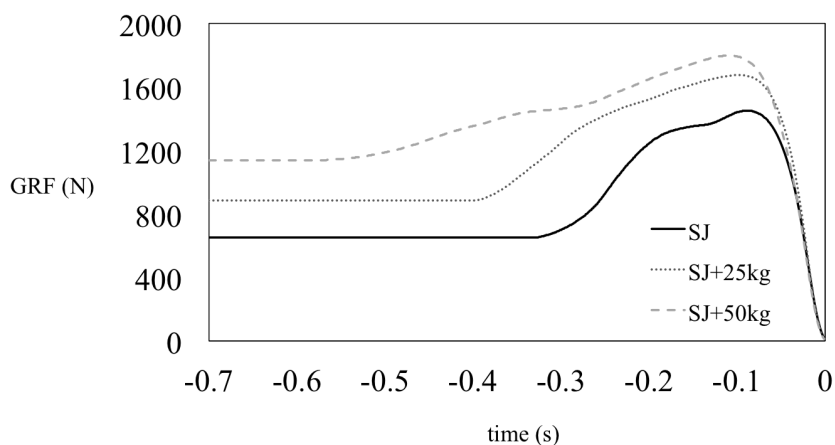


Figure 2.17: Vertical ground reaction forces recorder for the best jump (jump height) for each condition (SJ, SJ+25kg, SJ+50kg), synchronized at the toe-off. Peak GRF was reached at 0.109s, 0.098s, 0.089s from SJ+50kg, SJ+25kg, SJ, respectively. Value 0 for the abscissa represents the instant of the toe-off.

tatively information about muscle activation patterns (Figure 2.20). Figure 2.18 shows rectified sEMG of the SJbw best trial. The timeline represents 0.6s before the toe-off and a progressive increase or decrease activation is highlighted for all tested muscles. Figure 2.19 shows when recorded muscles reached the sEMG peak (rms) during the jump. For almost all conditions the peak occurred around the 50% of the propulsive phase. Peak values are reports in Table 2.5. Table 2.6 reports best squat jumps kinematic data, Table 2.7 describes kinematic characteristics in two separate instants: start of the propulsive phase, toe-off.

2. Experimental measurements

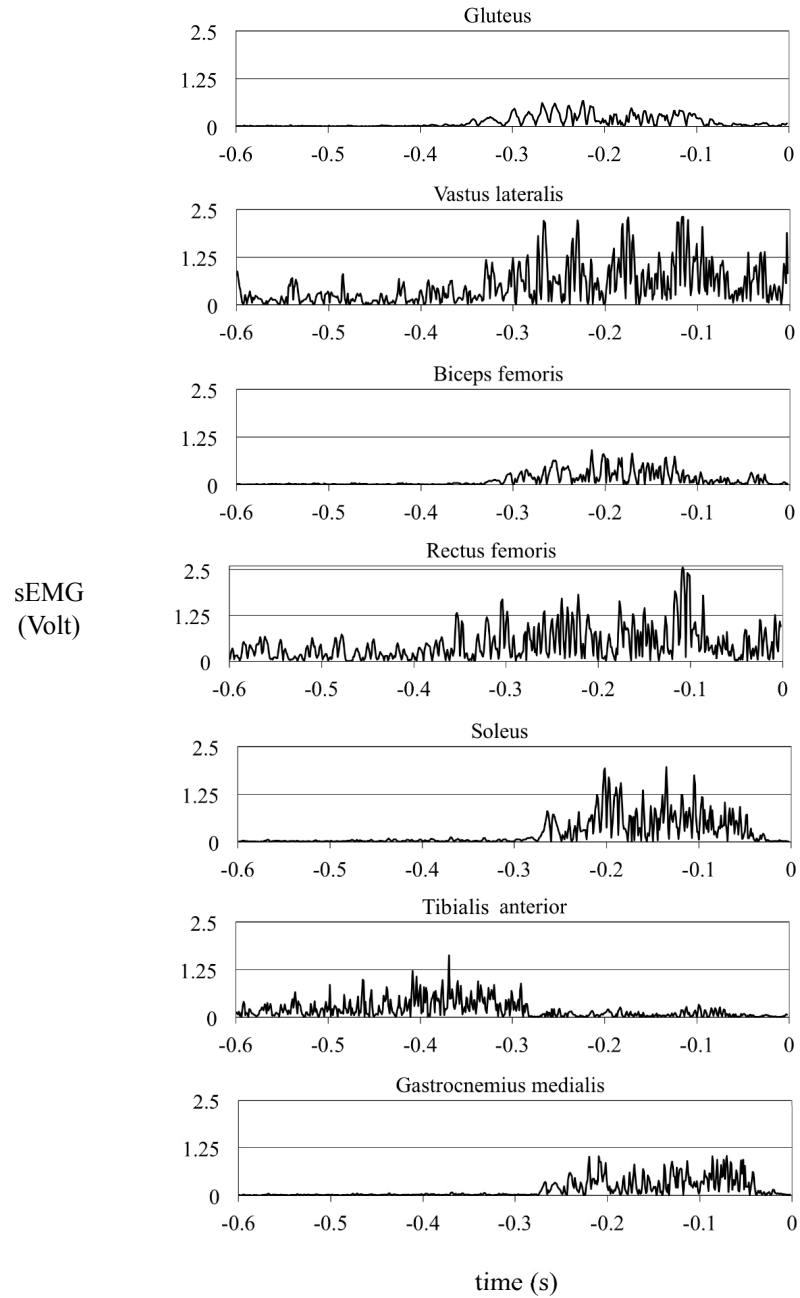


Figure 2.18: Squat Jump bandpass (10-400Hz) rectified sEMG data example. Charts show the last 600ms before the instant of the toe-off. The start of the propulsive phase occurred at -0.334s from the toe-off (0s). Main monoarticular and biarticular muscles were investigated.

2. Experimental measurements

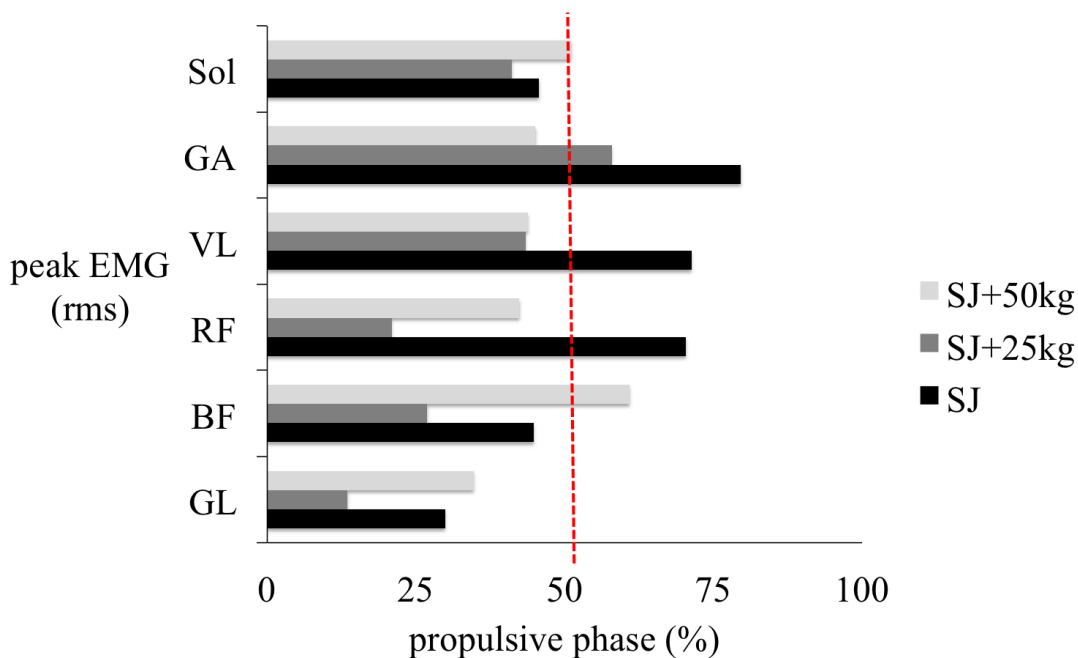


Figure 2.19: Peak EMG (rms) with respect to time expressed as percentage of the propulsive phase. The toe-off instant is 100%. This simple analysis suggests that if one wants to model the active state of muscles, it has to be considered to allow to reach the maximal activation by the half propulsive phase of the jump for all conditions. Otherwise, a simulation model could give as result a low jump height performance, since the magnitude of the activation would not be enough to reproduce a jump. Further, it seems there is a tendency which show that squat jumps with extra load need a shorter the time to reach the activation peak.

	SJ	SJ+25kg	SJ+50kg
muscle	(mV)	(mV)	(mV)
GL	0.39	0.60	0.26
BF	0.45	0.55	0.28
RF	1.25	1.08	0.74
VL	1.24	1.26	0.64
GA	0.56	0.54	0.29
SOL	0.93	0.70	0.50

Table 2.5: sEMG (rms) peak values. RMS was calculated over a window of 50ms. GL=gluteus; BF=biceps femoris; RF=rectus femoris; VL=vastus lateralis; GA=gastrocnemius medialis; SOL= soleus.

2. Experimental measurements

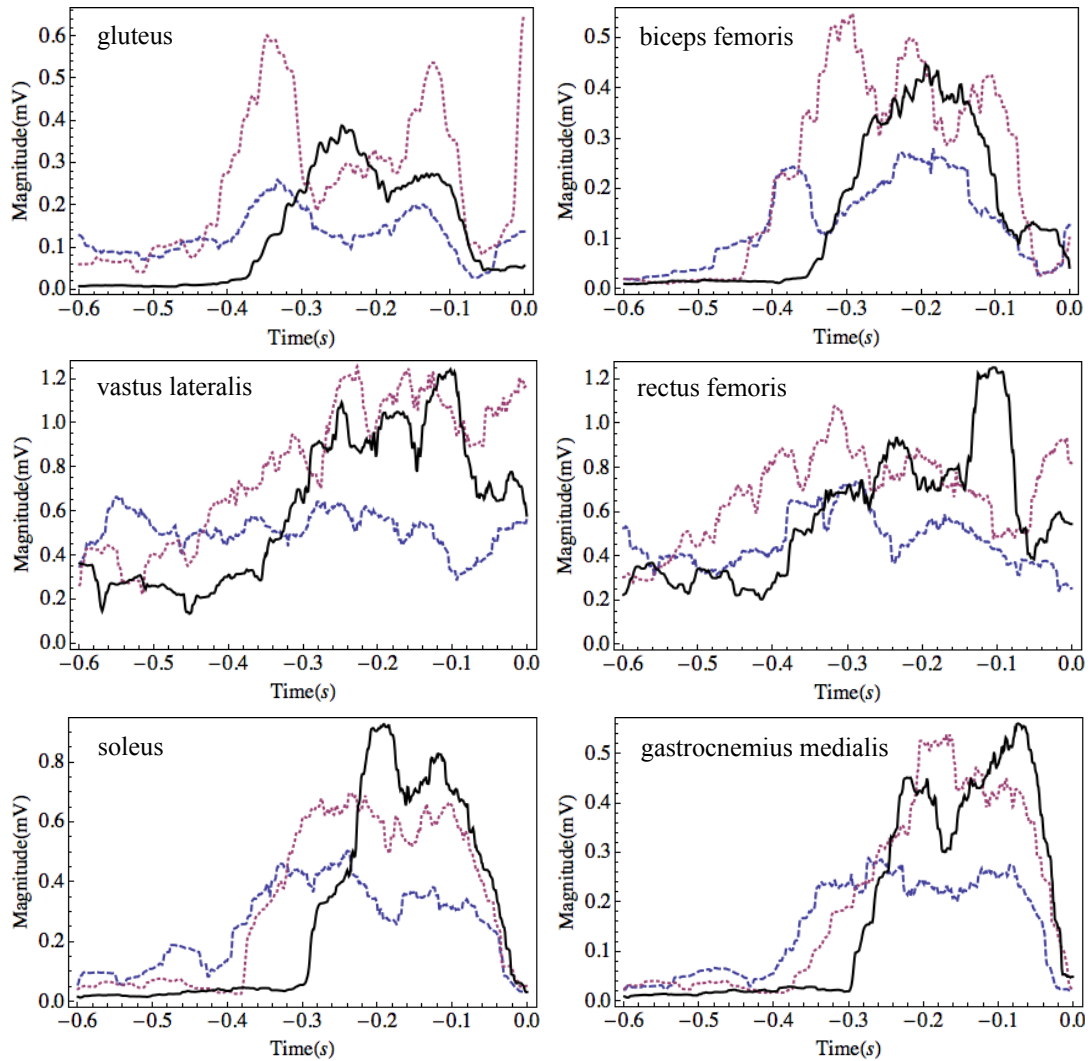


Figure 2.20: Surface EMG (rms). Signal was sampled at 960Hz and Band-Pass filtered (10-400Hz). RMS was calculated over a window of 50ms. Signals are synchronized at the toe-off. Abscissa represent time to toe-off. Solid line=SJ; shaded line=SJ+25kg; dotted line=SJ+50kg. Monoarticular muscles are on the left side, whilst biarticular muscles are in the right side.

2. Experimental measurements

Kinematic results are reported in Figure 2.21, three squat jump trials are shown as example. The same analysis was done for all conditions (SJ, SJ+25kg, SJ+50kg). In the Figure 2.21, trial 3 represents the best squat jump in terms of jump height. Kinematic analysis underpin matching simulation framework: angular and angular velocity time history were used to minimize differences between actual and simulated performance. The angular velocity time history shows a particular feature of the movement. For each joint, angular velocity increases starting from the beginning of the propulsive phase to reach a peak before the toe-off instant. Actually, velocity roughly slows down after the peak. Probably, this is because antagonist muscles activate to brake joint movements avoiding to violate anatomical constraints and in addition a neural inhibition could occur to reduce the force produced [88].

	Toe-off COM ω ($rad \cdot s^{-1}$)	COM height (m)	GRF _{peak} (N)	Fly _t (s)	Push-off _{phase} (s)
SJ	0.038	0.239	1450	0.441	0.334
SJ+25kg	0.031	0.163	1674	0.365	0.401
SJ+50kg	0.025	0.104	1797	0.292	0.568

Table 2.6: Kinetic and jump height characteristics of the best jump for each given condition (SJ,SJ+25kg,SJ+50kg).

	Start θ (rad)			Toe-off θ (rad)			Toe-off ω ($rad \cdot s^{-1}$)		
	θ_h	θ_k	θ_a	θ_h	θ_k	θ_a	ω_h	ω_k	ω_a
SJ	1.58	1.55	-0.49	2.95	3.05	0.60	0.042	0.042	0.037
SJ+25kg	1.73	1.61	-0.48	2.93	3.01	0.56	0.036	0.036	0.031
SJ+50kg	1.74	1.51	-0.53	2.94	3.06	0.58	0.028	0.028	0.025

Table 2.7: Kinematic characteristics of the best jump for each given condition (SJ,SJ+25kg,SJ+50kg) at the start and at the toe-off instant of the jump.

2. Experimental measurements

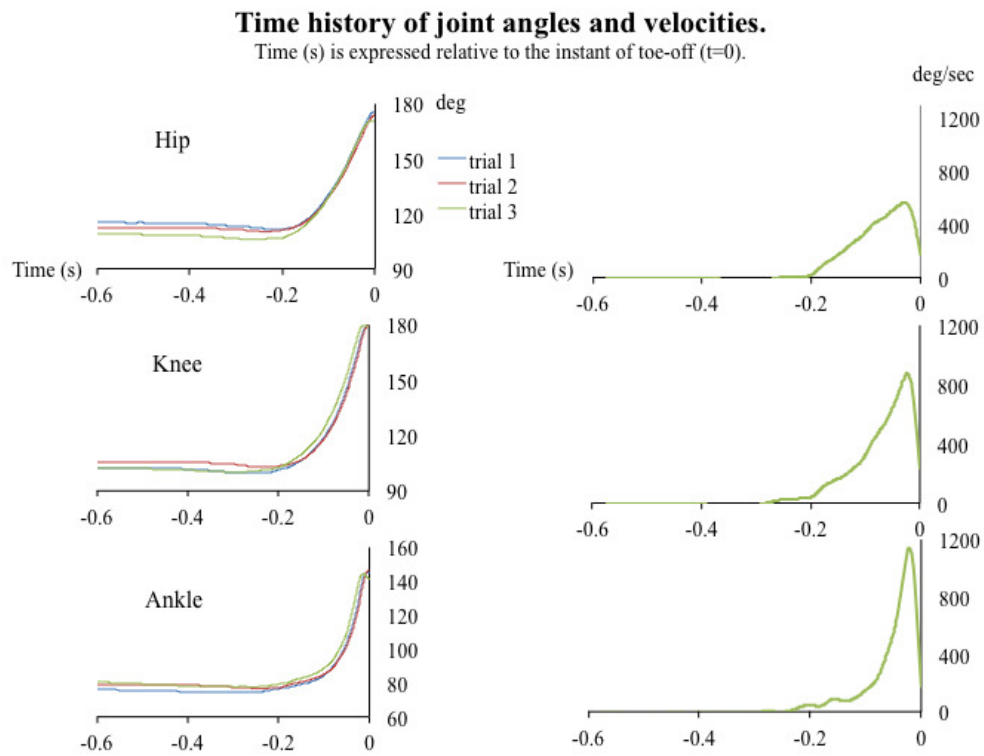


Figure 2.21: Squat jump joint angles and angular velocities time history. In the left side, angles time history of three squat jump trials are reported. Trial 3 is the best squat jump in terms of jump height and it was used as reference for the matching simulation. The right side of the figure shows angular velocities of the best trial for each joint.

2.4 Summary

This Chapter presented experimental data collected using the dynamometer to obtain torque measurements for the hip, knee and ankle joint. Further, kinetic and kinematic data were collected using a force plate and a camera system to obtain objective informations about squat jump performance (body weight and extra loaded). Surface EMG was also recorded a synchronized with kinetic and kinematic data during squat jump trials with and without extra load. The participant also performed the 1RM back half squat test. The maximal extra load that the subject was able to lift was considered the 1RM.

These data will be the base for creating models. Modelling part, is the topic of the next Chapter.

Chapter 3

Development of the jumping model

3.1 Whole-body 4 link rigid segment model

Human body was assumed to be constituted of rigid segments. Therefore, a two dimensional planar 4 link-rigid 3-actuator model, representing a subject-specific human body was built. The 4 link rigid segment model was based upon one healthy male subject (29yrs, 63kg, 1.74m). Subject characteristics are reported in Table 3.1. Segments model were linked by rotational joints, their position in

Table 3.1: Subject characteristics.

	Subject
Gender	male
Race	caucasian
Age (yrs)	29
Height (m)	1.74
Mass (kg)	63
Weight (N)	618
Sport	kickboxing

space were estimated by positional markers used during video-based kinematic analysis (Chapter 2 section 2.3). Briefly, markers were placed at specific anatom-

3. Development of the jumping model

ical locations in order to create custom-made segments in relation to the actual length. Upper body anatomical parts were represented by using one single rigid segment, assuming head, trunk, arms, forearms and hands fused together. Symmetry between the right and left sides was also assumed, consequently thighs and shanks were represented by only two linked segments. Marker centres situated at right head temple and at about the right great trochanter gave parameters to create the length of the upper body segment. Thigh segment length was estimated from the distance between the marker centre located at about the right great trochanter and the marker centre located at about the centre of rotation of the knee joint. Marker centers situated at about the knee joint centre and at malleolus gave a distance to create the shank segment length. Finally, in order to represent close to reality, the flexion of the foot at the ball and the movement of the ankle joint, a simple foot model was provided. A curved polygon and one elastic standard component of WM2D called *flexbeam* (composed of 5 equal separate parts, FB01-FB05 see Tab. 3.4) were built. The curved polygon had a length estimated from the distance of the ball of the foot to the posterior side of the shoe, whilst the distance between the ball of the foot and the great toe gave the total flexbeam component length. These two parts of the foot model enabled multiple ground contact points at the toe, the metatarsal-phalangeal joint and the heel. A comprehensive technical shape of the planar whole-body 4 link segment model is presented in Figure 3.1, whilst its parameter definitions are reported in Table 3.2.

3.1.1 Foot-ground interface

A human like foot object was required for the ground contact model. During ground contact, a kinematic vertical slot joint constraint at the toe prevented the toe from sliding. The friction of *foot polygon*, *flexbeam* component and *force plate* were set at 1. Thus, the horizontal forces associated with friction between the ground and the foot were also assisted by the vertical slot joint constraint. Vertical contact reaction forces were obtained by the sum of all vertical forces of the objects which created the foot. This system allowed the flexion at the ball

3. Development of the jumping model

Table 3.2: Parameter definitions of the planar model.

Parameters	Definition
<i>mass</i>	
m_{ub}	mass of the upper body (head+trunk+arms+forearms+hands)
m_t	mass of the thighs
m_s	mass of the shanks
m_f	mass of the feet (feet+shoes)
<i>length</i>	
ubl	upper body length
tl	thighs length
sl	shanks length
hbl	foot polygon length
btl	flexbeam total length
fl	total foot length
<i>input</i>	
Th	torque production at hip joint
Tk	torque production at knee joint
Ta	torque production at ankle joint
<i>angles</i>	
θ_h	hip angle joint
θ_k	knee angle joint
θ_a	ankle angle joint

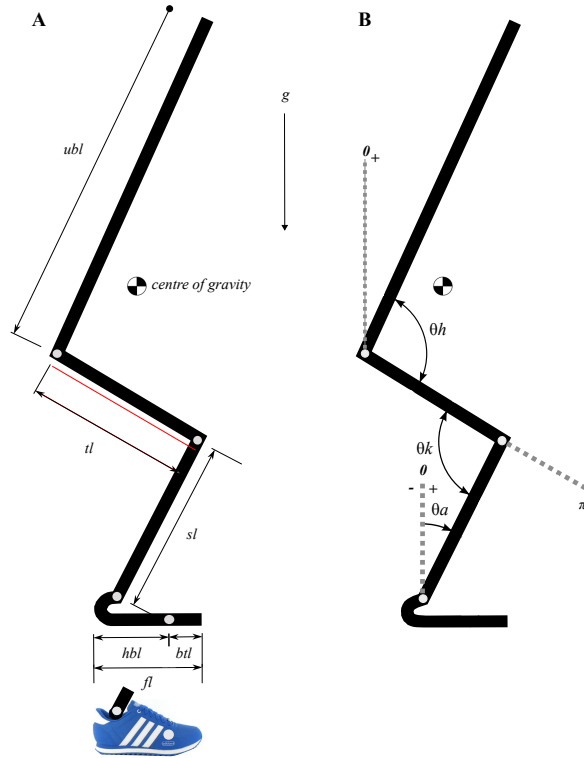


Figure 3.1: Technical model definition of the angles and segment lengths.

of the foot to vary depending on the rotational spring-damper that was set at an optimal value for running simulations at 60Hz. The spring k value was 1 and the damper b value was 0.1. Details of the foot-ground interface are shown in Figure 3.2.

3.1.2 Determination of subject-specific mass and centre of mass segments

A subset of the anthropometric measurements performed by a research group on six cadavers was selected and used [20]. This data set (Tab. 3.3), allowed to estimate, and then set up: 1) segment masses; 2) segment centre of mass positions, by assuming joint centres lay on the respective segment longitudinal axis. The weight of the shoes (0.7kg) was included in the final foot weight segment. By

3. Development of the jumping model



Figure 3.2: Detailed foot-ground interface of the model, which represent the feet of the subject. The five final segments linked by using springs allowed to better reproduce the natural movement of the foot during plantar flexion movement. The length of the foot segment was calculated measuring the length of the shoe used during the experiment. The vertical slot constraint attached at the toe was created to avoid sliding during the push-off phase of the jump.

3. Development of the jumping model

Table 3.3: Segment weight regression equations from Chandler et al. [20].

Segment	Weight (N)	COM location (%)	Prox. segment end
Head	$0.032 \cdot bw + 18.70$	66.3	Vertex
Trunk	$0.532 \cdot bw - 6.93$	52.2	C1
Upper arm	$0.022 \cdot bw + 4.76$	50.7	Shoulder joint
Forearm	$0.013 \cdot bw + 2.41$	41.7	Elbow joint
Hand	$0.005 \cdot bw + 0.75$	51.5	Wrist joint
Thigh	$0.127 \cdot bw - 14.82$	39.8	Hip joint
Shank	$0.044 \cdot bw - 1.75$	41.3	Knee joint
Foot	$0.009 \cdot bw + 2.48$	40	Heel

using the equations¹ reported in Table 3.3, it was possible to estimate the weight and the centre of mass positions of each segment of the 4 link rigid segment model. Subsequently, segment weight was calculated from segment weight. Weights for the model calculated from regression equations showed in Table 3.3, where ub is upper body, t_2 is thigh, s_2 is shank and f is foot segment:

$$\begin{aligned}
 ub = & [(0.032 \cdot 606.13 + 18.70) + (0.532 \cdot 606.13 - 6.93) \\
 & + 2 \cdot (0.022 \cdot 606.13 + 4.76) \\
 & + 2 \cdot (0.013 \cdot 606.13 + 2.41) \\
 & + 2 \cdot (0.005 \cdot 606.13 + 0.75)] = 417.96 \text{ N}
 \end{aligned} \tag{3.1}$$

$$t_2 = [2 \cdot (0.127 \cdot 606.13 - 14.82)] = 124.32 \text{ N} \tag{3.2}$$

$$s_2 = [2 \cdot (0.044 \cdot 606.13 - 1.75)] = 49.84 \text{ N} \tag{3.3}$$

$$f = [2 \cdot (0.009 \cdot 606.13 + 2.48)] = 20.31 \text{ N} \tag{3.4}$$

¹bw is the total body weight of the subject (606.13N)

3. Development of the jumping model

Table 3.4: Weight and mass of each model component. FB = flexbeam

	Weight (N)	Mass (kg)
Upper body	417.96	42.62
Thigh	124.32	12.68
Shank	49.84	5.08
Curved polygon	20.31	2.07
FB01	0.49	0.05
FB02	0.49	0.05
FB03	0.49	0.05
FB04	0.49	0.05
FB05	0.49	0.05

3.1.3 Subject-specific inertial data determination

Moment of inertia is the name given to rotational inertia, the rotational analog of mass for linear motion. It appears in the relationships for the dynamics of rotational motion. The moment of inertia must be specified with respect to a chosen axis of rotation. For a point mass the moment of inertia is just the mass (m) times the square of perpendicular distance to the rotation axis (r), in a system is the sum of the point mass moments of inertia (Eq. 3.5).

$$I = \sum_{i=1}^N m_i \cdot r_i^2. \quad (3.5)$$

where n indicates the number of elements in the system, m_i represents the mass of the i th element of the system, and r_i is the distance of the i th element from the axis of rotation. However, equation 3.5 is applied for systems that comprise few mass elements. For the whole human body or a human body segment, one way to determine the moment of inertia, is to use the pendulum method. It consists of suspending an object from a fixed point, setting it in motion by shifting it a few degrees from its resting position, and measuring, the time it takes to complete one period of oscillation. Equation 3.6 allow to calculate the moment of inertia

3. Development of the jumping model

about the suspension point:

$$I_0 = \frac{F_w \cdot h \cdot T^2}{4\pi^2} \quad (3.6)$$

where \mathbf{F}_w is the weight of the object, \mathbf{h} is the distance between the centre of mass and the suspension point and \mathbf{T}^2 is the period of one oscillation. The data set of the above section provided also mean values of body segments moments of inertia (somersault axis), measured using the pendulum method [20]. Data are shown in table 3.5. In summary, a video-based kinematic analysis during

Table 3.5: Segmental moment of inertia considering the somersault axis.

Segment	Somersault ($kg \cdot m^2$)
Head	0.0164
Trunk	1.0876
Upper arm	0.0133
Forearm	0.0065
Hand	0.0008
Thigh	0.1157
Shank	0.0392
Foot	0.003

Table 3.6: Whole-body 4 link rigid segment model parameters.

Model segment	Length (m)	Mass (kg)	COM location (offset from segment centre)	I ($kg \cdot m^2$)
Upper body	0.86	46.62	(x,y) 0, -0.08	1.1452
Shanks	0.42	5.08	(x,y) 0, 0.01	0.078
Thighs	0.39	12.67	(x,y) 0, 0.01	0.231
Foot with shoes	0.25	3.96	(x,y) 0.01, 0.065	0.006

vertical jumping and, a set of regression equations [20] gave all parameters to create a planar whole-body 4 link rigid segment model. Segment lengths was estimated by kinematic data, whilst regression equations gave inertial properties of each segment: mass, moment of inertia, centre of mass position (Tab. 3.6).

3.1.4 Barbell and plates inertial data determination

Moment of inertia of the olympic barbell and plates used during experiments (see Chapter 2) were calculated using the follow:

$$I = \frac{1}{2} \cdot m \cdot r^2 \quad (3.7)$$

Where m is the mass of the object and r is the radius of the object considering a 2 dimensional analysis. Details of the barbell and the plates are shown in Figure 3.3. Therefore, moment of inertia was calculated for the model using Equation 3.7. However, two plates of equal mass were added to the barbell. Considering a planar analysis the centre of mass of the whole object can be considered the centre of the object itself. The total moment of inertia (I_{tot}) was, therefore, the sum of each moment of inertia (barbell plus 2 plates):

$$I_{bar} = \frac{1}{2} \cdot m \cdot r^2 \quad (3.8)$$

$$I_{pla} = 2 \cdot \left[\frac{1}{2} \cdot (2 \cdot m) \cdot r^2 \right] \quad (3.9)$$

$$I_{tot} = I_{bar} + I_{pla} \quad (3.10)$$

Solving the above formulas for the 25kg (I_{25kg}) and for the 50kg (I_{50kg}) conditions (see Chapter 2) we have:

$$I_{bar} = \frac{1}{2} \cdot 20 \cdot 0.0025^2 = 0.0063 \text{ kg} \cdot \text{m}^2$$

$$I_{pla5kg} = \frac{1}{2} \cdot (2.5 + 2.5) \cdot 0.08^2 = 0.0160 \text{ kg} \cdot \text{m}^2$$

$$I_{pla30kg} = \frac{1}{2} \cdot (15 + 15) \cdot 0.17^2 = 0.4335 \text{ kg} \cdot \text{m}^2$$

3. Development of the jumping model

$$I_{25kg} = 0.0063 + 0.0160 = 0.0223kg \cdot m^2$$

$$I_{50kg} = 0.0063 + 0.4335 = 0.4398kg \cdot m^2$$

Table 3.7: Barbell and plates moment of inertia parameters.

	Mass (kg)	Weight (N)	I ($kg \cdot m^2$)
Barbell	0.86	46.62	0.006
Plate 2.5kg	0.42	5.08	0.008
Plate 15kg	0.39	12.67	0.217
Condition 25kg	0.25	3.96	0.022
Condition 50kg	0.25	3.96	0.440

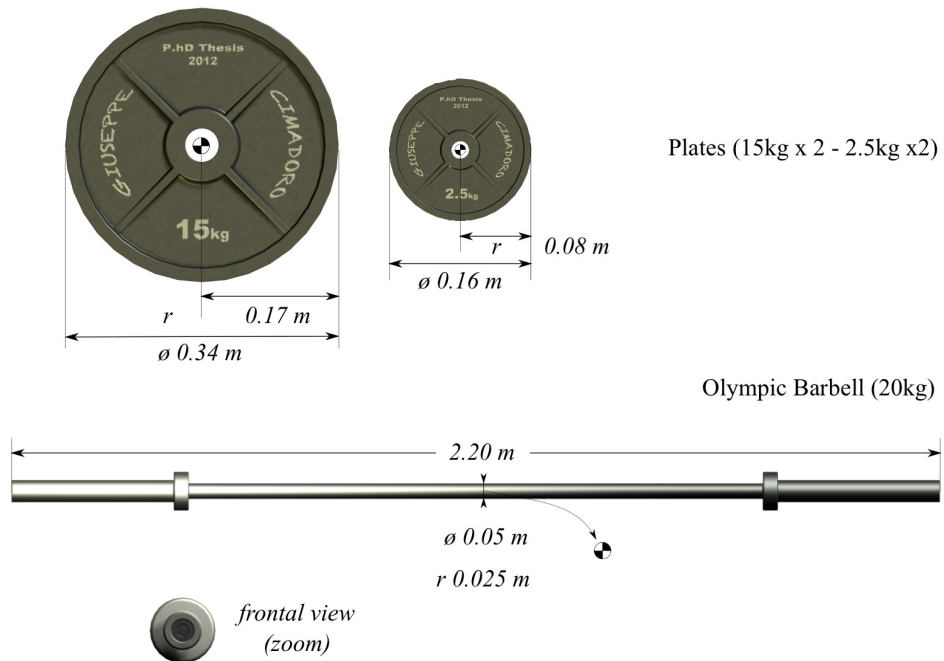


Figure 3.3: Olympic bar and plates measures used during the experiment.

3.2 Human muscle force modelling

Muscle force production is the most important input data for modelling, which will be implemented into simulation software package. A representation of muscle force, was described as resultant net torque at each considered joint. Torque models for hip, knee and ankle joints, therefore, were required to drive simulations. A *black box* approach was used, because experimental torque data were obtained from dynamometer measurements. Indeed, dynamometer system measurement does not allow deep knowledge of muscle contraction except resultant net torque during joint testing. Attempt to model, both eccentric and concentric muscle force contraction, is a difficult task. At my knowledge nobody proposed a single function for describing both phases, with regard to the tension-length and tension-velocity relationships. In spite of this fact, one main reference (already discussed in the earlier chapters) is known at least for the concentric phase: Hill's classic equation (Eq. 3.11) [38]:

$$(P + a) \cdot (V + b) = (P_0 + a) \cdot b \quad (3.11)$$

Where \mathbf{P} is the force, \mathbf{V} is the velocity and, \mathbf{a} , \mathbf{b} , $\mathbf{P0}$ are constants. Equation (3.11) is a rectangular hyperbola with asymptote at $\mathbf{P} = -\mathbf{a}$ and $\mathbf{V} = -\mathbf{b}$. It relates speed and load in a isotonic shortening.

This work was then inspired by Hill's equation. Two different functions described the concentric and the eccentric muscle contraction, separately.

3.2.1 Tension-velocity modelling (concentric-isometric)

According to the Hill's classic hyperbola for the concentric phase (CON) of muscle contraction [38], a rotational equivalent 2-parameter function (Eq. 3.12) to describe the *torque-angular velocity* was used [95]:

$$T(\omega) = \frac{CON}{(\omega_{con} + \omega)} - T_{con} \quad (3.12)$$

$$CON = T_{con} \cdot (\omega_{max} + \omega_{con})$$

$$T_{con} = T_0 \cdot \frac{\omega_{con}}{\omega_{max}}$$

Where T_0 is the isometric torque, ω_{max} the angular velocity at which the curve reaches zero torque and, ω_{con} defined by the vertical asymptote $\omega = -\omega_{con}$ (Fig. 3.4).

3.2.2 Tension-velocity modelling (eccentric-isometric)

A 2-parameter inverted rectangular hyperbola was used to represent the eccentric phase (ECC) [95]:

$$T(\omega) = \frac{ECC}{(\omega_{ecc} - \omega)} - T_{max} \quad (3.13)$$

$$ECC = -T_{max} - T_0 \cdot \omega_{ecc}$$

$$\omega_{ecc} = \frac{T_{max} - T_0}{k \cdot T_0} \cdot \frac{\omega_{max} \cdot \omega_{con}}{(\omega_{max} + \omega_{con})}$$

k^1 is the ratio of the slopes (eccentric and concentric) at $\omega=0$. ω_{con} defined by the vertical asymptote $\omega = -\omega_{con}$. T_{max} is the maximum eccentric torque.

3.2.3 Tension-length modelling

As reviewed in Chapter 1 (section 1.2), muscle force also depends on the length of muscle fibers at which the contraction occurs. Therefore, the torque at any angle was calculated using a quadratic torque-angle function (Eq.3.14) [48]:

¹ k was set at 4.3 as in the original model of Huxley [40]

3. Development of the jumping model

$$T_{\theta} = 1 - k_2 \cdot (\theta - \theta_{opt})^2 \quad (3.14)$$

Where k_2 is the width curve, θ is the angle and θ_{opt} is the optimal angle at which maximal torque can be produced (Fig. 3.5).

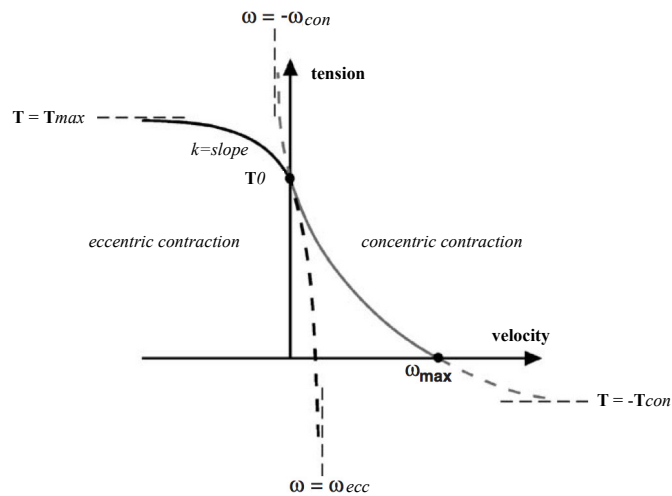


Figure 3.4: Representation of the parameters of the function that describe the torque-angular velocity relationship. From [95], *mod.*

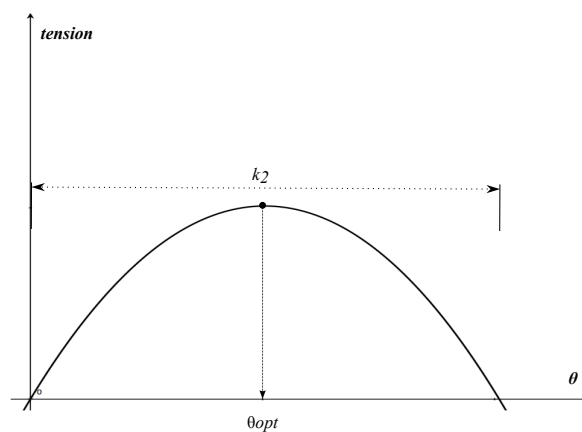


Figure 3.5: Graphic illustration of the tension-length relationship. k_2 is the width of the curve, θ_{opt} is optimal the angle.

3.2.4 Differential activation

A differential activation function¹ represents the neural inhibition mechanism evident for in-vivo measurements of torque which have suppressed torques at slow concentric velocities, and eccentric velocities [89] that are not apparent with in-vitro measurements [45]. Therefore, an exponential 3-parameter function (Eq. 3.15) used in the work of Lewis [49] was considered to represent this phenomena because it was computationally easier and therefore faster when incorporated in a whole-body simulation model.

$$a = a_{min} + \frac{1 - a_{min}}{1 + e^{-\frac{(\omega - \omega_1)}{m}}} \quad (3.15)$$

Where ***a_{min}*** is the lowest level of activation in the eccentric phase, ω_1 is the angular velocity at the point of inflection of the function, ***m*** governed the rate at which the activation increases with angular velocity (Fig. 3.6), $\frac{1}{m}$ was proportional to the slope at the point of inflection.

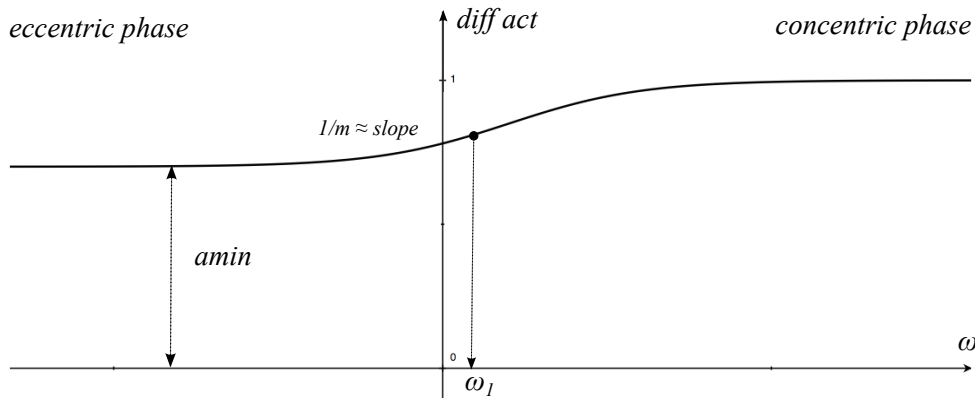


Figure 3.6: Graphic representation of the differential activation modelling.

¹The differential activation is based on physiological finding [89]. However, its role is to help the 5-parameter function to match as close as possible experimental data [49].

3.2.5 Subject-specific hip, knee, ankle joint modelling

3.2.5.1 Model-based on 5-parameter function

First simulations were based only on isometric and concentric modelling. Equation 3.12 on page 59 was used to fit isometric and concentric experimental values presented in Chapter 2 (sections 2.1.1 - 2.1.3). Fitting was obtained using surface toolbox implemented in Matlab (Matlab® 2010a, curve fitting toolbox 2.2) based on the nonlinear least squares method by means of the trust-region searching algorithm.

The 5-parameter (Tab. 3.8) **hip joint torque generator** represented the measured torque values collected over a hip joint range of motion (ROM) of 1.92 radians. Maximum isometric torque calculated was 19.3 % (37.6 N.m) lower than the measured one (157.6 N.m vs 195.2 N.m), the optimal angle calculated was at 1.66 rad whilst the measured isometric optimal angle was at 1.75 rad given a difference of 5.4%. The goodness of fit gave R^2 : 0.80. Figure 3.12 shows experimental data and fitted surface.

The 5-parameter (Tab. 3.9) **knee joint torque generator** represented the measured torque values collected over a hip joint ROM of 1.75 radians. Maximum isometric torque calculated was 1.3 % (2.9 N.m) greater than the measured one (230.2 N.m vs 227.3 N.m), the optimal angle calculated was at 2.18 rad whilst the measured isometric optimal angle was at 2.09 rad given a difference of 4.1%. The goodness of fit gave R^2 : 0.98. Figure 3.8 shows experimental data and fitted surface.

Finally, the 5-parameter (Tab. 3.10) **ankle joint torque generator** represented the measured torque values collected over a hip joint ROM of 1.22 radians. Maximum isometric torque calculated was 25.1 % (16.9 N.m) lower than the measured one (67.4 N.m vs 84.3 N.m), the optimal angle calculated was at -0.15 rad whilst the measured isometric optimal angle was at -0.17 rad given a difference of 13.3%. The goodness of fit gave R^2 : 0.89. However, the latter showed that the subject was clearly working sub maximally during biodex ankle testing sessions. Thus, it was necessary to multiply the ankle joint generator function by a factor S_a of 3.58 based on experimental data presented in Chapter 2 (sections 2.1.3). Figure 3.9 shows experimental data and fitted surface before and

3. Development of the jumping model

after the correction.

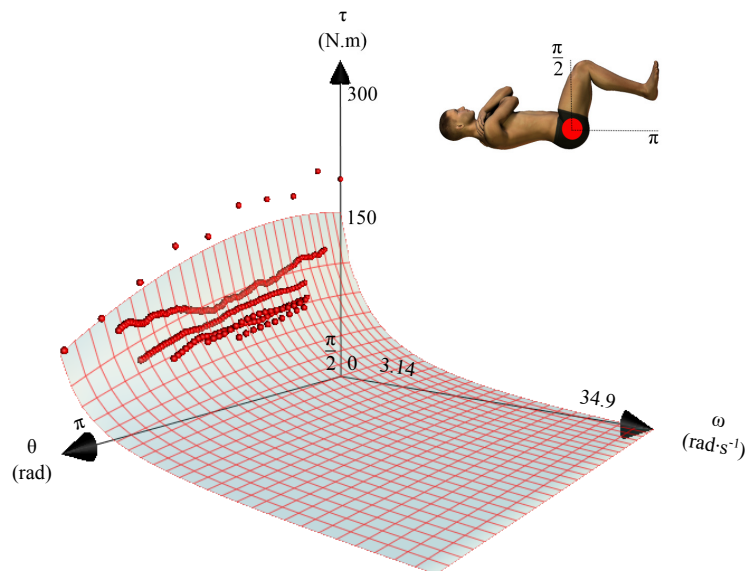


Figure 3.7: Hip extensors joint model obtained by the means of the trust region algorithm minimizing the difference between the model and the experimental data. Red points represent hip joint torque measured by using the dynamometer. The checkerboard surface represents the original fitting, whilst the uniform gray surface is the corrected model.

Table 3.8: Parameter of the hip joint torque model obtained from the statistical fitting.

Parameter	Description	Fitting value	Unit	Bounds (lower; upper)
k_2	Width of curve.	0.26		–inf; +inf
θ_{opt}	Angle at which max torque is exerted.	1.66	rad	± 0.08 exp. data
T_0	Isometric torque.	157.6	N.m	$\pm 20\%$ exp. data
ω_c	Vertical asymptote.	8.3	rad	1; 100
ω_{max}	Maximal shortening velocity.	34.91	rad·s ⁻¹	11.85; 34.91

3. Development of the jumping model

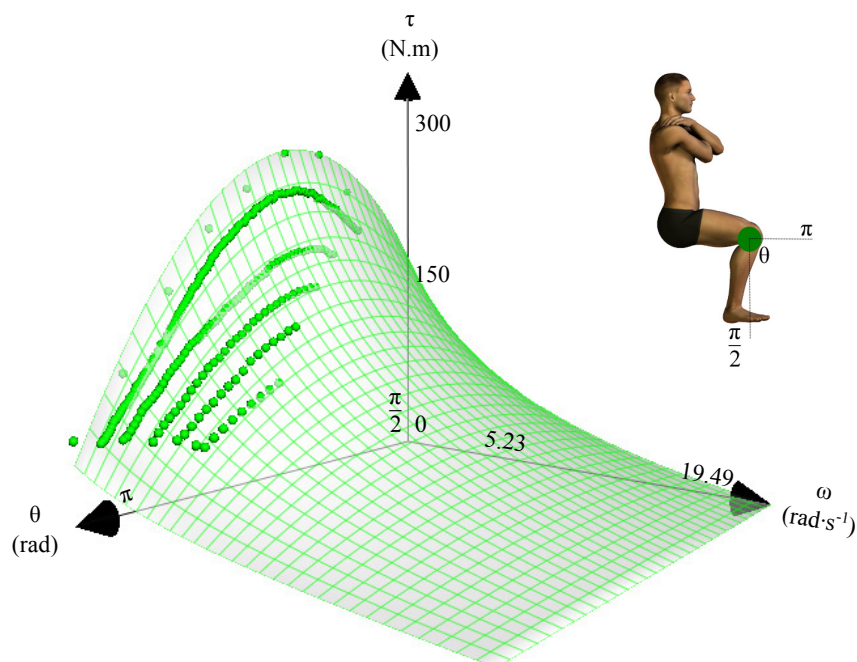


Figure 3.8: Knee extensors joint model obtained by the means of the trust region algorithm minimizing the difference between the model and the experimental data. Green points represent knee joint torque measured by using the dynamometer.

Table 3.9: Parameter of the knee joint torque model obtained from the statistical fitting.

Parameter	Description	Fitting value	Unit	Bounds (lower; upper)
k_2	Width of curve.	0.92		–inf; +inf
θ_{opt}	Angle at which max torque is exerted.	2.18	rad	± 0.08 exp. data
T_0	Isometric torque.	230.2	N.m	$\pm 20\%$ exp. data
ω_c	Vertical asymptote.	8.3	rad	1; 100
ω_{max}	Maximal shortening velocity.	19.49	$\text{rad}\cdot\text{s}^{-1}$	19.49; 34.91

3. Development of the jumping model

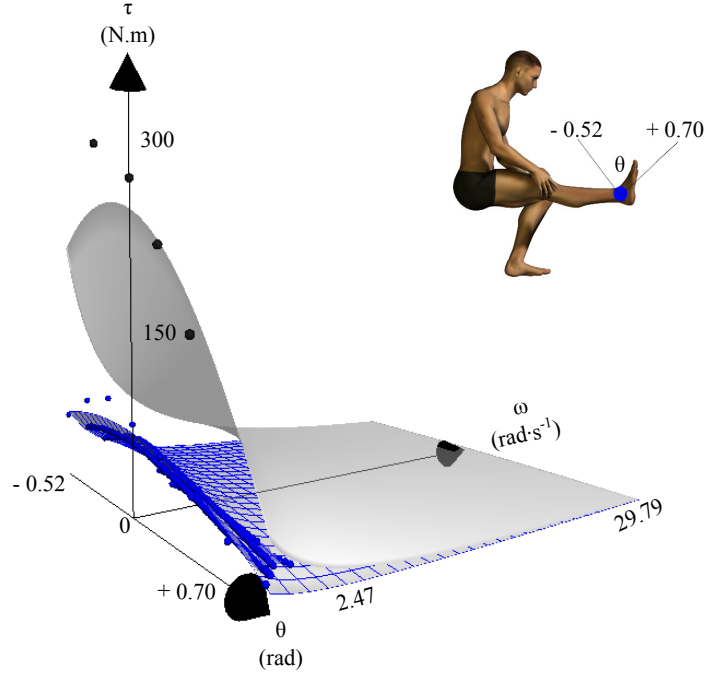


Figure 3.9: Ankle plantar flexors joint model obtained by the means of the trust region algorithm minimizing the difference between the model and the experimental data. Blue points represent ankle joint torque measured by using the dynamometer.

Table 3.10: Parameter of the ankle joint torque model obtained from the statistical fitting.

Parameter	Description	Fitting value	Unit	Bounds (lower; upper)
k_2	Width of curve.	1.14		$-\text{inf}; +\text{inf}$
θ_{opt}	Angle at which max torque is exerted.	-0.15	rad	± 0.08 exp. data
T_0	Isometric torque.	67.42	N.m	$\pm 20\%$ exp. data
ω_c	Vertical asymptote.	2.86	rad	1; 100
ω_{max}	Maximal shortening velocity.	29.79	$\text{rad}\cdot\text{s}^{-1}$	25.67; 34.91
S_a	Increasing factor	3.58		

3.2.5.2 Model-based on 9-parameter function

Another method was used to model the torque for each joint. The 9-parameter function for a single-joint torque generator was determined by minimizing the difference between measured joint torque data and the function derived from Equations 3.12 - 3.13 - 3.14 - 3.15. The simulated annealing algorithm was used to fit these experimental data using the following cost function (Eq. 3.16):

$$Cost = \sqrt{\frac{n+m}{n+m-f}} \cdot \sqrt{\frac{w_1 \sum_{i=1}^n \omega_i x_i^2 + w_2 \sum_{i=1}^m \omega_i y_i^2}{nw_1 \sum_{i=1}^n \omega_i + mw_2 \sum_{i=1}^m \omega_j}} \quad (3.16)$$

For data points where the measured torque was greater than the function: value $\mathbf{i} \rightarrow \mathbf{w}_1 = 100$ (target 10% more than the value), \mathbf{n} = the number of data points, \mathbf{x}_i = difference between measured torque and the function value. Likewise for data points where the measured torque was smaller than the function: value $\mathbf{j} \rightarrow \mathbf{w}_2 = 1$ (no weight), \mathbf{m} = the number of data points, \mathbf{y}_i = difference between measured torque and the function value, ω_i and ω_j = angular velocity, and \mathbf{f} = number of function parameters. Using a weighted RMS difference resulted in a 9-parameter subject-specific function that represented maximum voluntary joint torque rather than the average torque produced [49]. Therefore, the 9-parameter single-joint torque generator function represented the measured torques collected for the hip (extensors) the knee (extensors) and ankle (plantar-flexors) joints, respectively.

The 9-parameter (Tab. 3.11) **hip joint torque generator** gave an unbiased weighted RMS difference of 9.7 Nm (5% of maximum torque). However, this representation provided a surface only 39.7% of the experimental torque measurements were larger than the calculated torques which means underestimation. The calculated maximum torque isometric was 0.8% greater than the measured one. For the **knee joint torque generator** the 9-parameter (Tab. 3.12) gave an unbiased weighted RMS difference of 9.2 Nm (4% of maximum torque). This function provided a surface where 41.8% of the experimental torque measurements were larger than the calculated torques, also in this case the calculated

3. Development of the jumping model

torque was underestimated.

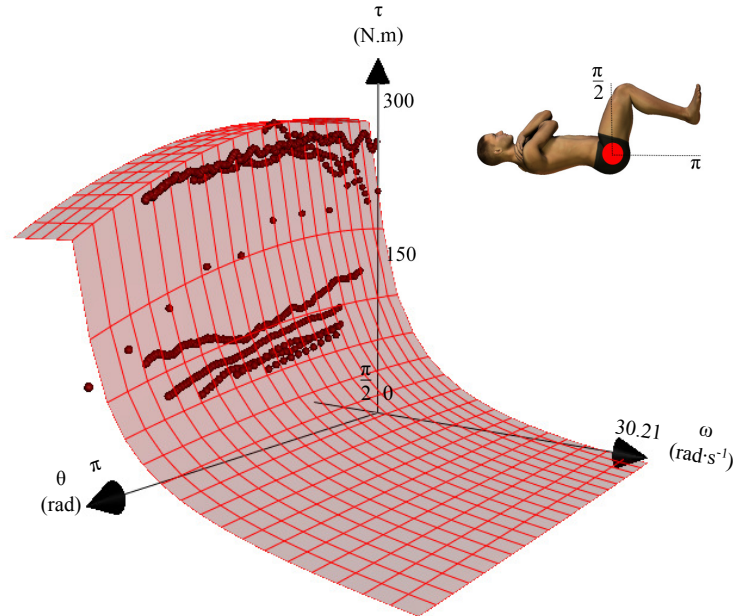


Figure 3.10: Hip joint modelling surface of the 9-parameter function. Eccentric and concentric phases are included. Red points are the experimental data.

The calculated maximum isometric torque was 1.7% greater than the measured one. Yet, the distal joint represented by the **ankle joint torque generator** (Tab. 3.13) gave an unbiased weighted RMS difference of 5 Nm (5.9% of maximum torque). For this latter case it was obtained a surface where 50% of the experimental torque measurements were larger than the calculated torques.

In summary, the model-based on 9-parameter function was calculated considering eccentric, isometric and concentric data (the previous model considered only concentric measured data). In addition, the simulated annealing algorithm was used instead of the trust region algorithm for fitting data.

3. Development of the jumping model

Table 3.11: Description, values and bounds of the 9 parameters used to fit the experimental data of the torque produced by the hip extensor muscle group.

Parameter	Description	Fitting value	Unit	Bounds <i>(lower; upper)</i>
a_{min}	Low activation level.	0.92		-0.5; +1
ω_1	Inflection point.	-0.31	rad/s	$-\pi$; $+\frac{\pi}{2}$
m	Slope	0.08	rad	0; 1
k_2	Width of curve.	0.17		0; 2
θ_{opt}	Angle at which max torque is exerted.	1.68	rad	± 0.08
T_0	Isometric torque.	193.00	N.m	exp. data $\pm 20\%$
T_{max}	Max eccentric torque.	270.20	N.m	
ω_c	Vertical asymptote.	4.53	rad	1.78; 17.46
ω_{max}	Maximal shortening velocity.	30.21	$\text{rad}\cdot\text{s}^{-1}$	11.85; 34.91

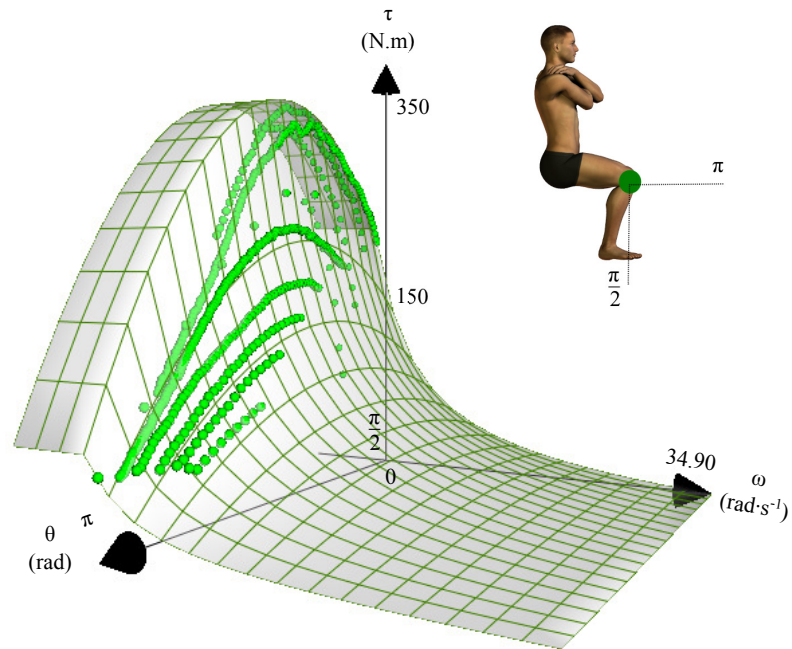


Figure 3.11: Knee joint modelling surface of the 9-parameter function. Eccentric and concentric phases are included. Green points are the experimental data.

3. Development of the jumping model

Table 3.12: Description, values and bounds of the 9 parameters used to fit the experimental data of the torque produced by the knee extensor muscle group.

Parameter	Description	Fitting value	Unit	Bounds (lower; upper)
a_{min}	Low activation level.	0.92		-0.5; +1
ω_1	Inflection point.	-1.27	rad/s	$-\pi$; $+\frac{\pi}{2}$
m	Slope	0.84	rad	0; 1
k_2	Width of curve.	0.86		0; 2
θ_{opt}	Angle at which max torque is exerted.	2.18	rad	2.1; 2.19 exp. data
T_0	Isometric torque.	230.82	N.m	$\pm 20\%$ exp. data
T_{max}	Max eccentric torque.	323.15	N.m	
ω_c	Vertical asymptote.	5.58	rad	5.24; 17.46
ω_{max}	Maximal shortening velocity.	34.91	rad·s ⁻¹	19.49; 34.91

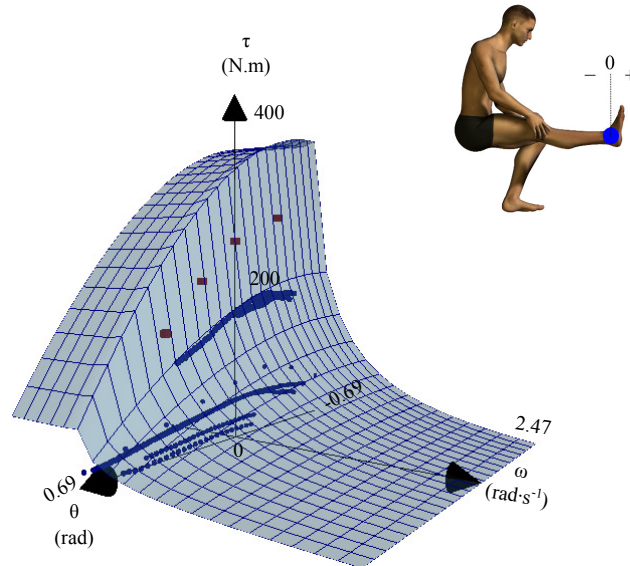


Figure 3.12: Ankle joint modelling surface of the 9-parameter function. Eccentric and concentric phases are included. Blue points are the experimental data. The 4 dark red points collected during the functional isometric ankle test were used to scale the torque starting from parameters showed in Table 3.13.

3. Development of the jumping model

Table 3.13: Description, values and bounds of the 9 parameters used to fit the experimental data of the torque produced by the ankle plantar flexor muscle group.

Parameter	Description	Fitting value	Unit	Bounds (lower; upper)
a_{min}	Low activation level.	0.98		-0.5; +1
ω_1	Inflection point.	-1.67	rad/s	$-\pi$; $+\frac{\pi}{2}$
m	Slope	0.17	rad	0; 1
k_2	Width of curve.	0.58		0; 2
θ_{opt}	Angle at which max torque is exerted.	-0.52	rad	± 0.08 exp. data
T_0	Isometric torque.	85.25	N.m	$\pm 20\%$ exp. data
T_{max}	Max eccentric torque.	119.36	N.m	
ω_c	Vertical asymptote.	3.85	rad	
ω_{max}	Maximal shortening velocity.	25.68	rad·s ⁻¹	25.67; 34.91

Table 3.14: Summary of the parameters obtained using two different models. For the hip and ankle joint the calculated isometric torque was lower in the 5-parameter function than in the 9-parameter one. Similar calculated optimal angle occurred for the hip and the knee joint. Maximal shortening velocity parameter (ω_{max}) was very different comparing the two different knee models.

Parameter	Hip		Knee		Ankle	
	5-par	9-par	5-par	9-par	5-par	9-par
a_{min}	-	0.92	-	0.92	-	0.98
ω_1	-	-0.31	-	-1.27	-	-1.67
m	-	0.08	-	0.84	-	0.17
k_2	0.26	0.17	0.92	0.86	1.14	0.58
θ_{opt}	1.66	1.68	2.18	2.18	-0.15	-0.52
T_0	157.6	193.0	230.2	230.8	67.4	85.3
T_{max}	-	270.2	-	323.2	-	119.3
ω_c	8.30	4.53	8.30	5.58	2.86	3.85
ω_{max}	34.91	30.21	19.49	34.91	29.79	25.68

3.3 The active state of skeletal muscle model

During movement at joints, the available of torque which can be exerted at any time t , is determined by multiplying the maximal torque calculated from the actuator parameters (based on fitted experimental data) by an activation. Therefore, each actuator which was a torque generator was controlled by a simple ramp function governed by four parameters. In this work, a quintic function¹ (Eq. 3.17) gave form to the muscle force rise up function, modelling neuromuscular patterns. Here, the quintic function, which has zero first and the second derivatives (Eq. 3.18, Eq. 3.19) at the endpoints.:

$$f(x) = x^3 \cdot (6x^2 - 15x + 10) \quad (3.17)$$

$$f'(x) = 30x^3 \cdot (x - 1)^2 \quad (3.18)$$

$$f''(x) = 120x \cdot \left(x - \frac{1}{2}\right) \cdot (x - 1) \quad (3.19)$$

However, neuromuscular activation as a function of the time, even when maximal is never instantaneous². Consequently, the activation Act was controlled in the model by the following equation that has taken form by the previous quintic function:

$$Act = 0 + (z)^3 \cdot (6z^2 - 15z + 10). \quad (3.20)$$

Where Act is the *active state* of mammalian skeletal muscle (recruitment and firing rate of alpha-motoneurons) and, the parameter z is:

$$z = \frac{t - d}{r}$$

Where t is *time*, d is the joint onset *delay* and r is the *ramp* time for building

¹Neuromuscular activation (Act) was created using a quintic function [94]. Act was forced not to exceeded the range between 0 and 1.

²Simplifying the model, we assumed that the activation could reach is maximal equal to 1.

3. Development of the jumping model

force. In order to avoid aberrations, simulations always start from an equilib-

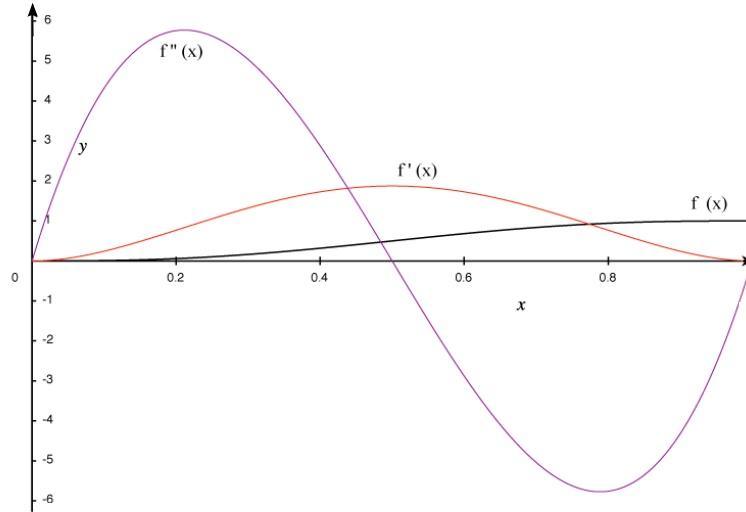


Figure 3.13: Quintic function $f(x)$ and its derivatives $f'(x)$ and $f''(x)$.

rium position. It required an initial activation level $a(\text{start})$, for this reason, Rt was the considered simulated rise time for building torque at joints. Rt was obtained by subtracting r by the time spent at equilibrium position (Fig. 3.14). However, attempt to model the neuromuscular activation means to represent as close as possible the neuromuscular activity. Latter is generally assessed by using surface electromyography (sEMG). Figure 3.15 (A-C) shows an overlap between a measured sEMG signals and an optimized ankle joint activation profile obtained from matching simulation of a squat jump trial in a time domain³.

In the panel **A** of the figure above, the *continuous thick line*, represents the simulated optimized activation profile (matching simulation of a squat jump +50kg loaded). The *continuous thin line*, is the linear envelope (low-pass filter 7Hz) of the sEMG of the soleus muscle (SOL), whilst the *dotted line* represents the gastrocnemius medialis muscle (GA). The panel **B** and **C** show the band-pass (10-400Hz) rectified sEMG of the GA (blue) and SOL (green), respectively.

³Data referred to the ankle joint of a squat jump with 50kg extra loaded trial, compared with the activation profile of its matching simulation.

3. Development of the jumping model

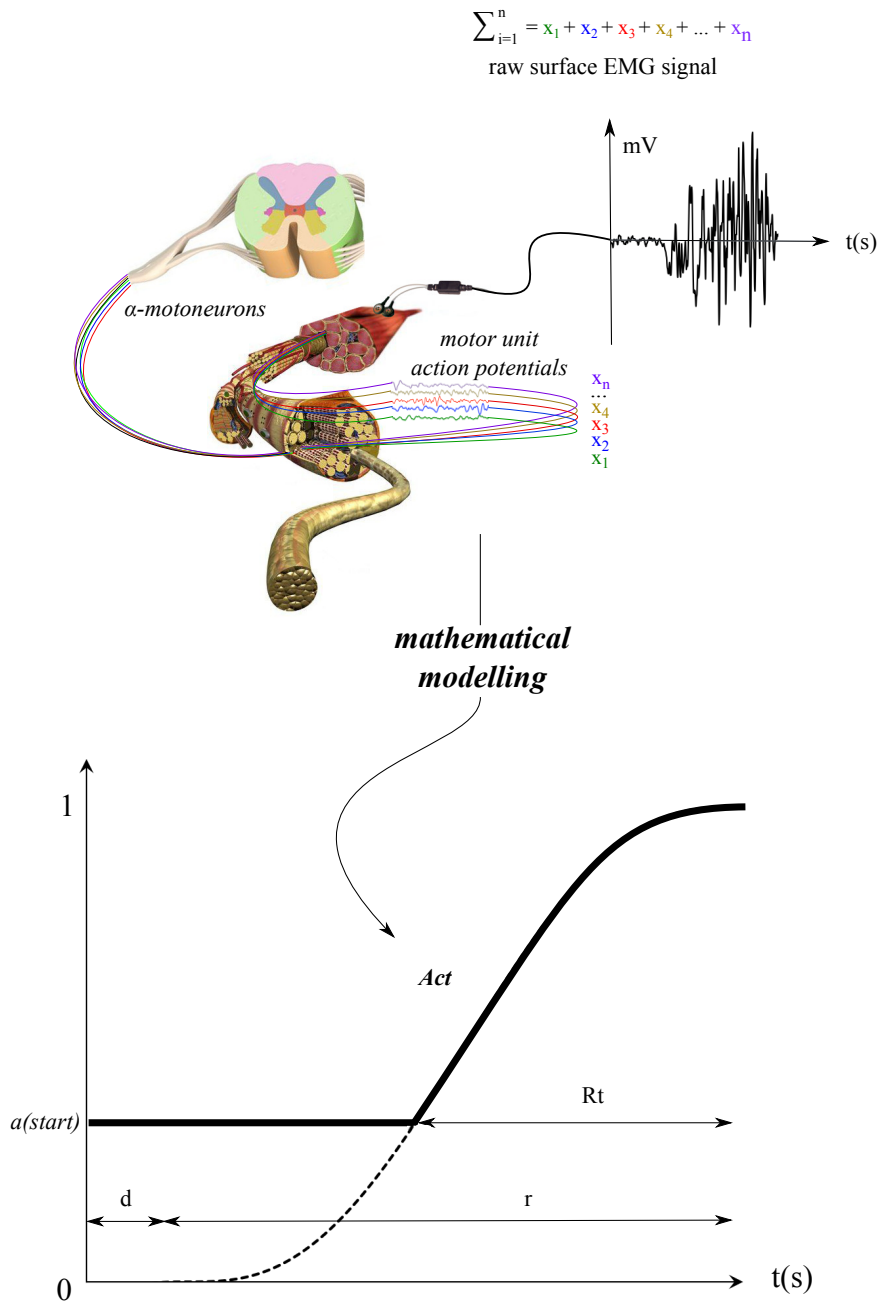


Figure 3.14: The way the human body activate muscles is simply represented by using a quintic function that is equivalent to the neuromuscular activation pattern.

3. Development of the jumping model

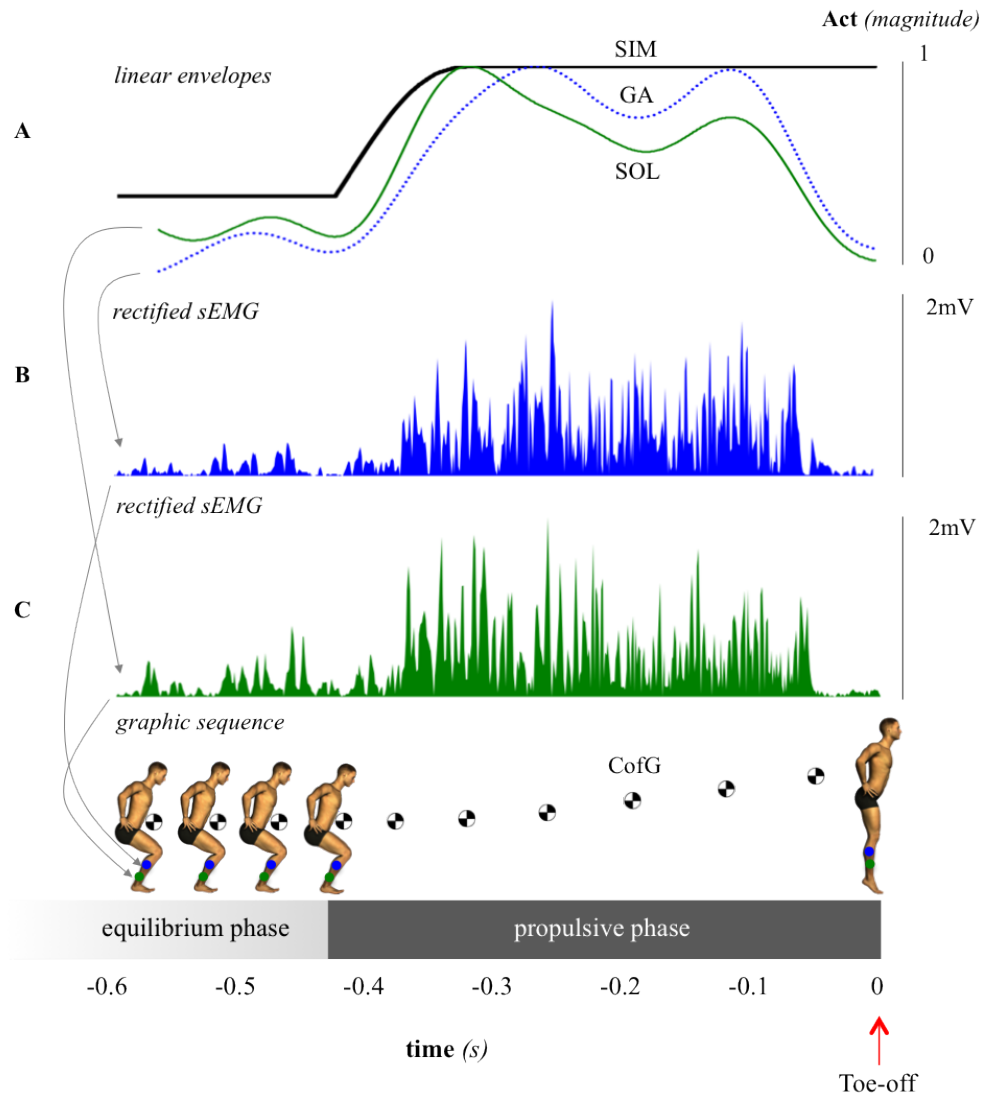


Figure 3.15: Example of the ankle joint activation profiles time history. The solid line is the activation modeling which is compared with the sEMG linear envelope and the rectified sEMG. GA and SOL are the gastrocnemius laterals and the soleus, respectively. The graphic sequence at the bottom of the figure help to understand the activation phenomena during the push-off phase of the squat jump.

3.4 Summary of joint torque generation

Different models were used to represent total net muscle force at any instant in time and parameters were all explained in the above sections. However, in order to encourage a clear understanding of all mathematical terms, the equation 3.21 describes in summary how input data inserted into actuators actually worked interacting each other for the model based on 9-parameter. Equation 3.22 summarize the model based on 5-parameter function. Equation 3.23 represents the activation which is multiplied for both 5-parameter or 9-parameter functions.

$$T(\theta, \omega) = \begin{cases} [1 - k_2 \cdot (\theta - \theta_{opt})^2] \cdot [a_{min} + \frac{1-a_{min}}{1+e^{-\frac{(\omega-\omega_1)}{m}}})] \cdot [(\frac{CON}{(\omega_{con}+\omega)} - T_{con})] & \text{if } \omega \geq 0 \\ [1 - k_2 \cdot (\theta - \theta_{opt})^2] \cdot [a_{min} + \frac{1-a_{min}}{1+e^{-\frac{(\omega-\omega_1)}{m}}})] \cdot [(\frac{ECC}{(\omega_{ecc}-\omega)} - T_{max})] & \text{if } \omega \leq 0 \end{cases} \quad (3.21)$$

$$T(\theta, \omega) = [1 - k_2 \cdot (\theta - \theta_{opt})^2] \cdot [(\frac{CON}{(\omega_{con}+\omega)} - T_{con})] \quad \text{if } \omega \geq 0 \quad (3.22)$$

$$T(t) = Act \cdot T(\theta, \omega) \quad (3.23)$$

3.5 Summary

A comprehensive description of the models was the goal of this Chapter. It was extensively described how the model was created in Working Model© environment. Regression equations were used to estimate subject-specific anthropometric and inertial parameters. Joint torque for the hip, knee and ankle was modeled by using two models. The first one was based on the 4-parameter function, the second one on the 9-parameter function. The active state of skeletal muscle was described by using a quintic function. These models are now predisposed to be implemented into simulations. The next Chapter is about evaluation models, based on result of matching simulations against the actual performance.

Chapter 4

Torque-driven model evaluations: results and discussion

4.1 Vertical jumping modelling evaluations

Modelling human performance requires representing main human neuromuscular characteristics. However, evaluation of a proposed models must be a routine part of a research design project. Actually, before a simulation model is used to investigate research questions it should be demonstrated that a recorded movement can be reproduced with accuracy. Here, results of squat jump simulation evaluations, which we call *matching performance* are presented. At first, two squat jump models (**Model A** and **Model B**) were created using two different methods and compared to each other to establish which model gave the better result in matching performance compared to the actual performance. This first evaluation will establish the way to create models about squat jump +40% of the body weight and squat jump +80% of the body weight. Figure 4.1 illustrates how the two first squat jump models were created to find the optimal solution that best matched the experimental squat jump considered. Simulations were run using two different search algorithms to fit torque data and to find the optimal solution for matching performance purpose: the brute-force and the simulated annealing algorithm. Further, the **Model A** used the 5-parameter function (concentric phase and activation equations), whilst the **Model B** used the 9-parameter func-

4. Torque-driven model evaluations

tion (concentric-eccentric phase, differential activation and activation equations), explained elsewhere (see Chapter 3).

By the end of this section, it has to be mentioned that in simulation the root-mean-square deviation (RMSD) or root-mean-square error (RMSE) is a frequently used measure of the differences between values predicted by a model or an estimator and the values actually observed. Here, comparisons are based on the RMSE to establish the accuracy of the tested model.

In summary, in this work the first model evaluation was used to establish which model had to be used to run other matching simulations, to optimize squat jump height (body weight and extra load) and finally to make predictions.

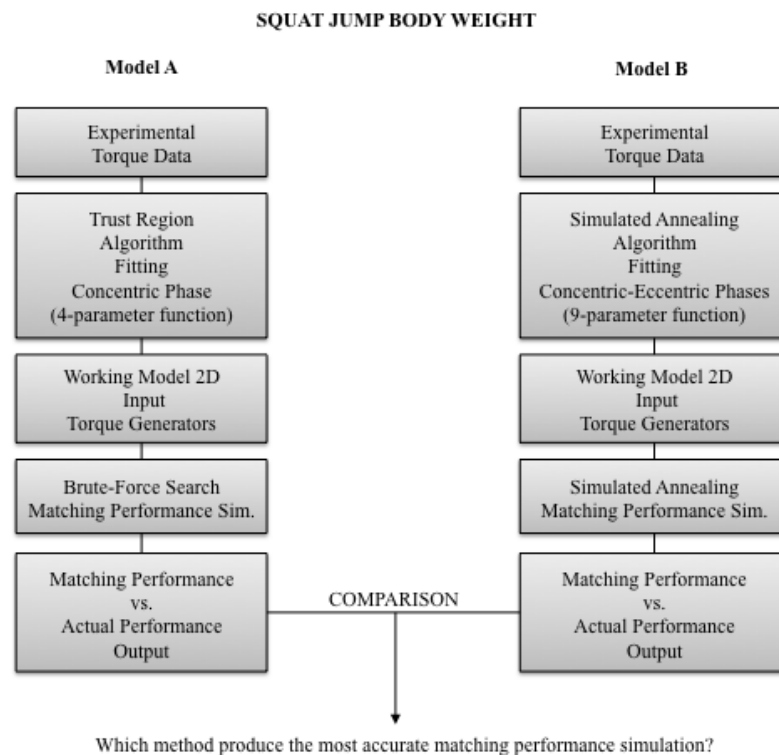


Figure 4.1: Diagram of the two squat jump model (A-B). They are compared to each other for the matching performance simulation purpose.

4.2 Cost functions

Vertical jumping optimization problems in this thesis, consist of minimizing (matching performance) or maximizing (optimize performance) a cost function by systematically choosing input values from within an allowed set of variables, then computing the value of the cost function. Actually, the result of the cost function is a minimized or maximized score. Therefore, the goal is to select optimal elements (with regard to some criteria) from some set of available alternatives. However, for these kind of problems (vertical jump height human performance), the cost function includes joint vertical velocities, centre of mass velocity (vertical and horizontal), peak ground reaction force, joint displacement or joint angle at a given instant (toe-off), etc [4; 48; 90]. Two cost functions were used in this work, the first one contained joint angles and hip vertical velocity at the instant of the toe-off. It was used to obtain a score for the **Model A** for matching simulation. The second cost function also included the vertical velocity of the centre of gravity of the system. The second cost function was used to obtain a score of the **Model B** for matching simulation.

$$S = \sqrt{\frac{\sum_{i=1}^n (s_i - a_i)^2}{n}}. \quad (4.1)$$

$$S = \sqrt{\frac{\sum_{i=1}^n (s_i - a_i)^2 + \sum_{j=1}^m 50 \cdot (s_j - a_j)^2}{n + m}}. \quad (4.2)$$

where \mathbf{S} is the score, \mathbf{i} is angle variables and \mathbf{j} is velocity variables, \mathbf{s} is the value of variable from simulated performance, \mathbf{a} is the value of variable from actual performance. The total number of the \mathbf{i} and \mathbf{j} variables were given by the sum of \mathbf{n} and \mathbf{m} . If the cost function included a variable about velocity a weight of 50 was chosen making $0.20 \text{ m/s} \equiv 10 \text{ degrees error}$ (Eq. 4.2), otherwise the unweighted equation was used (Eq. 4.1). A weight of 50 was chosen because it was already studied that 1 degree (joint angle) was comparable to 1% error [90].

4.3 Squat jump matching performance

4.3.1 Squat jump Model A: 5-parameter function, trust region algorithm for fitting input data and, brute-force search method for matching simulations.

The first attempt to simulate a real squat jump was performed using the equations 3.12 and 3.14 (Page 59, Page 61) as input for torque generators and the brute-force search for obtaining the more close result in relation to the actual performance. This model was named **Model A**.

Before to run simulations boundaries concerning torque rise time and onset torque generators were chosen based on physiological knowledge.

Torque rise time for the hip, knee and ankle joint was set between 90 ms [18] (lower bound) to 300 ms (upper bound). Due to the computational time cost of the exhaustive search (brute-force algorithm) an upper value greater than 300ms was discouraged. For upper limits no physiological data are available.

Experimental data based on sEMG were used to estimate muscle onsets: the average value was calculated for each recorded muscle over a period of 900ms during a rest phase immediately before the start of the movement. When the average value increased three times the standard deviation, this instant in time was chosen as the onset threshold. Therefore, 56 ms was the calculated delay between the gluteus and the soleus. Therefore, the gluteus activated as first muscle during SJbw whilst the soleus was the last one. However, still due to the high computational time cost onset joints time was set for simulations between 0 ms to 30 ms.

The cost-function 4.1 was used to minimize the difference between the actual performance and the simulation by varying 6 torque generator activation timings. Each iteration took about 1.8 s and thousands of simulations were run for up to four days long. Results are presented and discussed in section 4.3.3.

4.3.2 Squat jump Model B: 9-parameter function, Simulated Annealing (SA) algorithm for fitting input data and, SA method for matching simulations.

The **Model B** differently from the **Model A** was created using the 9-parameter function explained in Chapter 3. Another crucial difference in relation to the **Model A** was the search method (algorithm) to converge to the optimal solution. Indeed, the simulated annealing algorithm was implemented into the script program, since it seems suitable for this kind of problems [22]. A general explanation about SA is reported elsewhere (Chapter 1, section 1.3.2). Here the pseudocode of the SA used for matching simulations:

```
T0(T and a lowercase 0)    Starting temperature
Iter    Number of iterations
alpha   The cooling rate

1. Set T = T0 (T and a lowercase 0)
2. Let x = a random solution
3. For i = 0 to Iter-1
4. Let f = fitness of x
5. Make a small change to x to make x1
6. Let f1 = fitness of new point
7. If f1 is worse than f then
8.     Let p = PR(f1, f, Ti (T with a lowercase i))
9.     If p > UR(0,1) then
10.        Undo change (x and f)
11.     Else
12.        Let x = x1
13.     End if
14.     Let Ti(T with a lowercase i) + 1 = alpha Ti(alpha and T with a lowercase i)
15. End for

Output: The solution x
```

Here the cooling rate was set at 10% and the starting temperature was set at 10.

For matching performance, torque rise time for the hip, knee and ankle joint was set between 90 ms [18] (lower bound) to 350 ms (upper bound). Onset time bounds were 0ms (lower bound) and 60ms (upper bound), based on experimental sEMG finding. The SA converged to the optimal solution in 24h for each simulated condition after 38400 total iterations. To determine the acceptance probability of a new solution vis-a-vis the current solution, an elaborate procedure is followed that takes into account the domination status of the new solution

with the current solution, as well as those in the archive. Results are extensively presented and discussed in next sections.

4.3.3 Model A *vs.* Model B *vs.* actual performance

This section compares the **Model A** *vs.* **Model B** *vs.* **actual performance**. Initial conditions are showed in the Table ???. Starting position was set as for the squat jump performed during the experimental session (the best trial in terms of jump height).

4.3.3.1 Jump height

The squat jump **Model A** gave a jump height of 32.2% lower than the actual performance. The **Model A** jumped 16.2 cm, the **Model B** 20.1 cm against 23.9 cm of the actual performance. This gave a difference of 7.7 cm and 3.8 cm, respectively. If one consider the jump height as the main parameter, then the **Model B** was better in matching this parameter. The jump height reached by the **Model B** can be considered a great achievement. In fact, in subject-specific vertical jumping model simulations this is not an easy result to obtain. Lewis presented two models, one based on assumption of monoarticularity, the other considering biarticular muscles [49]. Both models, struggled to achieve a jump height of 50% of that measured for the participant. Subsequently, he included strength increase factors ranged from 1.1 to 1.6 in order to match the actual jump height. Here, only the ankle joint required a torque correction (3.58). Lewis [49] in his work justified the weakness of his models arguing that the participant clearly worked submaximally during dynamometer testing sessions. This means an underestimated fitting of dynamometer data.

4.3.3.2 Kinetic

A shorter propulsive phase was found in both the **Model A** and the **Model B** in relation to the actual performance: 260 ms (A) *vs.* 217 ms (B) *vs.* 334 ms (actual). In this case, the **Model A** was more close to the actual propulsive phase than the **Model B**. The peak GRF (Fig. 4.2) was 1450 N for the actual performance, 1297 N for the **Model A** (underestimated) and, 1631.8 N for the

Model B (overestimated). A RMSE % of 10.63% for the GRF (percentage of the average GRF over the propulsive phase) was calculated over the propulsive phase for the **Model A**, 17.1% for the **Model B**.

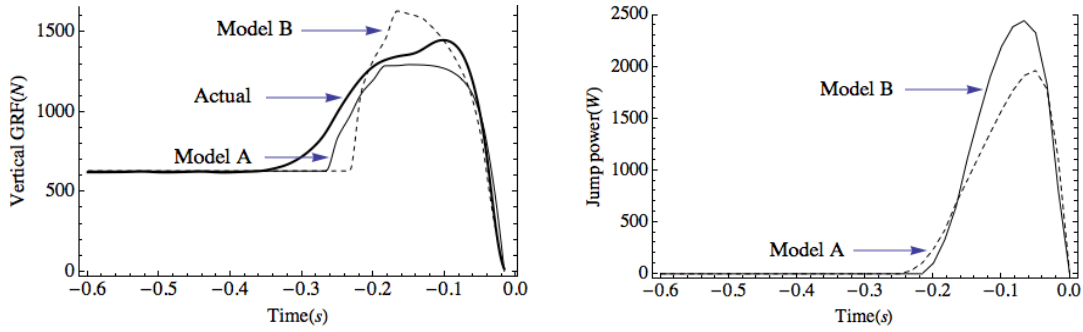


Figure 4.2: In the left side: **Model A vs. Model B vs. actual performance** (SJ GRF). In the right side: **Model A vs. Model B** (global power output). The abscissa 0 value correspond to the instant of the toe-off.

Considering, these first parameters two questions are open. 1) *why do models execute the jump in a shorter time than the actual one?* The GRF provided clear evidence of the simulation models ability to generate an important impulse in a short duration of the ground contact phase (Fig. 4.2). This means that much force is available with respect to time. At first, this could be due to the assumption that serie elastic elements do not play a relevant role in relation to the pure concentric phase of the movement. Actually, as well explained by Patel et al. [69] the actual path of force transmission is also dependent from the tendon stretch before to obtain a mechanical movement of the contiguous segment. Considering the nature of the tendon in this terms, elastic components in this case would delay a force production instead of to recoil energy and a force dispersion could probably occur. This might be macroscopically translated in a strengthen system such as a torque generator which consider only the contractile component of the muscle-tendon complex. In this case the difference is 74 ms for the **Model A** and 117 ms for the **Model B** means that the **Model A** is weak with respect to the **Model B**, since the peak force is underestimate for the **Model A** and overestimate for the **Model B**. In addition a clearly evidenced is that the **Model A** jumped only 16.2 cm. Indeed, the **Model A** is not strong as the **Model B**

4. Torque-driven model evaluations

(see 3.14, Page 71 → hip and ankle isometric torque). However, it has to be said that the exact mechanism of the force transmission from the myosin filament to the tendons is still not completely understood [59; 69]. In addition, it could also be speculated that muscle tissue conditions at the moment of the experimental session is important since potential damages (as scar tissue), might limit the force transmission from muscles via the tendon of insertion to the skeleton [53].

2) *Why despite the fact that the difference at the peak GRF is in the order of 150 N for both models, the **Model A** considering the RMSE seems more accurate in matching GRF than the **Model B** ?* In previous studies [49] GRF was also included to evaluate simulation models. RMSE % can be in relation to the peak GRF or the average force produced during the propulsive phase. The latter is the case in this thesis and a low value was found for the **Model A**. However, first results, suggest that the squat jump **Model A** is quite far from the actual performance, especially in terms of jump height performance.

4.3.3.3 Torque output

For **Model A**, peak torque was 164.9 N.m, 142.7 N.m, 185.2 N.m for the hip, knee and ankle joints, respectively. The hip reached the peak torque after 17 ms followed by the ankle (67 ms) and, the knee at 100 ms. However, the **Model B** gave a greater peak torque at hip and knee joint and, a similar torque at ankle joint (196.0 N.m → hip; 213.7 N.m → knee; 181.2 N.m → ankle). Figure 4.3 show a comparison between the **Model A** and the **Model B** about torque exertion in matching squat jump simulation. At first, it should be pointed out that both

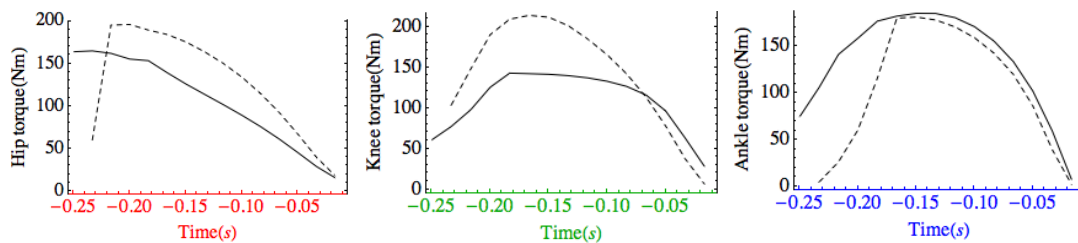


Figure 4.3: Torque exerted by the **Model A** and **B**. Charts show a comparison between the two models for matching performance. Dashed line = Model B; solid line = Model A.

4. Torque-driven model evaluations

theoretical models (5-parameter and 9-parameter functions) used a big amount of available torque, for the matching simulation. Indeed, both models exerted at each joint 80% up to 95% of the predicted torque. This means, the models worked close to their maximal capacity.

4.3.3.4 Kinematic

If we consider a movement, then a kinematic comparison is required in simulations. In these terms, an important difference was found when comparing the ankle joint angle of the **Model A** at the instant of the toe-off: 13.9 degrees from the actual performance was obtained, whilst the **Model B** showed to be more accurate. This is clearly highlighted by the Figure 4.4. Slight differences were

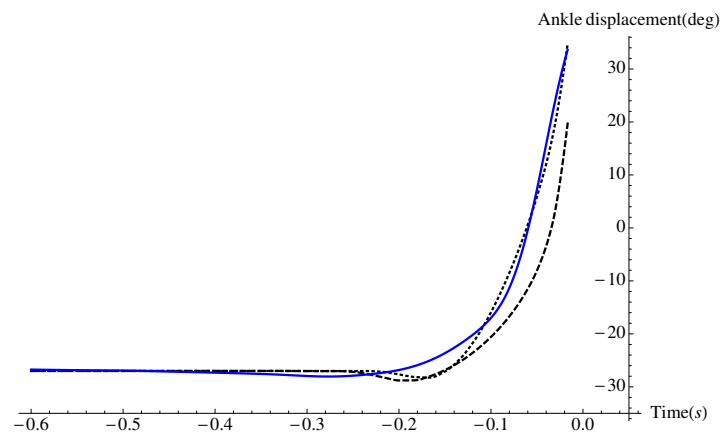


Figure 4.4: Ankle displacement. Comparison between **Model A** (dashed line) , **Model B** (dotted line) and actual performance (solid line). These two models showed very similar results in relation to the knee joint displacement.

found for the hip and knee joint at the instant of the toe-off between the accuracy of the **Model A** and the **Model B** (Fig. 4.5, Fig. 4.6).

Table 4.1 reports angle data at each joint for a given starting condition and the instant of the toe-off. Thus, for kinematic analysis the **Model A**, the **Model B** and, the actual performance can be compared considering the displacement or the instant of the toe-off. In the light of these data, it is an evidence that

4. Torque-driven model evaluations

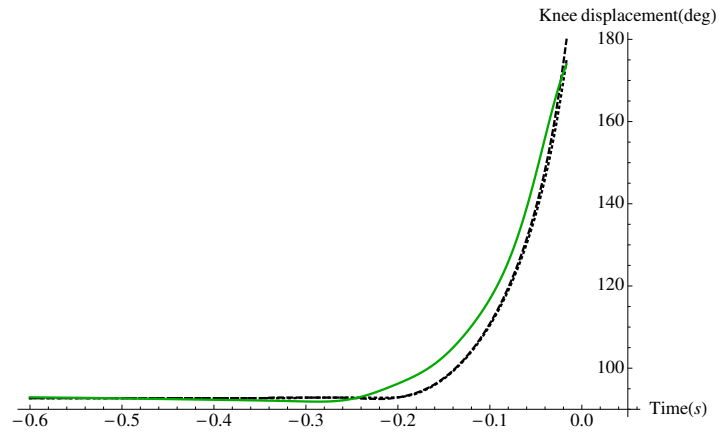


Figure 4.5: Knee displacement. Comparison between **Model A** (dashed line) , **Model B** (dotted line) and actual performance (solid line).

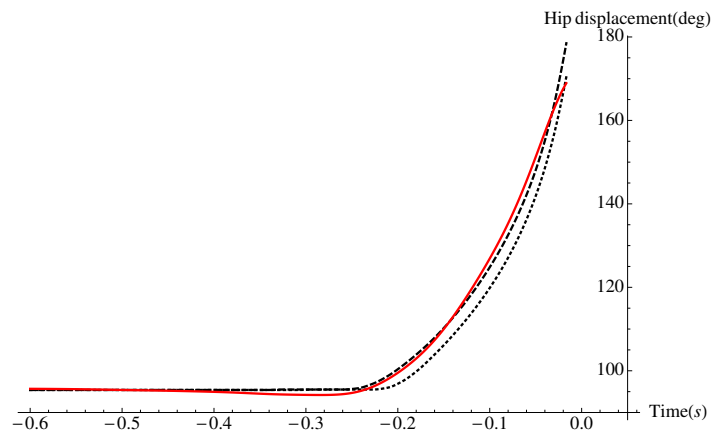


Figure 4.6: Hip displacement. Comparison between **Model A** (dashed line) , **Model B** (dotted line) and actual performance (solid line).

4. Torque-driven model evaluations

the **Model B** provided a good overall agreement with the participant kinematics (joint displacement).

Table 4.1: Kinematic data: SJ conditions compared for starting and toe-off angles. RMSE is calculated over the whole jump, whilst the column *difference* (deg) is about the instant of the toe-off.

	Initial condition (deg)	Toe-off instant (deg)	difference (deg)	RMSE (deg)
θ_{hip} actual	90.5	168.9		
θ_{hip} A	90.5	178.5	9.6	1.7
θ_{hip} B	90.5	170.4	1.5	4.2
θ_{knee} actual	88.8	173.9		
θ_{knee} A	88.8	179.9	6.0	3.9
θ_{knee} B	88.8	174.9	1.0	4.4
θ_{ankle} actual	-28.07	33.6		
θ_{ankle} A	-28.07	20.0	13.6	6.2
θ_{ankle} B	-28.07	34.8	1.2	1.7

In contrast, for the actual performance, peak angular velocities reached 578.5 deg/s, 866.0 deg/s, 840.2 deg/s for hip, knee and ankle joint, respectively. Considering these data, an important difference was obtained for both the **Model A** and the **Model B**. Indeed, at the instant of the toe-off the angular velocity at hip, knee and ankle joint reached more than 2 time the correspondent value obtained in experimental conditions. Figures 4.7, 4.8 and 4.9 show angular velocities throughout the jump. Actually, before the toe-off in experimental conditions angular velocities suddenly decrease. Here, it was found that angular velocities increased from the beginning to the end of the jump (toe-off). Reasons are to be found in the way in which these two models were created. It is to be reminded that neither the **Model A** nor the **Model B** incorporated antagonist muscles or biarticular muscles. Early works of van Soest [86] showed the same problem arguing that this happen when antagonist muscles are not considered. Probably other reasons are behind this phenomena such as anatomical constraints (tendons, ligaments, etc.) and neural inhibition. Actually, sEMG data (Page 43 and Page 90) show that the magnitude decreased close to the instant of the toe-off. However, it sounds fair to hypotesized that when performing explosive movements humans

4. Torque-driven model evaluations

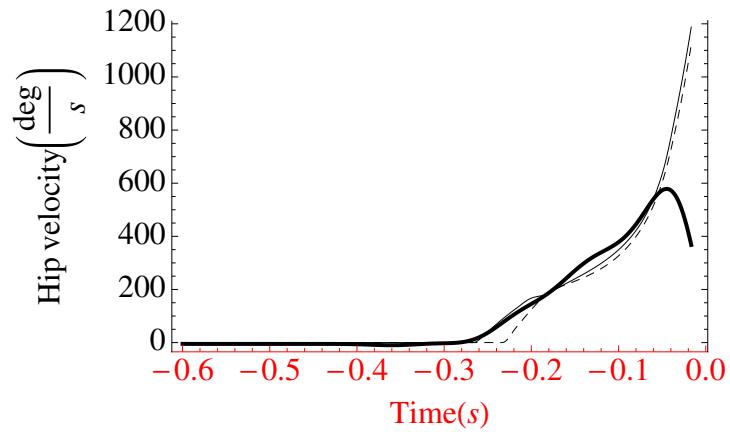


Figure 4.7: Hip angular velocity. Solid thick line=actual performance; solid thin line=Model B; Dashed line=Model A.

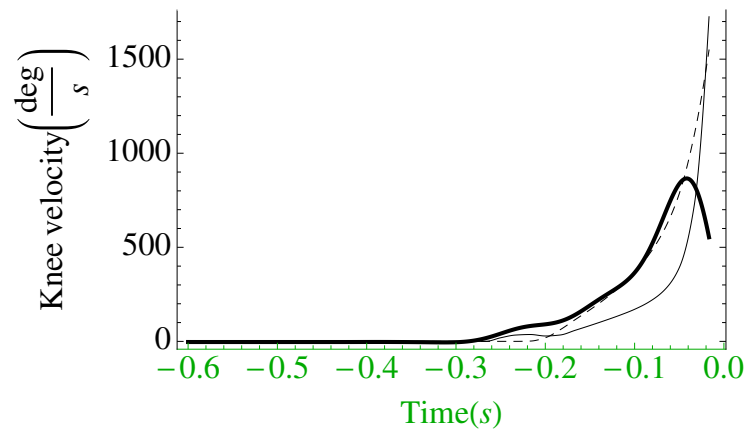


Figure 4.8: Knee angular velocity. Solid thick line=actual performance; solid thin line=Model B; Dashed line=Model A.

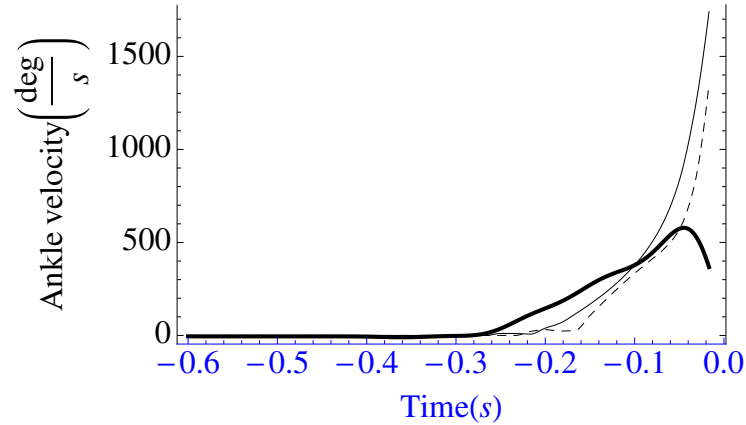


Figure 4.9: Ankle angular velocity. Solid thick line=actual performance; solid thin line=**Model B**; Dashed line=**Model A**.

benefit from unconsciously protective mechanism to avoid body damages (e.g. avoiding to violate anatomical range of motion or joint dislocations).

4.3.3.5 Activation pattern profiles

Activation patterns were qualitatively close when the experimental squat jump was compared against the shape of the slope of the linear envelopes of the sEMG as shown in Figure 4.10 and Fig. 4.11 (only sEMG for monoarticular muscles). The quintic function presented in Chapter 3 was used to activate each torque generator. One parameter managed the ramp time, whilst an other parameter was responsible of the delay (onset) between joints. In order to simplify the model, the activation patterns were allowed to reach the full activation and keep it until the toe-off phase. Based on sEMG experimental measurements (see Page 44), it was allowed to reach the full activation by the half of the whole propulsive phase. The hip joint reached the full activation at first, followed by the ankle and the knee joints. Slightly differences can be noticed between the **Model A** and the **Model B**, but in both cases a proximal-to-distal activation sequence was found confirming data from the literature [9; 14; 68].

4. Torque-driven model evaluations

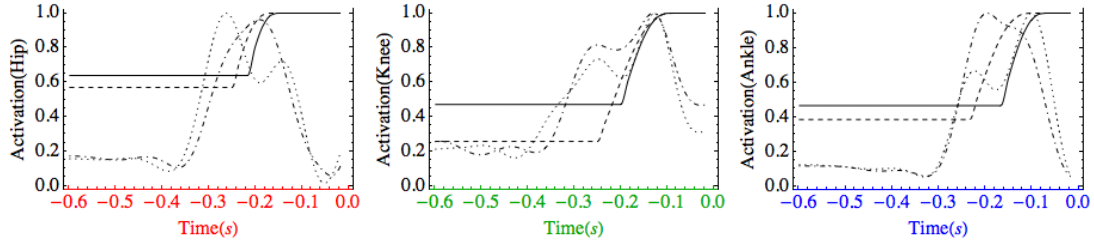


Figure 4.10: Squat jump activation profiles: Model (A) vs. Model (B) vs. sEMG. sEMG linear envelope: gluteus (GL), biceps femoris (BF), vastus lateralis (VL), rectus femoris (RF), gastrocnemius lateralis (GL), soleus (SOL). Hip joint (left, red): solid line= B, dashed line=A, dotted line=GL, dotted dashed line=BF. Knee joint (centre, green): solid line= B, dashed line=A, dotted line=RF, dotted dashed line=VL. Ankle joint (right, blue): solid line= B, dashed line=A, dotted line=GA, dotted dashed line=SOL.

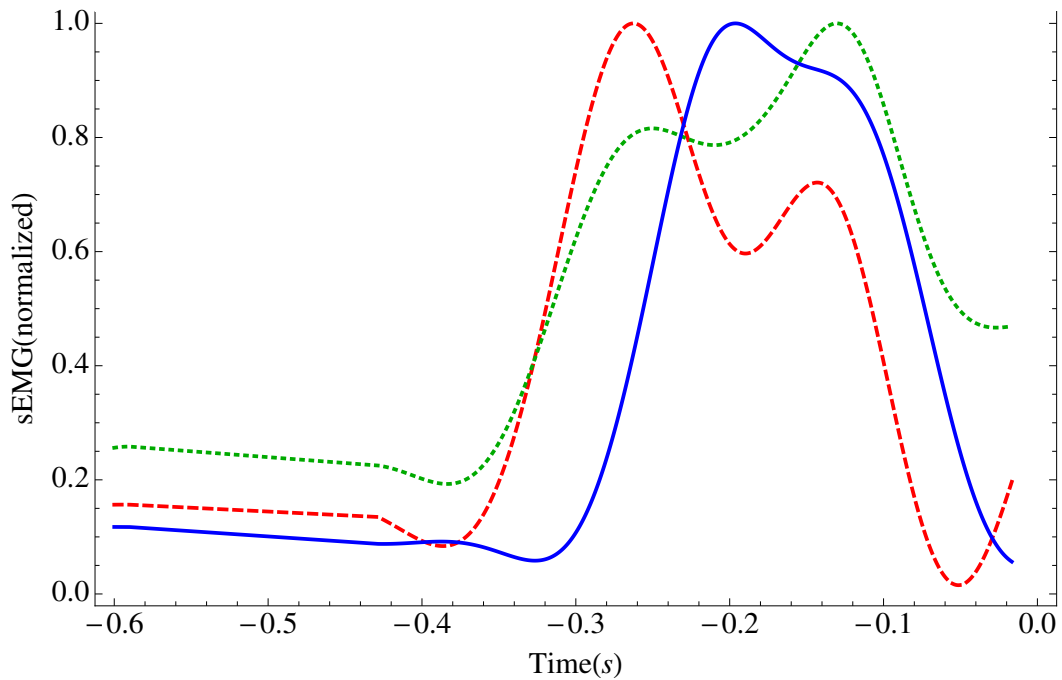


Figure 4.11: sEMG linear envelope. The signal was first Band-Pass filtered (10Hz-400Hz) then Low-Pass filtered at 7Hz. The chart shows the sEMG path of the monoarticular muscle recorded: dashed red line = gluteus; dotted green line = vastus lateralis; blue line = soleus.

4.3.3.6 Joint power output

In this thesis an inverse dynamic calculation using experimental data was not considered. As extensively reported in the current Chapter, for evaluations it was therefore decided to compare only kinematic and ground reaction force data between actual performance and models (A-B). However, by using output of

Table 4.2: Activation timing set for the squat jump matching simulation. **Model A** (A), **Model B** (B). Graphical representation is presented in Figure 4.10. *Ramp time* represents the time that the torque generator needs to reach the full activation. A proximal-to-distal activation pattern could be noticed (from the hip to the ankle).

	Ramp time	Onset time
	(ms)	(ms)
Hip A	99	0
Hip B	78	0
Knee A	171	8
Knee B	140	5
Ankle A	160	14
Ankle B	120	45

the **Model A** and the **Model B** matching simulations, it was at least possible to compare, between these two models, joint power exertion during the jump (Fig. 4.12). The **Model B** produced more power at the hip joint (peak power = 771.8 W), whilst the **Model A** was powerful at the knee (1484.8 W vs. 1175.4 W) and ankle joint (1012.7 W vs. 993.8 W). Gregoire [35] for his model stated that the monoarticular muscles (gluteus, vastus medialis and soleus) are active during all push phase, which means that they contribute power as soon as they shorten. This is what happened in this work, the only difference is that it was considered the vastus laterals instead of the vastus medialis to represent the monoarticular muscle of the thigh. However, it could be noticed that at the knee and ankle joint differences are reduced when comparing model A and B in relation to the hip joint. Now, in the future the interest would be to compare actual performance against the model by using the inverse dynamic. *Would the model be able to close predict power output at joints?* In the light of results here presented, it would be

4. Torque-driven model evaluations

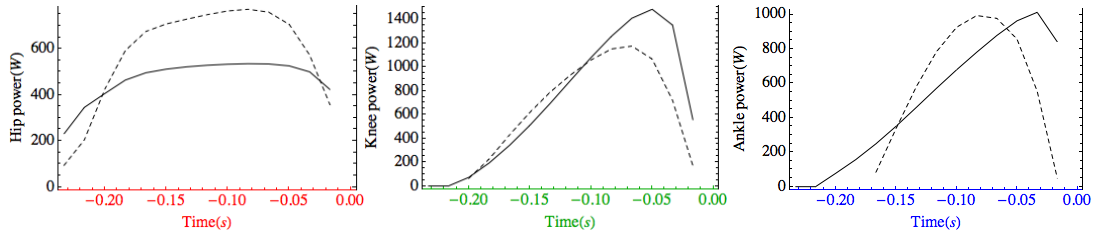


Figure 4.12: Joint power production during simulated squat jump (matching performance). Solid line = **Model A**, dashed line = **Model B**.

too ambitious to believe the model is already enough complex to make accurate predictions about joint power output (see angular velocity issues for both models A and B). At this stage of the research the model seems not able to give much support for athletes, coaches and scientists about joint power parameters, since a comparison with the actual performance is needed. In spite of this fact, the same previous results allow to think that this challenge is not an unfeasible matter: jump height is well matched, activation patterns are qualitatively comparable with sEMG, joint displacement well match actual performance. Thus, improving the accuracy of the model it may be possible to obtain interesting power output results.

In conclusion, next sections present and discuss results about matching simulations (squat jump extra load) obtained using the **Model B**.

4.4 Matching simulations for SJ with extra load

Results of the previous section based on the **Model A** were less accurate than the results of the **Model B** in relation to the actual performance (e.g. errors for jump height and angles). For this reason it seems acceptable to evaluate only the **Model B** vs. other experimental conditions: squat jump extra load (SJ+25kg, SJ+50kg). Therefore, results about squat jump +25kg extra load (SJ+25kg) and squat jump +50kg extra load (SJ+50kg) obtained from the **Model B** vs. actual performances are presented in this Chapter.

Despite the fact that SJ results (**Model B**) were presented in the previous section, some SJ result is presented again in order to allow a simplified comparison

with extra load matching performances, without the need to have a look in the previous section.

4.4.1 Jump height evaluation

The **Model B** matched well the jump height reached during the experimental session. In fact, 14.9cm and 10.8cm were the jump heights reached in the matching simulation for SJ+25kg and SJ+50kg, respectively. Therefore, for the SJ+25kg the difference in relation to the actual performance was -1.4cm and +0.4cm for the SJ+50kg. These results derived from the velocity of centre of gravity of the whole body at the instant of the toe-off: 1.709m/s, 1.455m/s were the velocity for the SJ+25kg and SJ+50kg, respectively. Table 4.3 shows the results above described (including SJ). Only these data could suggest that the heavier the extra load, the more accurate. Actually, this could not surprise since torque data were collected from dynamometry. Indeed, available experimental data ranged at slow velocities in relation to the angular velocity obtained during the squat jump at each joint (more than 500 deg·s⁻¹) [14]. Thus, since experimental data were collected up to 300 deg·s⁻¹, data fitting might be more accurate at slow velocity giving as result a strong torque generator for “slow” movements.

Table 4.3: Result of the jump height for actual performance and relative COM velocity at toe-off. **Model A** and **Model B** are shown. Differences (diff.) between the **Model A** against the **Model B** and, between the **Model B** vs. the actual (act) performance are reported. COM (centre of mass).

	COM vel. (<i>m/s</i>)	Jump Height (<i>cm</i>)	diff. (A-B) (<i>cm</i>)	diff. (B-Act) (<i>cm</i>)
bw sim A	1.790	16.2		
bw sim B	1.980	20.1	+3.9	-3.8
bw act	2.164	23.9		
25kg sim B	1.709	14.9		-1.4
25kg act	1.791	16.3		
50kg sim B	1.455	10.8		+0.4
50kg act	1.433	10.4		

Further, using a huge search space to run the simulation the chance to find

a better solution for matching performance increased. However, a substantial difference was present between the matching simulation obtained from the **Model A** and the **Model B** suggesting that the last one was more appropriate if the comparison is about jump height.

4.4.2 Kinetic evaluation

Ground reaction forces (GRF) were also compared over the duration of the propulsive phase for a given condition (Table 4.4, Fig. 4.13, Fig. 4.14, Fig. 4.15). It has to be mentioned that GRF was not include in the cost function during simulations.

GRF of the **Model B** against the actual performance gave an RMSE of 13% for the SJ+25% and an RMSE of 13.6% for SJ+50kg. Peak GRF for SJ+25kg and SJ+50kg (actual performances) was 1674N and 1797N, respectively (Fig. 4.14, Fig. 4.15). The **Model B** a peak GRF of 1788.3N for SJ+25kg and, 1887N for SJ+50kg. Thus, a difference of 6.8% and 5% was found for SJ+25kg and SJ+50kg, respectively. It is clear that the **Model B** have the tendency to overestimate the peak GRF and, as for the jump height, the heavier the extra load, the more accuracy.

Table 4.4: Data of the GRF are reported in this table for matching simulations. Result of the GRF for actual performance, **Model A** and **Model B** are shown. The RMSE was calculated over the propulsive phase of the jump in relation to the actual performance of the given condition.

Squat Jump	Peak GRF	RMSE
	(N)	(%)
bw sim A	1297	10.6
bw sim B	1632	17.1
bw act	1450	
25kg sim B	1788	13.0
25kg act	1674	
50kg sim B	1887	13.6
50kg act	1797	10.4

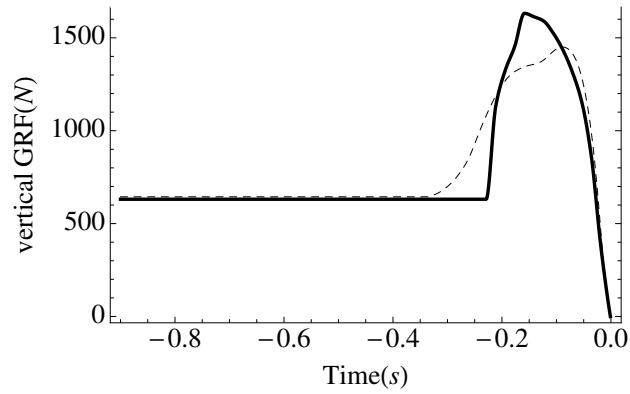


Figure 4.13: GRF for the squat jump matching simulation. **Model B** *vs.* actual performance. The matching simulation is represented by the solid line.

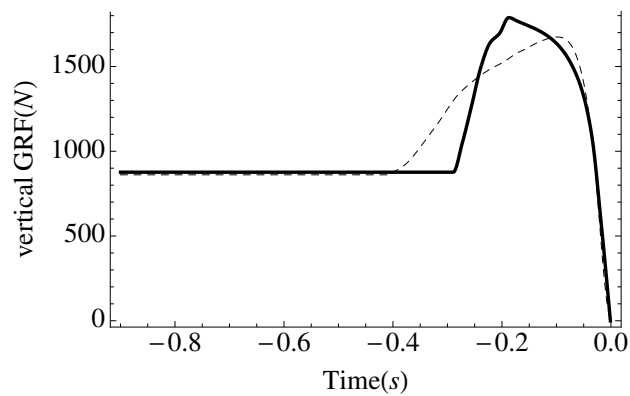


Figure 4.14: GRF for the squat jump +25kg matching simulation. **Model B** *vs.* actual performance. The matching simulation is represented by the solid line.

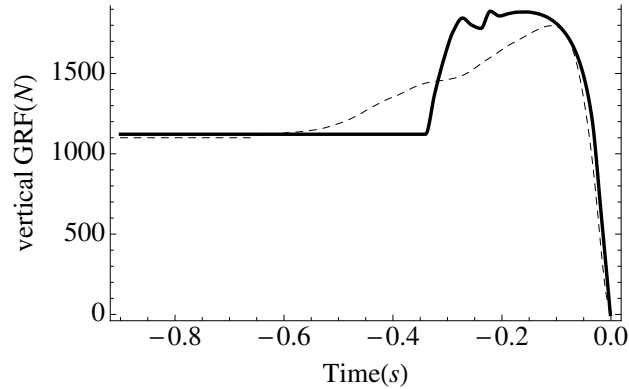


Figure 4.15: GRF for the squat jump +50kg matching simulation. **Model B** vs. actual performance. The matching simulation is represented by the solid line.

The question could be: *Why GRF are not accurately simulated?*. Allen [4] explained that in order to reproduce realistic ground reaction forces in pin-linked simulation models of jumping, a requirement for a high level of compliance (70 mm) at the foot-ground interface has been reported and attributed to a lack of wobbling masses [77]. In addition, Allen [4] concluded his study affirming that a pin-linked simulation model can reproduce realistic GRFs if additional compliance is allowed at the foot-ground interface. Any of these features was incorporated in this model, the foot-ground interface was created with a rigid polygon and a standard elastic component (flex beam) which helped the foot to only behave like humans. Therefore, it could be speculated that the collision between these rigid bodies did not help the model to reproduce with accuracy GRF. An other question is: *What is the impact of inaccuracy of GRF on measuring squat jump performance?*. At first, inaccurate GRF obviously provoke a bigger error in matching simulations, whilst global power output will suffer indirectly, since the power is the product between GRF and velocity of the centre of mass of the system. However, here GRF did not affect jump height outcomes.

4.4.3 Torque output

Matching simulations gave joint torque values. Considering all conditions (SJ, SJ+25kg, SJ+50kg), maximum torque values were obtained for the SJ+50kg

4. Torque-driven model evaluations

matching simulation (Fig. 4.16). Table 4.6 presents peak torque values expressed as percentage of the predicted maximum isometric torque (T_0 parameter) for each joint. SJ+50kg is the heavier condition and the fact that maximal torque values occurred for that condition does not surprise. However, angular velocities values at which the maximum torque occurred were surprisingly low especially for the SJ+25kg (knee, ankle joints), in relation to the SJ+50kg. One would expect similar or at least slightly differences in angular velocity values between SJ and SJ+25kg. The extra load (25kg) cannot be considered "heavy" and especially is lower than the SJ+50kg condition. Contrarily, as expected low angular velocities values at which the maximum torque occurred were found for the SJ+50kg at hip and knee joints, but not for the ankle joint. However, SJ+50kg peak torque values were 259.2N.m, 311.7N.m, 210.2N.m for hip, knee and ankle joints, respectively. Smaller peak torque values were obtained for the SJbw matching simulation: hip, knee and ankle joints gave 196.0N.m, 213.7N.m, 181.2N.m, respectively. Table 4.5 reports torque, velocity values and angle at which maximum torque occurred.

Table 4.5: Torque (τ), velocity (ω) values for matching simulations (match). Angles (θ) at which the maximal torque occurred are reported for each conditions and each joint.

	SJ match	SJ+25kg match	SJ+50kg match
Hip joint			
τ (N.m)	196.0	219.4	259.2
θ (deg)	97.5	98.0	96.5
ω (deg/s)	124.4	105.7	63.1
Knee joint			
τ (N.m)	213.7	255.5	311.7
θ (deg)	95.1	92.2	92.2
ω (deg/s)	115.2	19.8	9.4
Ankle joint			
τ (N.m)	181.2	196.6	210.2
θ (deg)	-27.1	-28.6	-26.8
ω (deg/s)	107	80.1	133.8

4. Torque-driven model evaluations

Table 4.6: Matching simulation peak torque (τ , 2 legs) expressed as the percentage of the predicted maximum isometric torque (T_0).

	SJ (%)	SJ+25kg (%)	SJ+50kg (%)
Hip joint	50.8	56.8	67.2
Knee joint	46.3	55.4	67.5
Ankle joint	29.7	32.3	34.4

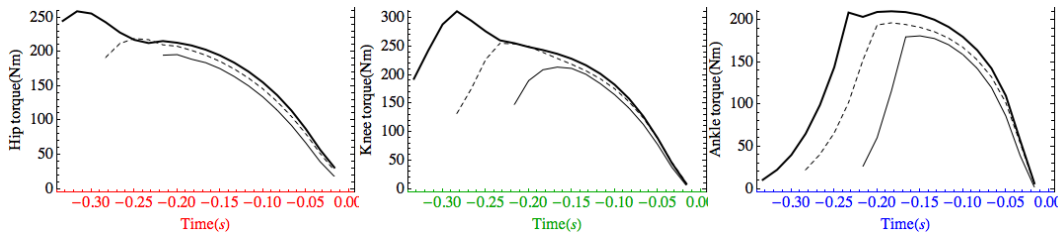


Figure 4.16: Torque output obtained from matching simulations. Thin solid line = SJ; dashed line = SJ+25kg; thick solid line = SJ+50kg.

4.4.4 Joint power output

If we look at power exertion for each joint, the SJ matching simulation gave maximal values for all joints. Table 4.7 shows complete set value for each joint and each condition. For the SJ the highest power value was obtained at the knee joint (1175.4W) which occurred at 126.1 degrees flexion with a velocity of 594.8 deg/s. The ankle joint exerted a peak power of 993.8W at -9.8 degrees (plantar flexion). Finally, the lower power output was obtained for the hip joint (771.8W). It occurred at 126.5 degrees (hip flexion) with a velocity of 384.9 deg/s. There is a tendency for which joint power output decrease as load increased. Angular velocities at which maximal power occurred ranged from 384.9 deg/sec up to 401.5 deg/sec for the hip joint. The range was 519.6 deg/sec up to 594.8 deg/sec for the knee joint and, 337.8 deg/sec up to 399.2 deg/sec for the ankle joint. However, as previously mentioned (see section 4.3.3.6) inverse dynamic calculation was not considered so that a comparison between joint power output of the model and the actual performance was not possible.

4. Torque-driven model evaluations

Table 4.7: Power (P) , velocity (ω) values for matching simulations (match). Angles (θ) at which the maximal torque occurred are reported for each conditions and each joint.

	SJ match	SJ+25kg match	SJ+50kg match
Hip joint			
P (W)	771.8	740.1	716.8
θ (deg)	126.5	137.9	141.5
ω (deg/s)	384.9	401.5	359.4
Knee joint			
P (W)	1175.4	1173.7	1155.8
θ (deg)	126.1	129.2	133.5
ω (deg/s)	594.8	540.9	519.6
Ankle joint			
P (W)	993.8	961.0	968.4
θ (deg)	-9.8	-5.9	-2.6
ω (deg/s)	399.2	360.4	337.8

4.4.5 Kinematic evaluation

Angles during the whole propulsive phase were compared to actual performances. For the SJ the **Model B** was more accurate than the **Model A** especially for the ankle joint displacement. However, for the SJ+25kg the hip (Fig. 4.17) and

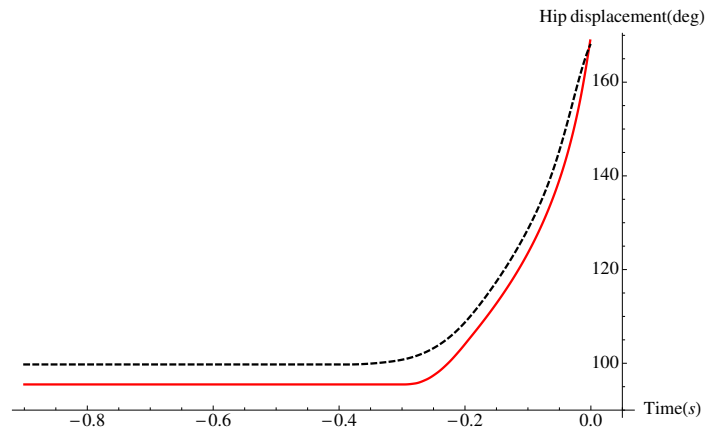


Figure 4.17: Hip displacement (SJ+25kg). Comparison between actual performance (dashed line) and simulation (solid line).

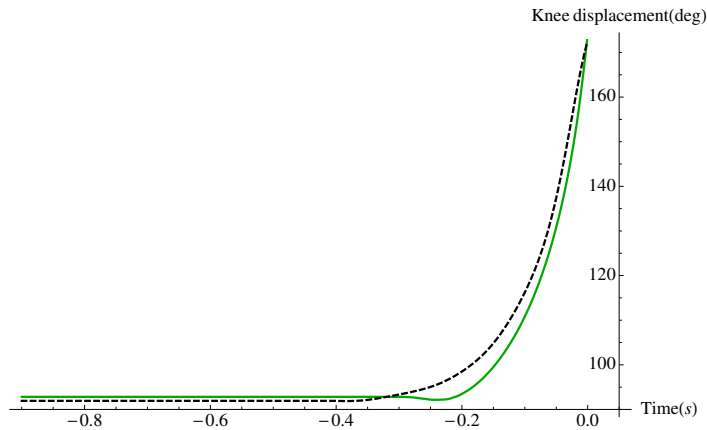


Figure 4.18: Knee displacement (SJ+25kg). Comparison between actual performance (dashed line) and simulation (solid line).

knee (Fig. 4.18) displacements were more close to the actual performance (4.4deg, 4.1deg) than the ankle (Fig. 4.19) displacement (6.4deg).

4. Torque-driven model evaluations

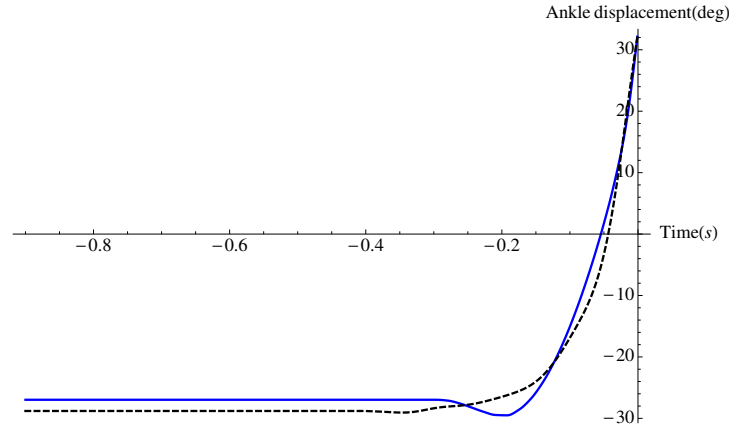


Figure 4.19: Ankle displacement (SJ+25kg). Comparison between actual performance (dashed line) and simulation (solid line).

Finally, for SJ+50kg the RMSE for the hip displacement was 5.8deg (Fig. 4.20), for the knee 5.9deg (Fig. 4.21) and 14.2deg for the ankle joint (Fig. 4.22). Considering the kinematic pattern of each joint it does not seem that the heavier, the better matched. Now if we consider that jump height is derived from the velocity of the centre of gravity at the instant of the toe-off, it does not matter how this velocity is achieved (considering only the jump height parameter). For this reason kinematic evaluation is important to establish how good is a model since joint displacements are also taken into account. One consideration is about the duration of the propulsive phase. For each condition (as for the SJ) the simulated (matching) jump was shorter than the actual performances. It seems logic that kinematics is related to the way in which the model generate movement. Either the **Model A** or the **Model B** are based on the assumption that for pure concentric movement with extra load, elastic components of the muscle-tendon complex are not crucial. This is the reason why only the contractile component was considered. However, as explained in the previous section, one reason could be that tendons might delay the transmission of the force which would mean a longer time for generating an action [69]. Here, torque generators immediately transfer energy to segments accelerating them from the very beginning of the movement. However, this issue is about physics arguments (body contacts and collisions) but they are not the goal of this work.

4. Torque-driven model evaluations

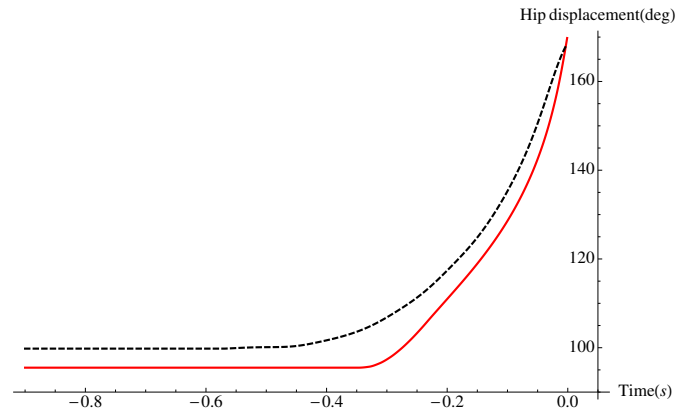


Figure 4.20: Hip displacement (SJ+50kg). Comparison between actual performance (dashed line) and simulation (solid line).

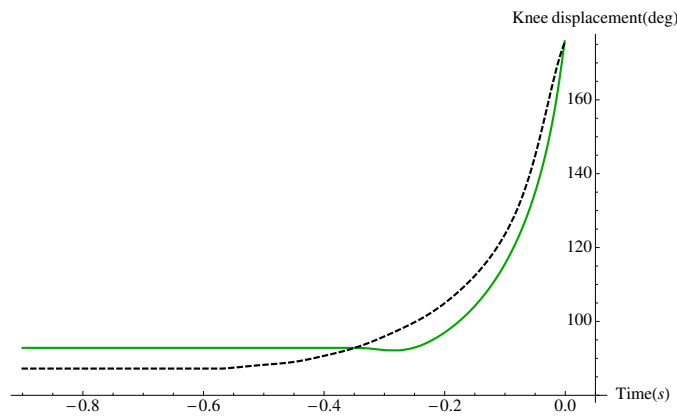


Figure 4.21: Knee displacement (SJ+50kg). Comparison between actual performance (dashed line) and simulation (solid line).

4. Torque-driven model evaluations

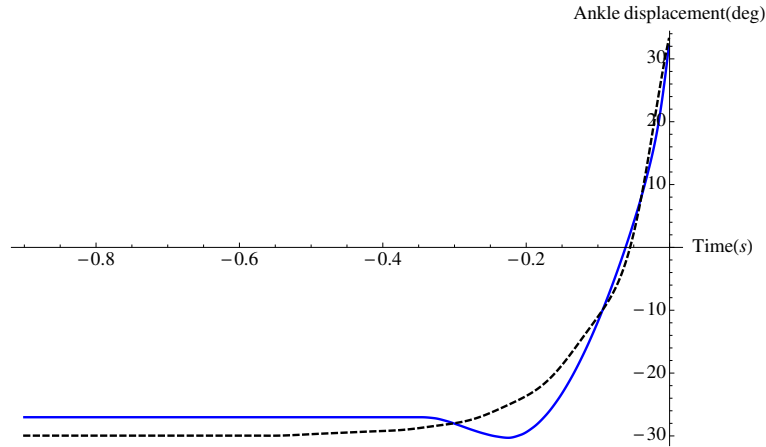


Figure 4.22: Ankle displacement (SJ+50kg). Comparison between actual performance (dashed line) and simulation (solid line).

For SJ+25kg and SJ+50kg, angular velocities at each joint are similar to the actual performances at the beginning of the movement. Differently from the actual performances, when the jump is approaching the toe-off instant, angular velocities still increase. Therefore, also for the SJ+25kg and the SJ+50kg condition, angular velocity had the same issue found for the SJ matching simulation (see Figures 4.7, 4.8 and 4.9). These results suggest a probable importance of including at least a representation of antagonist muscles in order to decrease the angular velocity when the jump is close to the toe-off phase.

Table 4.8 shows complete data about joint angles at the instant of the toe-off for all matching simulations and actual performances. In summary, the evidence is that the **Model B** better matched the actual squat jump and that RMSE for SJ+25kg and SJ+50kg were reasonable.

4. Torque-driven model evaluations

Table 4.8: Angle values (matching simulation) for each joint at the instant of the toe-off for SJ, SJ+25kg, SJ+50kg. The RMSE error refers to the whole propulsive phase comparing actual performances against the models.

	Toe-off instant (deg)	RMSE (deg)
Squat jump		
SJ act hip	168.9	
SJ act knee	173.9	
SJ act ankle	32.9	
SJ A hip	178.5	1.7
SJ A knee	179.9	3.6
SJ A ankle	19.7	30.5
SJ B hip	168.9	3.8
SJ B knee	173.9	4.5
SJ B ankle	33.6	1.9
Squat jump + 25kg		
25kg act hip	167.9	
25kg act knee	172.2	
25kg act ankle	32.9	
25kg B hip	168.9	5.1
25kg B knee	172.8	4.4
25kg B ankle	32.1	4.6
Squat jump + 50kg		
50kg act hip	168.5	
50kg act knee	175.5	
50kg act ankle	33.7	
50kg B hip	169.8	6.7
50kg B knee	175.9	6.3
50kg B ankle	33.1	3.1

4.4.6 Activation patterns for SJ extra load matching simulations

Matching simulations for SJ+25kg (Fig. 4.23) and SJ+50kg (Fig. 4.24) gave a set of activation patterns that best matched actual performances. A simple activation profile was used for the scope as for the previous matching simulation about SJ Model A vs. Model B. Actually, the magnitude of the activation could have a minimum level (equilibrium position) up to value 1. Indeed, for all simulations full activation was obtained around the 50% of the duration of the jump. After all, if the model was not allowed to reach the full activation early (especially for extra load conditions), probably it would have not jumped enough. However, this suggestion came from the analysis of the peak sEMG (rms) presented in Chapter 2 (see Page 44).

A clear proximal-to-distal sequence of muscle activation (from hip to knee to ankle) was obtained for both SJ+25kg and SJ+50kg matching simulations. This, as for the SJ matching simulation confirmed data from literature in vertical jumping simulations [14; 16; 68]. Figure 4.25 shows an overlap of the activation profile obtained during matching simulation. This allows to compare results of SJ, SJ+25kg and SJ+50kg. Table 4.9 reports activation timing data which represent the muscle coordination for matching simulation purpose.

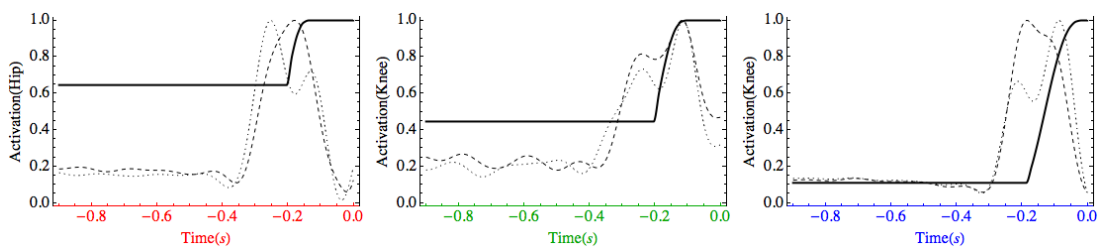


Figure 4.23: SJ+25kg activation profiles for matching simulation. Dashed lines are matching activation results, solid lines represent the jump height optimization. Thin lines are sEMG envelopes of gluteus, vastus lateralis, soleus for hip, knee and ankle joint, respectively.

4. Torque-driven model evaluations

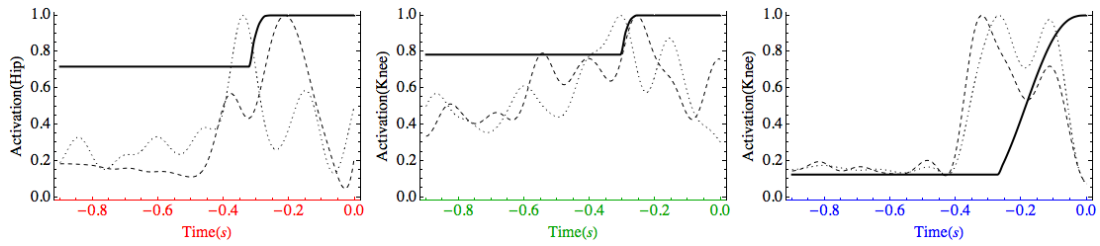


Figure 4.24: SJ+50kg activation profiles for matching simulation. Dashed lines are matching activation results, solid lines represent the jump height optimization. Thin lines are sEMG envelopes of gluteus, vastus lateralis, soleus for hip, knee and ankle joint, respectively.

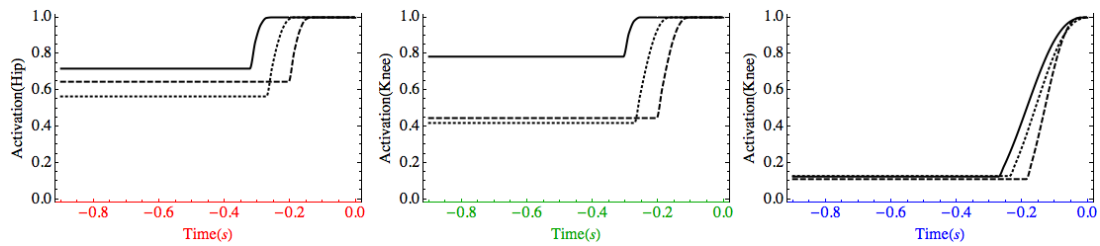


Figure 4.25: SJ+50kg activation profiles for matching simulation. Dashed lines are matching activation results, solid lines represent the jump height optimization. Thin lines are sEMG envelopes of gluteus, vastus lateralis, soleus for hip, knee and ankle joint, respectively.

Table 4.9: Activation and onset timing obtained from matching simulations for SJ, SJ+25kg and SJ+50kg.

	Ramp time (ms)	Onset (ms)
Hip joint		
SJ	78	start
SJ+25kg	102	start
SJ+50kg	76	start
Knee joint		
SJ	140	5
SJ+25kg	123	5
SJ+50kg	76	10
Ankle joint		
SJ	120	45
SJ+25kg	106	42
SJ+50kg	280	52

4.5 Summary

In conclusion of this first part of this thesis, it could be stressed that a model is able to give an acceptable representation of the reality since some important parameter of the performance investigated was well reproduced: jump height and joint displacements. This was true for the **Model B** and not for the **Model A**. However, a good mathematical representation of the torque-angle and torque-angular relationship is required if the goal is to match a specific-subject performance. In addition, a suitable solver has to be chosen to avoid a misleading solution. The simulated annealing offered a better results in finding the optimal solution as demonstrated from the onset parameters set when the **Model A** and the **Model B** are compared (Pag 91).

Next two Chapters are two accepted works for the 34th Annual International Conference of the IEEE Engineering in Medicine and Biology Society (2012) and, for the 36th annual meeting of the American Society of Biomechanics (2012). These two papers do not add extra informations with respect to the current Chapter. Some result could be slight different because for these two works simu-

4. Torque-driven model evaluations

lations were only run by using the brute-force algorithm. However, it was decided to include them, since they were about the model evaluation. The Chapter 7 will continue this first part presenting and discussing optimization results starting from matching simulations.

Chapter 5

Validation of a subject 3-actuator torque-driven model in human vertical jumping

(paper format)

G. Cimadoro, M.R. Yeadon, J. Van Hoecke, G. Alberti, N. Babault, and A.E. Minetti.

5.1 Abstract

In this study, a forward dynamic subject specific 3-actuator torque-driven model of the human musculoskeletal system was created based on measurements of individual characteristics of a subject. Simulation results were compared with experimental vertical squat jumping with and without adding weights. By analyzing kinematic and kinetic experimental data at the instant of the toe-off for the same initial conditions, it was shown that a simple computer simulation using a suitable cost function could reproduce the real task performed by humans. This investigation is the first step in a wider project that will incorporate elastic components, and that will evaluate the advantages of the individual subject approach in modeling.

5.2 Introduction

Nowadays computer simulation has been invaluable in furthering our understanding of the mechanics and physiological behavior of human movement. For example, sport scientists used simulations to better understand human motion, by optimizing sport techniques of common tasks such as walking, running, and vertical jumping [68] or even by optimizing more complex movements such as gymnastic and athletics abilities [47]. Generally, one could use two different approaches: (1) considering average muscle characteristics to provide general predictions, where the model is usually constructed from generic parameters and thus it does not represent any of the subjects it is compared against; (2) investigations based on single subject where model parameters are equal to those measured on a given subject and compared with the subjects best performance. The computational approach enables the control of many test conditions, avoiding lengthy sessions in the lab. This approach also allows to independently control the individual variables that affect performance and various training conditions.

Here, one-subjects characteristics were incorporated into simple computer simulations to address questions about his individual response to different jump conditions. The goal of this paper was to propose and validate a subject specific 3-actuator torque driven 2D jumping simulator to examine actual performance of different conditions in squat jump exercises with and without adding weights.

5.3 Methods

5.3.1 Forward Simulation Model

A subject specific whole body model was built using Working Model 2D (WM2D, Design Simulation Technologies, Inc. USA). The model consisted of four linked rigid segments representing upper body (head, trunk and arms together), thighs, shanks and feet (Fig. 6.1). Three torque generators drive simulations: hip, knee and ankle joints. The model was limited by an assumption of monoarticularity. The motivation is to create a simple model in order to investigate the macroscopic features of human performance on vertical jumping with and without adding

weights. Foot-ground interface was modeled using two linked bodies, one rigid component representing the segment of the foot from the heel to the ball and one elastic standard component of WM2D called flexbeam to represent, close to the reality, the flexion of the foot at the ball (Fig. 6.1).

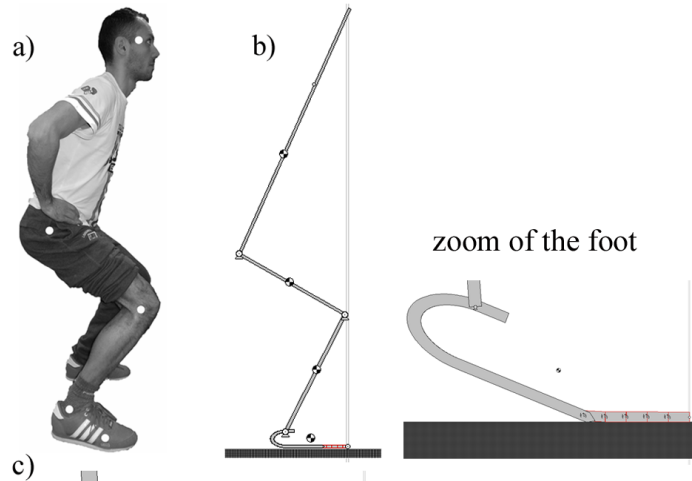


Figure 5.1: a) Subject position and markers location, b) four linked rigid segments model, c) foot details: the part from the ball to the end of tips was modeled using the flexbeam WM2D script.

5.3.2 Experimental Data

Kinematics, vertical ground reaction force (GRFz) and surface electromyography (sEMG) data were synchronized and collected for a series of bilateral jumps by an individual male athlete (29yrs, 1.74m, 63Kg) and the best performance in terms of jump height was analyzed for each condition. The participant was asked to perform three different types of squat jumps starting from approximately 1.57 rad posterior knee joint angle:

- Maximal height squat jump body weight (SJbw)
- Maximal height squat jump with an added 40% of the body weight ($SJ_{+40\%}$)
- Maximal height squat jump with an added 80% of the body weight ($SJ_{+80\%}$)

Kinematics were collected using a Vicon Nexus motion analysis system (Oxford Metrics, Oxford, UK) sampling at 120 Hz. Markers were placed on the right side of the body on head temple, greater trochanter, malleolus and foot ball. Raw data were low pass filtered at 6Hz using a 4th order zero lag butterworth filter according to Winter recommendations [91]. GRFz data were recorded using Kistler platform sampling at 960Hz and raw data were filtered using a 4th order zero lag butterworth low pass filter at 3Hz. sEMG activities (SMART-BTS, Milan, Italy) were recorded (960 Hz frequency) on the subject's right side for the tibialis anterior (TA), soleus (SOL), gastrocnemius medialis (GA) rectus femoris (RF), vastus lateralis (VL), the biceps femoris long head (BF) and gluteus (GL). The skin was shaved and cleaned with alcohol to ensure low impedance. The interval between electrodes was 2 cm. In accordance with the recommendations of International Society for Electromyography and Kinesiology [56], raw sEMG signals were first bandpass filtered between 10 and 400 Hz and then full-wave rectified and filtered using a 10Hz low-pass filter to obtain a linear envelope. Maximum torque (T, N.m) profiles of the hip, knee extensors, and ankle plantar flexors were determined via isokinetic dynamometer (Biodex,USA) at different angles (θ , rad) and concentric angular velocities (ω , rad/s). Positional data were also corrected to ensure real bone alignment [80].

5.3.3 Muscle Model

Muscle-tendon complex (MTC) is generally categorized into a three-component assembly: series elastic element (SEE), contractile component (CC) and parallel elastic elements (PEE). Muscle force is governed by two relationships: (1) muscle tension increase and decrease depending on fibre length that is known as a parabolic length-tension relation [48]; (2) muscle tension decreased as the velocity of shortening increased generating a relation know as tension-velocity [38]. However, according to the nature of the squat jump and, especially a squat jump with added weight, the model considers only CC, in order to simplify its conception. In our model CC is represented by rotational actuators, and the converted features are torque-angle (T, θ) and torque-angular velocity (T, ω) relationships at hip, knee and ankle joints.

5.3.4 Model Input Data

Torque data were fitted [95] using a 4-parameter hyperbolic function for the concentric phase between T and ω (Equation 5.1), where T_0 is the isometric torque, ω is the angular velocity, ω_{max} is the angular velocity at which the curve reaches zero torque, and ω_c defined by the vertical asymptote $\omega = -\omega_c$ of the classic Hill hyperbola.

$$T(\omega) = \frac{C}{(\omega_{con} + \omega)} - T_c \quad (5.1)$$

$$C = T_c \cdot (\omega_{max} + \omega_c)$$

$$T_c = T_0 \cdot \frac{\omega_c}{\omega_{max}}$$

The torque-angular relationship was represented by a nonlinear quadratic function [48; 95] showed in Equation 5.2, where k_2 = width curve, θ = angle, θ_{opt} = optimal angle

$$T_\theta = 1 - k_2 \cdot (\theta - \theta_{opt})^2 \quad (5.2)$$

Active state, i.e. muscle activation (recruitment and firing rate of alpha-motoneurons), even when maximal is never instantaneous and was controlled in the model by a simple activation ramp function showed in Equation 5.3. Therefore, the fraction of torque, which can be exerted at any time t , is determined by multiplying the maximal torque calculated from the torque generator parameters by an activation Act . Each activation profile ramps were forced not to exceed the range between 0 and 1 (see appendix section Fig. 6.3). Detailed information is described elsewhere [95].

$$Act = 0 + (z)^3 \cdot (6z^2 - 15z + 10). \quad (5.3)$$

$$z = \frac{t - d}{r}$$

Where t is time, d is the delay of activation between joints and r is the rise time for building force. The optimal solutions that best matched a subjects actual SJbw, SJ+40% and SJ+80% were calculated with a brute-force optimization algorithm using a cost-function to minimize SIM vs actual performance (Equation 5.4) including hip, knee and ankle angles and the vertical velocity of the hip at toe-off for the SJbw and adding the vertical velocity of the barbell for the SJ+40% and SJ+80%. For the velocity at toe-off a value for the weighting (50) was decided as 0.17 rad angle equivalent to 0.2m/s velocity error (Equation 5.5).

$$S = \sqrt{\frac{\sum_{i=1}^n (si - ai)^2}{n}}. \quad (5.4)$$

$$S = 50 \cdot \sqrt{\frac{\sum_{i=1}^n (si - ai)^2}{n}}. \quad (5.5)$$

Where S is score; si is value of variable i from simulated performance; ai is value of variable i from actual performance and n is number of variables in objective function part. The brute-force algorithm was set using five variables: Hr (hip ramp force), Kr (knee ramp force), Ar (ankle ramp force), Kd (knee onset), Ad (ankle onset). Ramp force variables were allowed to vary in a range between 0.090s and 0.284s, onset variables between 0 and 0.020s.

5.4 Results

Quantitatively, the model corresponds well to real jump conditions. SIM gave a set of activation patterns that best matched actual performances (Table 5.1). A proximal-to-distal sequence of muscle activation (from hip to knee to ankle) confirmed data from literature [68]. Joint displacements from the start position

to the instant of the toe-off showed a good correspondence.

SIM conditions	Activation parameters t(s)				
	Hr	Kr	Ar	Kd	Ad
SJbw	0.101	0.176	0.154	0.005	0.012
SJ+40%	0.091	0.166	0.136	0	0.006
SJ+80%	0.093	0.091	0.108	0.002	0.003

Table 5.1: Data set obtained from matching simulation at 60Hz for SJbw , SJ+40% and SJ+80%. Hr, Kr and Ar are the rise time for building torque of hip, knee and ankle joints respectively. Kd and Ad are the onset delay of the knee and the ankle joints with regard to the hip joint.

Actual	GRFz	Jump height	Propulsive phase
	Peak (N)	Height (m)	Time (s)
SJbw	1450	0.239	0.334*
SJ+40%	1674	0.163	0.401*
SJ+80%	1797	0.104	0.568*

Table 5.2: Jump height was calculated using the flight time method; * the start of the propulsive phase was located when the force value was greater than three time the deviation standard of the average value of the start equilibrium position before to jump.

SIM	Peak	RMSE	Height	Error	Time	Error
	(N)	(%)	(m)	(%)	(s)	(%)
SJ+bw	1297	15.3	0.162	32.2	0.260	22.1
SJ+40%	1537	18.9	0.100	38.6	0.310	29.4
SJ+80%	1610	9.8	0.072	30.8	0.426	25

Table 5.3: Jump height was calculated using the flight time method. RMSE % is calculated with respect to the average vertical GRF.

Kinematic data (θ) at the instant of toe-off are shown in the appendix section (Table 5.4). However, quantitatively the general tendency of all SIM conditions was to underestimate actual performances:

5.4.1 Squat Jump bw

Jump height of the SIM SJbw was 32.2% lower than the actual SJbw, SIM SJbw propulsive phase was 22.1% lower than the real propulsive phase, the RMSE expressed as percentage (%), of the peak GRFz, was 15.3% (Table 5.2 - 5.3).

5.4.2 Squat Jump +40%

SIM SJ+40% showed the greater percentage error compared with its actual performance between all three conditions. Jump height of the SIM SJ+40% was 38.6% lower than the actual SJ+40%, SIM SJ+40% propulsive phase was 29.4% lower than the real propulsive phase, the RMSE (%), of the peak GRFz, was 18.9% (Table 5.2 - 5.3).

5.4.3 Squat Jump +80%

The RMSE (%), of the peak GRFz for the SIM SJ+80% was 9.8%, the lower error between GRFz over all conditions (Fig. 6.1). Jump height difference of 30.8% also was the lower difference for jump height between all conditions. Finally the SIM SJ+80% propulsive phase was 25% lower than SJ+80% (Table 5.2 - 5.3).

5.5 Discussion

The purpose of this work was to create a model and compare it with a specific subject for testing its validity. Although we built a simple model, according to other musculoskeletal models, a proximo-distal activation sequence was observed [68]. The corresponding result of SIM GRFz (Fig. 6.2) showed a good matching. However, in all simulations the propulsive phase was faster than in reality. This could be explained by the lack of SEE structures in the model. They generally slow down the rise up of the force [49], which is useful to produce more muscle power

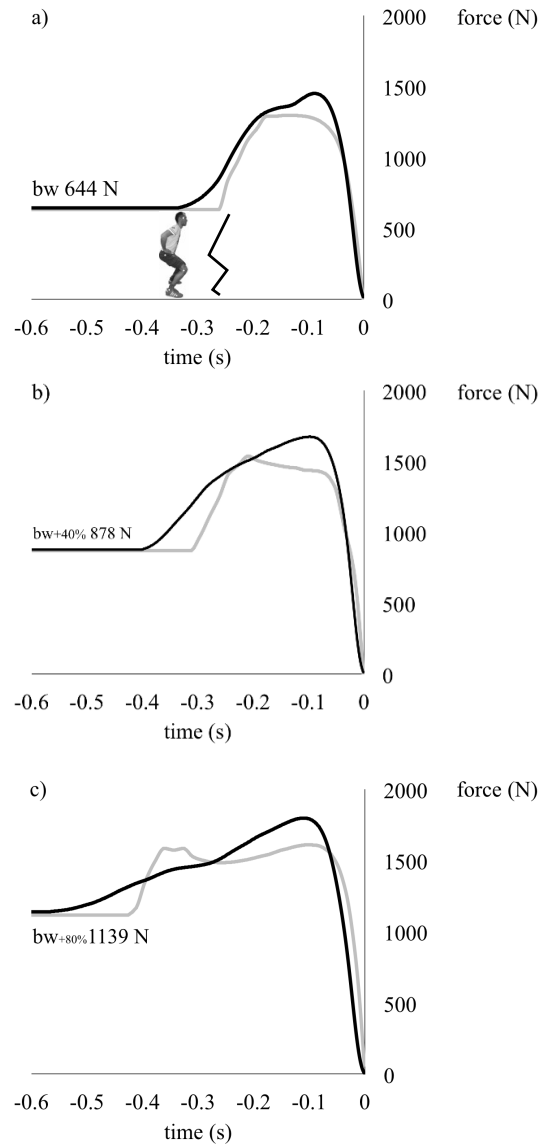


Figure 5.2: Vertical ground reaction force curves. Black line is the actual performance, gray line is the SIM. a) SJbw, b) SJ+40%, c) SJ+80%. Subject picture and stick diagram, in the a panel, show the starting position for actual and SIM performance, respectively. The subject picture and the stick diagram are synchronized with the instant of the propulsive phase start. 0 = instant at the toe-off.

since the beginning of the movement occurs at low velocity when the muscle is stronger. That could be the reason why the peak GRFz of all SIM occurs earlier than reality and lower jump heights were obtained. Also, we did not include biarticular muscles in the model. It has been shown that biarticularity is crucial in order to achieve an optimal jump height in modeling. Not taking that into account could result in less than 50% of the actual jump height [68]. In contrast with that prediction, our model was able to achieve more than the 61% for all SIM conditions with regard to the actual performance. Further, the SIM SJ+80% was the more accurate condition, showing that the heavier the barbell weight, the more accurate the model. However, the simulator is strongly influenced by input data, and it is possible that the subject used in this study was more familiar and capable to express his strength limits during dynamometer testing sessions. In summary, a specific 3-actuator torque driven model could be a successful tool to investigate and determine different training strategies of a single athlete, since it represents specific muscle characteristics of the subject. This is the main important feature of this model, as it could potentially predict squat jump (with and without weights) performances. Here, we considered just concentric movements; we are currently working on a set of experiments and simulations on large applications to confirm the preliminary data presented in this paper. However, this model is a first step of an extensive project about modelling applied to strength and conditioning performance. The next challenge now is to validate a further developed jumping model including eccentric, isometric and concentric phases, with the presence of elastic structures.

5.6 Acknowledgment

The authors would like to thank Petar Bozadzhiev, Yves Ballay, Matt Pain, Glen Blenkinsop for their contribution to experiments.

5.7 Appendix

Jump height was calculated using the fly time method, which is described in Equation 5.6 where v is the velocity at the toe-off instant, g is 9.81 and t_{flight} is

the fly time phase in seconds.

$$v = \frac{g \cdot t_{flight}}{2} \quad (5.6)$$

		Start position Θ (rad)		Toe-off instant Θ (rad)	
		actual	SIM	actual	SIM
SJbw	Hip	1.58	1.58	2.95	3.12
	Knee	1.55	1.55	3.05	3.14
	Ankle	-0.49	-0.49	0.60	0.34
SJ+40%	Hip	1.73	1.73	2.93	2.83
	Knee	1.61	1.61	3.01	3.14
	Ankle	-0.48	-0.48	0.56	0.30
SJ+80%	Hip	1.74	1.74	2.94	3.01
	Knee	1.51	1.51	3.06	3.14
	Ankle	-0.53	-0.53	0.58	0.32

Table 5.4: Data set obtained from matching simulation at 60Hz for SJbw, SJ+40% and SJ+80%. Hr, Kr and Ar are the rise time for building torque of hip, knee and ankle joints respectively. Kd and Ad are the onset delay of the knee and the ankle joints with regard to the hip joint.

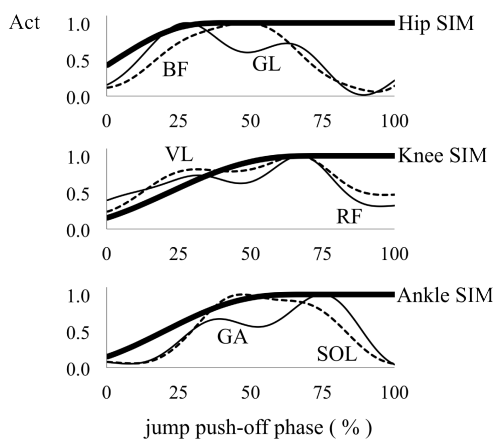


Figure 5.3: Activation profiles example (SJbw). Bold lines represent SIM results. Activations are shown as function of percentage jump push-off phase. Toe-off = 100%. (GL, BF, RF, VL, GA, SOL = sEMG envelopes low-pass filtered at 7Hz).

Chapter 6

Comparison between squat jump *vs.* weighted squat jump: simulation study

(paper format)

Giuseppe Cimadoro, Alberto Minetti, Matt Pain, Jacques Van Hoecke, Giampiero Alberti, Nicolas Babault, Fred Yeadon.

6.1 Introduction

Computer simulation has been used in sport science to better understand human motion, by optimizing sport techniques of common tasks such as walking, running, and vertical jumping [68]. Biomechanical models often use average muscle characteristics to provide general predictions. In this process the model is usually constructed from generic parameters and thus the model does not represent any of the subjects it is compared against and may not even represent an average of the subjects. An alternative is to use subject specific models where model parameters are equal to the same parameters measured on the subject, and compare a simulation to the single subject performance. Here one-subjects characteristics were incorporated into computer simulations that were used to address questions about his individual response to different jump conditions. From a mechanical

point of view, vertical jumping can be compared to an inverted pendulum and, many authors have investigated neuromuscular function in a computational way using different kind of software packages to explore neuromechanical perspectives in the study of jumping. The aim of this study was to examine differences in technique between a squat jump and a squat jump with added weight by utilizing a subject specific model implemented in Working Model 2D©.

6.2 Methods

A subject specific four segment whole body model was constructed using Working Model 2D©. An individual male athlete performed body weight squat jumps (SJbw) and squat jumps with an added 40% of body weight (SJ+40%). Anthropometric characteristics were calculated from the subject according to Chandler (1975) [20]. Maximum torque (T, N.m) profiles of the hip and knee extensors, and ankle plantar flexors were determined via dynamometer measurements (Biodex©,US) at different angles (θ , deg) and concentric angular velocities (ω , deg/s), coupled with force plate isometric corrections to the ankle torques. Positional data were also corrected to ensure real bone alignment. Torque data

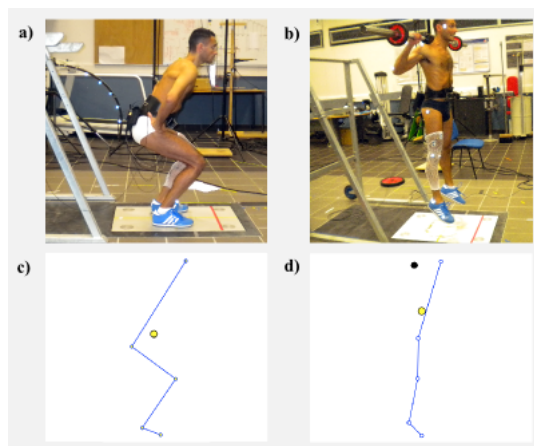


Figure 6.1: a) SJbw start position; b) Subject performing SJ+40%; c) and d) stick models, SJbwstart position and SJ+40% fly phase.

were fitted with a 4-parameter hyperbolic function and neuromuscular activa-

tions were represented using a quintic function [95]. Kinematic and force plate data from a subject were obtained for matching purposes (Fig. 6.1). The optimal solutions that best matched a subjects actual SJbw and SJ+40% were calculated with a brute-force optimization algorithm using a cost-function including hip, knee and ankle angles and the vertical velocity of the hip at toe-off for the SJbw and adding the vertical velocity of the barbell for the SJ+40%.

6.3 Results and discussion

SIM gave a set of activation patterns (Table 6.1) that best matched actual performances. A proximal-to-distal sequence of muscle activation (from hip to knee to ankle) confirmed data from literature [68]. Height jump was 0.24m (SJbw),

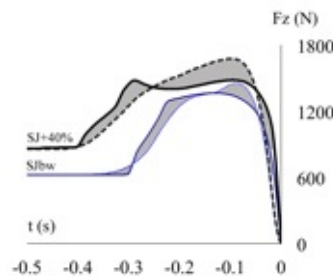


Figure 6.2: Vertical component of the ground reaction force: SJbw *vs.* SIM SJbw, RMS error=6.5%; SJ+40% *vs.* SIM SJ+40%, RMS error=9.8%. Solid lines=actual jumps; dashed lines=SIM. Shaded area represents difference in relation to the net impulse.

0.21m (SJbwSIM), 0.16 (SJ+40%), 0.15 (SJ+40%SIM). The SJbw vertical GRF peak was 1450N *vs.* 1361N SJbwSIM, (SJbw +6.14%); SJ+40% gave 1674N *vs.* 1482N SJ+40%SIM (SJ+40% +11.5%); (Fig. 6.2). Net power was calculated for SJbw 955W *vs.* SIM SJbw 798W (SJbw +16.4%) and, SJ+40% 999W *vs.* SIM SJ+40% 856W (SJ+40% +14%). Mechanical energy was greater for both actual jumps with regard to simulations, data are shown in Table 6.2. Rectified sEMG (Fig. 6.3), showed that the model should take into account activation decrease, in fact SIM GRF with full activation are both greater than actual jumps close to toe-off phase.

Data/Joints	Hip	Knee	Ankle
SJbw Opt_{ramp} (s)	0.099	0.171	0.160
SJbw Opt_{onset} (s)	-	0.008	0.014
SJ+40% Opt_{ramp} (s)	0.075	0.164	0.136
SJ+40% Opt_{onset} (s)	-	0.003	0.007

Table 6.1: Data set obtained from matching simulation at 60Hz for SJbw and SJ+40%

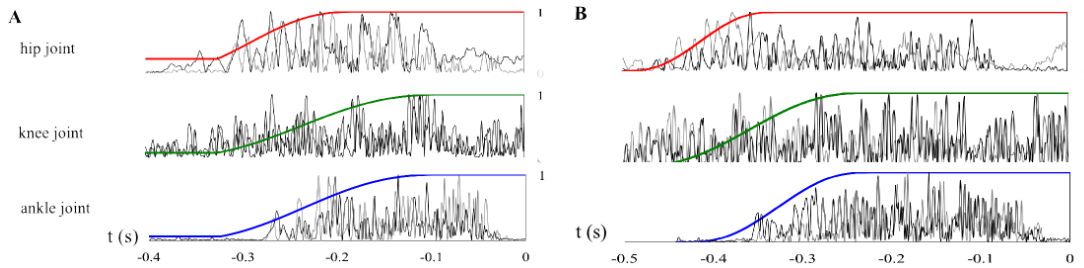


Figure 6.3: Activation function compared with normalized rectified sEMG. A) SJbw chart; B) SJ+40%. 0=Toe-off.

Parameters	SJbw	SIM SJbw	SJ+40%	SIM SJ+40%
Hip (θ , deg)	169.3	166.2	167.9	145
Knee (θ , deg)	174.5	173.9	172.2	158.4
Ankle (θ , deg)	34.2	34.8	31.9	35.1
Hip (Y vel.,m/s)	2.38	2.285	2.067	1.910
Barbell (Y vel.,m/s)	-	-	2.216	1.999
Ek (J)	148	131	142	132
Ep,g (J)	945	676	1100	1066
Ek + Ep,g (J)	1093	807	1242	1198

Table 6.2: Parameters at the instant of the toe-off for both SJbw and SJ+40%.

6.4 Conclusions

Further investigations to improve the accuracy of the current model are strongly recommended to make predictions more precise.

Chapter 7

Model optimization - predictions: results and discussion

7.1 Squat jump optimization

In mathematics and computer science, an optimization is the selection of a best element (with regard to some criteria) from some set of available alternatives. Here, optimization refers to the capacity of the model to maximize the jump height. The latter is the cost function that will be maximized by a specified solver. Briefly, we want to know whether the model (which was tested against actual performances) is able to jump more than in matching simulation, without kinematic constraints. It has to be reminded that in matching simulation, the model want to match the actual performance in order to evaluate whether we can consider the model a good representation of the reality. Therefore, once the model has been evaluated, it can take the place of the subject. This allow to test whether the subject was operating sub-maximally or not. Further, the model is able to predict what would happen by changing initial conditions.

In optimized performance, any kinematic constraint was used. Consequently, the model was able to jump freely in the space to see whether the jump height could be increased. However, in order to avoid unlikely human movements, some penalties were established: the model could not jump breaking anatomical constraints. The hip and knee joints could extend up to 180 degrees. The ankle joint

7. Model optimization - predictions

had a range of movement of 80 degrees, starting from -40 degrees (dorsi flexion) to 40 degrees (plantar flexion). In order to be sure that *wrong simulations* were not considered, if the model broke these constraints, then a penalty gave the jump height 10 cm lower than the original simulation jump height result.

The parameters governing activation were the initial activation, the rate of increase in activation (ramp time) and the time at which activation started to ramp (onset). The ramp function at each jump was allowed to ramp up once only in the simulation and when at the maximum level, remained there until the end of the simulation. Activation could be a minimum of 0.001 (initial activation), not zero, as this produced errors in the mathematical calculations of torque, and a small activation such as this would be a realistic lower bound. The maximum activation was set as 1.0 (full activation). The time for activation to ramp from zero to 1.0 (rate of increase in activation) was given a lower bound of 70 ms [18]. Upper limits for the ramp time were set loosely to minimise the search space, typically of the order of 350 ms, and were selected based on a manual approach of selecting parameters which could produce similar jump kinematics. Boundaries are showed in Table 7.1. Onset time could be a minimum of 0 up to 56 ms based on sEMG experimental finding (see Page 80).

Table 7.1: Parameter boundaries used to optimize squat jump conditions by using the simulated annealing algorithm.

	Ramp Time		Onset Time	
	Lower Bound (ms)	Upper Bound (ms)	Lower Bound (ms)	Upper Bound (ms)
Hip joint	70	350	0	56
Knee joint	70	350	0	56
Ankle joint	70	350	0	56

As for matching performance the simulated annealing was used to find the optimal solution. The initial temperature was set at 10 whilst the cooling rate decreased of 20% at each temperature iteration. For each temperature 300 iterations were run and the solver converged to the optimal solution after 7h performing 42 temperature iterations. Each iteration took about 2 s. Subsequently, starting from the optimal solution, an other simulation was run to be sure that the solver

was not able to find a better solution. Otherwise, the new optimal solution was finally considered. This method was used for all optimized simulations.

7.1.1 Jump height performance optimized for SJ, SJ+25kg and SJ+50kg

Figure 7.1 shows the jump height tendency under different extra load conditions between matched (SJ, SJ+25kg, SJ+50kg) and optimised simulations. As expected the heavier, the lower COM velocity at the toe-off. The latter is completely in accord with the theoretical tension-velocity relationship [38].

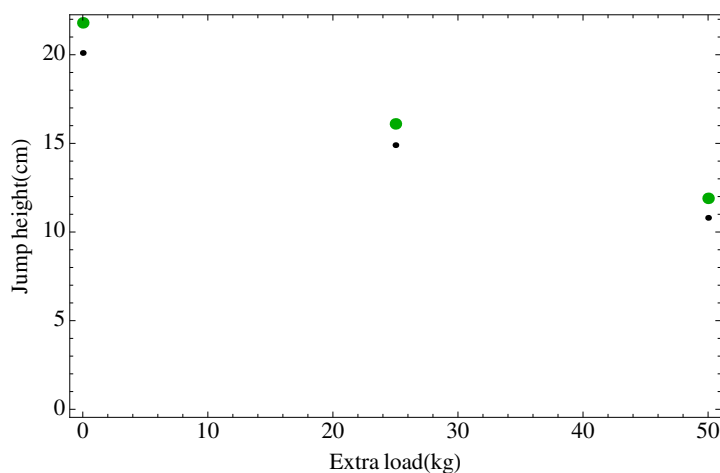


Figure 7.1: Jump height differences between matching and optimized simulations for SJ, SJ+25kg and SJ+50kg. Large points represent optimized jump heights, whilst small points represent jump height output in matching simulations. These data suggest that the jump height was not maximal in matching simulations.

The jump height (h) performance comes from knowledge of the velocity of jumper's COM velocity at the instant of the toe-off. By applying the law of conservation of mechanical energy, a relation between jump height and COM velocity at the toe-off can be obtained. The mechanical energy of the jumper is the sum of the kinetic energy and gravitational potential energy. In vertical jumping the effect of air resistance is negligible. The mechanical energy of the jumper at one instant is therefore the same as the mechanical energy at any other

7. Model optimization - predictions

instant. We consider the changes in mechanical energy between the instant of toe-off and the instant the jumper reaches the peak of the jump [50]. Therefore, equation 7.1 was used to obtain jump heights:

$$h = \frac{v^2}{2 \cdot g} \quad (7.1)$$

where \mathbf{h} is the jump height, gravity is represented by \mathbf{g} and \mathbf{v} is the COM velocity at the toe-off.

The improvement in the jump height from the matched simulations to the optimized simulations came from different activation patterns (Table 7.2). The

Table 7.2: Optimized activation patterns for SJ, SJ+25kg and SJ+50kg. Match = matching simulation; Opt = Optimized simulation.

	Jump Height (cm)	Hr (ms)	Kr (ms)	Ar (ms)	Ht (ms)	Kt (ms)	At (ms)
SJ Match	20.1	78	140	120	0	5	45
SJ Opt	21.8	75	129	106	0	5	50
SJ+25kg Match	14.9	102	123	252	0	5	42
SJ+25kg Opt	16.1	113	137	185	0	11	43
SJ+50kg Match	10.8	76	76	280	0	10	52
SJ+50kg Opt	11.9	91	77	229	0	21	40

tendency is that ramp time at each joint decreases with respect to the matching performance and onset time increases between joints. This control strategy was already noticed in a study about the sensitivity of vertical jumping performance to changes in muscle activation onset [16]. In this research, it was showed that jump height is sensitive to errors in the delay between activation onset times of plantar flexors [16]. In relation to this thesis, it could be stated that data confirming previous data in the literature, but in addition it was found that when ramp time decreased, onset time increased except for 50kg ankle joint condition (Table 7.2, optimized performance). The importance of coordination in explosive jumps was also demonstrated in an other study that showed how a premature activation of soleus has a dramatic effect on vertical jumping performance [52]. However, further simulations (comparing matching simulation vs. optimized simulation)

should be performed to better understand the control strategy in squat jump with extra load. Indeed, here the goal was to simulate only 2 different extra loads so that future simulations (with other different extra loads) could help to obtain more informations.

7.1.2 Activation patterns optimized

Data mentioned in the previous section (Table 7.9) anticipated the role played by activation timing and sequences to optimize the vertical velocity of the centre of gravity of the system in order to maximize the jump height for each squat jump condition. Graphic activation profile time histories give a clear idea about optimized simulation in relation to activation timing and joint onset. Figures 7.2, 7.3, 7.4 show the activation profile time history of the SJ, SJ+25kg and SJ+50kg, respectively.

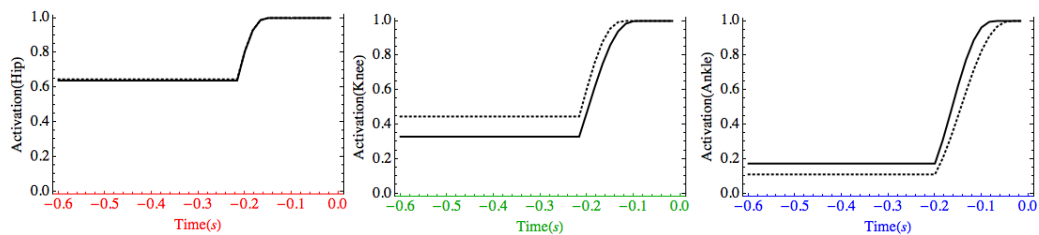


Figure 7.2: Activation profiles time history of the squat jump. The dotted line is the matching performance whilst the continuous line is the optimized performance. This condition shows slightly differences between the matching and the optimized performance.

The result of the activation patterns is strongly influenced by the algorithm search method used during optimization process. In this work the simulated annealing algorithm was used and it was set according to the explanation gave in the section 7.1. Since the SA has a randomized nature, if the number of iterations at each temperature is big enough to analyze many solutions, the final result should be the global optimum. However, WM2D software is a graphic-numeric based computation package in which it was implemented the SA to search the activation patterns optimum. Consequently, there was an high computational time cost issue because of graphical-numerical computation. This is the reason why

7. Model optimization - predictions

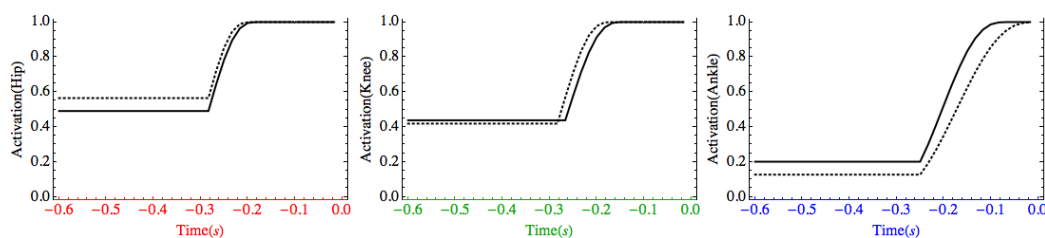


Figure 7.3: Activation profiles time history of the squat jump with 25kg extra load. The dotted line is the matching performance whilst the continuous line is the optimized performance. This condition shows slightly differences between the matching and the optimized performance.

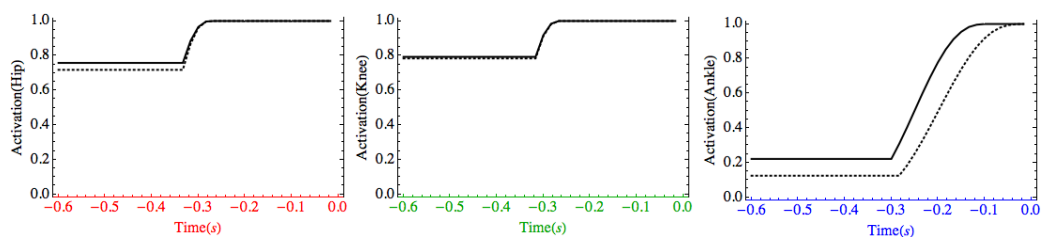


Figure 7.4: Activation profiles time history of the squat jump with 50kg extra load. The dotted line is the matching performance whilst the continuous line is the optimized performance. For each joint the ramp time obtained from the optimized performance is slower than in the matching performance profiles.

7. Model optimization - predictions

300 iterations at each temperature state were performed which could give a local optimum for some optimized condition. It was assumed that optimal solutions were found. Therefore, the number of iterations was chosen to get the result in a reasonable time.

7.1.3 Torque output

Torque output for optimized simulations are shown in Table 7.3 and compared with matching simulations from SJ, SJ+25kg and SJ+50kg.

Table 7.3: Peak torque (τ) for matching and optimized simulations (match, opt). Angles (θ) and velocity (ω) at which the maximal torque occurred. Match = matching simulation; opt = optimized simulation.

Hip joint		SJ	SJ+25kg	SJ+50kg
match	τ (N.m)	196.0	219.4	259.2
opt	τ (N.m)	203.5	243.8	256.6
match	θ (deg)	97.5	98.0	96.5
opt	θ (deg)	102.7	101.1	104.4
match	ω (deg/s)	124.4	105.7	63.1
opt	ω (deg/s)	175.7	110.1	105.2
Knee joint				
match	τ (N.m)	213.7	255.5	311.7
opt	τ (N.m)	214.4	256.1	303.3
match	θ (deg)	103.4	92.2	92.2
opt	θ (deg)	95.0	98.1	91.1
match	ω (deg/s)	115.2	19.8	9.4
opt	ω (deg/s)	106.3	45.9	10.5
Ankle joint				
match	τ (N.m)	181.2	196.6	210.2
opt	τ (N.m)	188.7	212.0	234.6
match	θ (deg)	-27.1	-28.6	-26.8
opt	θ (deg)	-25.1	-28.0	-30.3
match	ω (deg/s)	107.0	80.1	133.8
opt	ω (deg/s)	189.0	103.9	18.2

7. Model optimization - predictions

The optimized models showed that a greater peak torque was used as the extra load increased. The peak torque for the SJ was 52.7%, 46.4%, 30.9% for the hip, knee and ankle joints, respectively. The SJ+25kg gave a peak torque of 63.2%, 55.5% and 34.7% for the hip, knee and ankle joints, respectively. The last simulated condition (50kg) gave a peak torque of 66.5%, 65.7% and 38.4% for the hip, knee and ankle joint, respectively. Table 7.4 shows peak torques for each condition and each joint compared with the correspondent matching simulation.

Table 7.4: Peak torque (τ) for matching and optimized simulations expressed as percentage of the predicted maximum isometric torque at each joint (T_0). Match = matching simulation, Opt = optimized simulation.

		SJ	SJ+25kg	SJ+50kg
		(%)	(%)	(%)
match	τ	50.8	56.8	67.2
opt	τ	52.7	63.2	66.5
match	τ	46.3	55.4	67.5
opt	τ	46.4	55.5	65.7
match	τ	29.7	32.3	34.4
opt	τ	30.9	34.7	38.4

7.1.4 Joint power output

Power in mechanical systems is the combination of forces and movement. In particular, power is the product of a force on an object and the object's velocity, or the product of a torque on a shaft and the shaft's angular velocity. Mechanical power is also described as the time derivative of work. Instantaneous power is given by force times velocity. However, in rotational systems power is the product of the torque τ and angular velocity ω (Eq. 7.2):

$$P(t) = \tau \cdot \omega \tag{7.2}$$

where ω measured in radians per second and the unit of measure is Watt (W).

7. Model optimization - predictions

However, power is a parameter often used in the field by trainers, especially in power sports (athletics, powerlifting, etc.). Simulations allowed to estimate the global power for each given extra load condition. At first a theoretical model of the available power at each joint was created by using Equation 7.2. These models are showed in Figure 7.5, Figure 7.6, Figure 7.7.

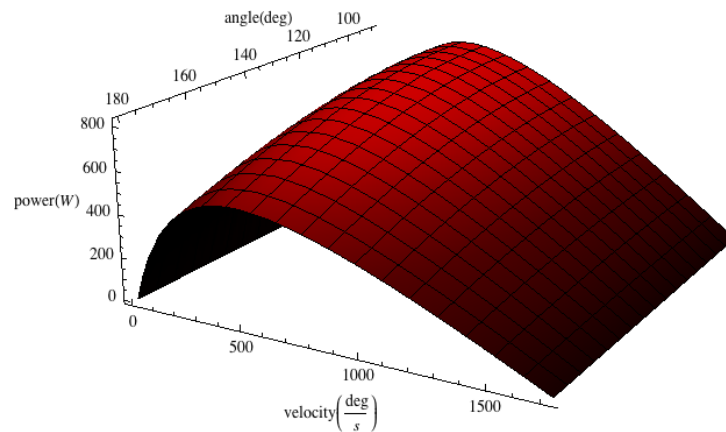


Figure 7.5: Theoretical hip joint power model (considering 2 legs). The maximal value is 820.9 W.

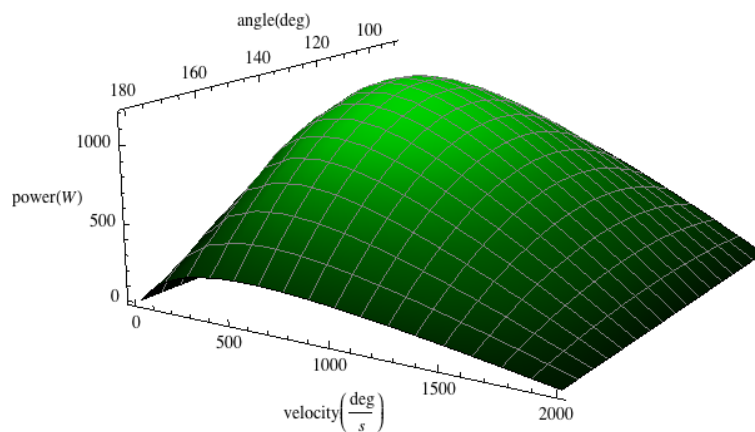


Figure 7.6: Theoretical knee joint power model (considering 2 legs). The maximal value is 1193.0 W.

7. Model optimization - predictions

Table 7.5 shows joint power simulation outcomes expressed as percentage of the

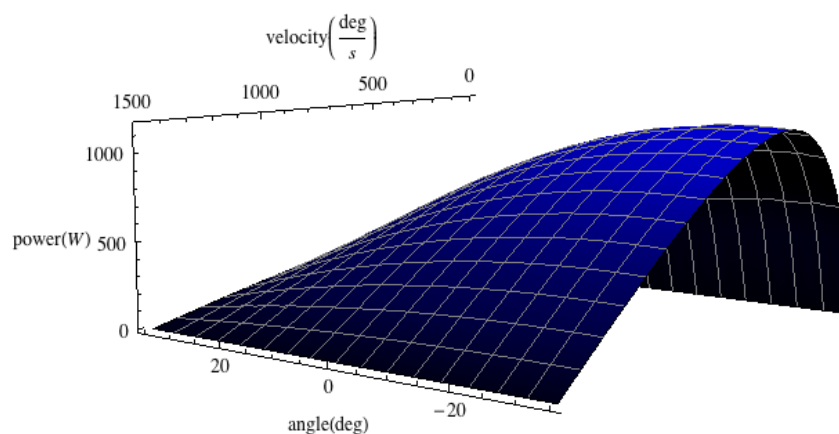


Figure 7.7: Theoretical ankle joint power model (considering 2 legs). The maximal value is 1153.9 W.

maximal power of the theoretical model. Optimized simulations gave results very close to the predicted maximal values. This means that the model worked well close to its limits. This is also showed in Table 7.6.

Table 7.5: Power (P) of hip, knee and ankle joint expressed as percentage of the maximal power of the theoretical model.

		SJ	SJ+25kg	SJ+50kg
		(%)	(%)	(%)
Hip joint				
match	P	94.0	90.2	87.3
opt	P	94.4	91.8	89.4
Knee joint				
match	P	98.5	98.4	96.9
opt	P	98.6	98.7	97.7
Ankle joint				
match	P	86.0	83.3	83.9
otp	P	91.1	88.8	88.0

7. Model optimization - predictions

Table 7.6: Power (P) , velocity (ω) values for matching simulations (match). Angles (θ) at which the maximal torque occurred are reported for each conditions and each joint.

		Hip joint	SJ	SJ+25kg	SJ+50kg
match	P (W)		771.8	740.1	716.8
opt	P (W)		774.9	753.4	733.8
match	θ (deg)		126.5	137.9	141.5
opt	θ (deg)		124.1	103.0	137.3
match	ω (deg/s)		384.9	401.5	359.4
opt	ω (deg/s)		373.7	120.6	365.1
Knee joint					
match	P (W)		1175.4	1173.7	1155.8
opt	P (W)		1176.2	1177.6	1166.1
match	θ (deg)		126.1	129.2	133.5
opt	θ (deg)		127.2	127.2	130.2
match	ω (deg/s)		594.8	540.9	519.6
opt	ω (deg/s)		637.6	535.2	490.8
Ankle joint					
match	P (W)		993.8	961.0	968.4
opt	P (W)		1051.3	1024.2	1014.9
match	θ (deg)		-9.8	-5.9	-2.6
opt	θ (deg)		-10.1	-7.8	-8.2
match	ω (deg/s)		399.2	360.4	337.8
opt	ω (deg/s)		394.5	355.4	320.0

7.1.5 Global power output

Instantaneous global power of the simulated jumps means the product of the vertical GRF times the COM velocity over the whole propulsive phase until the instant of the toe-off. For this reason, it seems evident how crucial is the accuracy of these two variables during simulation: GRF and COM velocity. GRF also depends on how body collisions are computed by the simulation software. Thus, an appropriate foot-ground interface could help the model to be close to the actual performance. COM velocity is dependent on the capacity of joints to increase its height and vertical velocity. It was shown that the amount to which rotation of a segment contributes to increase the vertical velocity, depends on simple geometric factors [14]. Figure 7.8 shows jump power for SJ, SJ+25kg and SJ+50kg for optimized simulations. Peak power was obtained for the SJ (2362.8 W). SJ+25kg gave a peak of 2316.9 W whilst the SJ+50kg gave 2291.9 W. Global

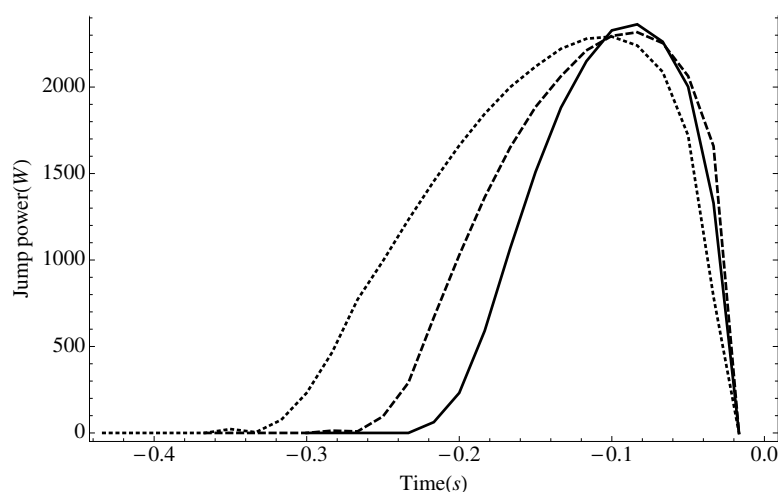


Figure 7.8: Global power meant as jump power for optimized simulations. SJ (solid line), SJ+25kg (dashed line) and SJ+50kg (dotted line).

peak power was obtained for these 3 conditions, the evidence is that although an increase of the extra load, the peak power is similar between conditions. The peak power was reached in a shorter time in the SJ+50kg than in the other 2 conditions. An interesting perspective would be to simulate other extra loads to see if the global peak power could be obtained using an optimal extra load.

7.2 Predictions

The final goal of this thesis was to use the model to predict jump height using different extra loads in the squat jump exercise. Successively, it was predicted the maximal load that the model can lift. This is also referred as 1RM test (half squat exercise). A model was created from the jump height obtained with different extra loads simulations. This allowed to calculate the load at which the model cannot jump.

7.2.1 Impact of extra loads on jump height in squat jump

Simulations were run to predict what would have been the jump height reached by the model using different extra loads. A total of 11 extra load conditions were simulated: 0kg, 10kg, 15kg, 20kg, 25kg, 30kg, 35kg, 40kg, 45kg, 50kg, 55kg. The maximized jump height for each condition was 21.8cm, 19.5cm, 18.4cm, 17.2cm, 16.1cm, 15.0cm, 14.2cm, 13.3cm, 12.6cm, 11.9cm, 11.1cm, respectively. It was

Table 7.7: Jump Height results for matching and optimized simulations.

	Jump Height (cm)
SJ Matching	20.1
SJ Optimized	21.8
SJ+10kg	19.5
SJ+15kg	18.4
SJ+20kg	17.2
SJ+25kg Matching	14.9
SJ+25kg Optimized	16.1
SJ+30kg	15
SJ+35kg	14.2
SJ+40kg	13.3
SJ+45kg	12.6
SJ+50kg Matching	10.8
SJ+50kg Optimized	11.9
SJ+55kg	11.1

7. Model optimization - predictions

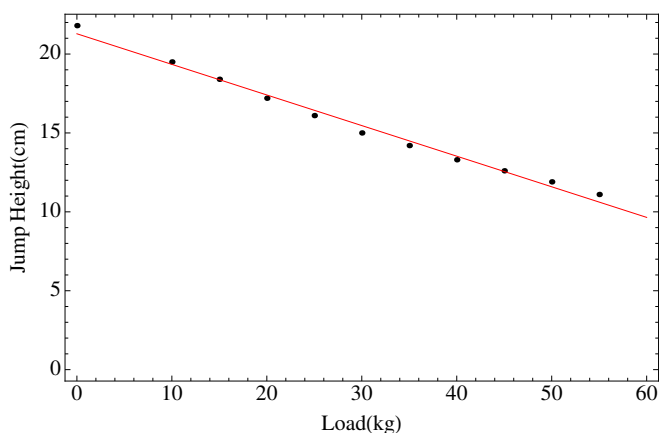


Figure 7.9: Jump height prediction model. A linear decrease in jump height was found simulating different squat jump extra loaded. Jump height decreased as extra load increased.

obtained an average decrease of 2.5% each 5kg added extra load with respect to the previous load. A model was created based on simulation results (jump height) using a linear regression showed in Figure 7.9 and explained in Equation 7.2.1.

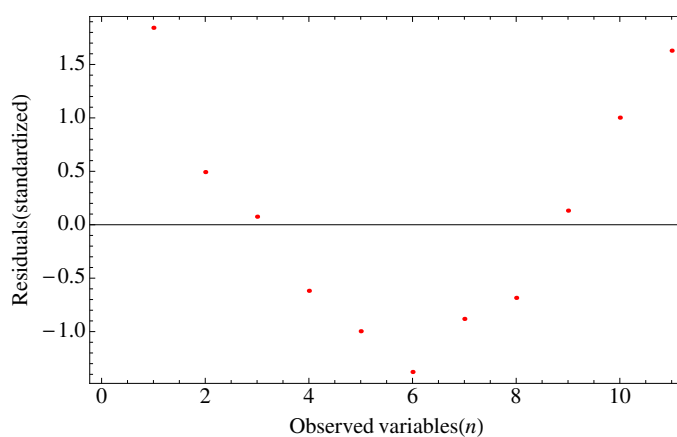


Figure 7.10: Standardized residuals of the jump height model.

$$H = \beta_0 + \beta_1 l_i \quad (7.3)$$

7. Model optimization - predictions

where H is the predicted jump height (cm), β_0 is the maximal jump height in squat jump (cm), β_1 is the rate of changing of the extra load and l_i is the load (kg).

Table 7.8: Jump height vs. load predictions: estimated parameters. $R^2 = 0.99$

	Estimate value	Standard Error	t-Statistic	P-Value
β_0	21.285	0.219	97.292	$6.49391 \cdot 10^{-15}$
β_1	-0.194	0.006	-30.033	$2.45959 \cdot 10^{-10}$

By solving the Equation 7.2.1 for $H = 0$ (the model will not be able to jump) we have:

$$0 = 21.285 - 0.194l_i$$

$$-0.194l_i = -21.285$$

$$l_i = \frac{-21.285}{-0.194} = 109.7kg$$

Therefore, 109.7kg was the predicted load at which the model would not be able to jump. Predictions also gave an optimal activation patterns set which is reported in Table 7.9.

Considering the ramp time for each joint and condition, a slightly tendency to increase the time needed to reach the full activation was obtained. For each condition the extra load became heavier. Therefore, the longer ramp time for heavy conditions does not surprise because muscles need more time at short velocity to exert more force [12] to succeed in lifting tasks.

However, activation pattern results confirmed once again a proximal-to-distal sequence. This result was obtained for all conditions and it could be considered an unexpected phenomena since this model was based on monoarticularity assumption. Indeed, Selbie and Caldwell [76] investigated about how initial jumping

7. Model optimization - predictions

Table 7.9: Activation parameters set for each given optimized squat jump condition. Onset time is always in relation to the hip joint that showed to be the first joint activated for each condition.

	Ramp Time			Onset Time		
	hip joint (ms)	knee joint (ms)	ankle joint (ms)	hip joint (ms)	knee joint (ms)	ankle joint (ms)
SJ	75	129	106	0	5	50
SJ+10kg	82	102	107	0	25	51
SJ+15kg	88	119	118	0	14	57
SJ+20kg	85	103	107	0	20	57
SJ+25kg	113	137	185	0	11	43
SJ+30kg	87	114	176	0	9	45
SJ+35kg	92	87	189	0	19	41
SJ+40kg	110	111	227	0	17	38
SJ+45kg	119	104	227	0	17	49
SJ+50kg	91	77	229	0	21	40
SJ+55kg	80	82	250	0	8	37

posture affected vertical jump performance using a four-segment planar model driven by three torque actuators. They did not find a proximal-to-distal activation sequence explaining that the result may have been due to the model not incorporating antagonist or biarticular muscles. In these terms, this model was similar and that suggests that biarticular muscles could not have an impact on the coordination of the activation sequence. However, a research group investigated for vertical jumping the relationships between muscle actions, movement pattern and jumping achievement. They obtained a proximal-to-distal sequence [14; 16]. Other studies investigated optimal muscular control strategies for squat jumping showing that the optimal control strategy comprised a proximal-to-distal sequence of muscle activation from hip to ankle [68]. It could be argued that it is an evidence that a proximal-to-distal sequence occurs for vertical jumping tasks. Despite this fact, if a different sequence is found, then it should be better understood why this did not happen. Probably, other reasons could have a bigger impact on the activation sequence than biarticular muscles which are may be crucial for other aspects of vertical jumping (e.g. height achievement).

7.2.2 1RM prediction

Strength capacity is an important ability for athletes. They spend long time during training to develop their maximal strength. The back half squat exercise is one among basic exercises for athletes. It is generally used at the beginning of the season in the annual training plan. Indeed, this exercise allow to massively stimulate the strength capacity by improving different aspects of the neuromuscular system. However, a big role is played by the system nervous. Different equations are available to predict the 1RM (maximum load) in back half squat. However, the most common Equation (7.4) was proposed by Brzycki in 1993 [17]:

$$\frac{bw}{(1.0278 - (0.0278 \cdot n_r))} \quad (7.4)$$

where \mathbf{bw} is the body weight (N), \mathbf{n}_r is the maximum number of repetition that the subject is able to perform with a given load (generally not more than 10 repetitions).

Here, the purpose was to see whether the model was also able to predict the back half squat 1RM. The simulation included a cost function to minimize differences at hip, knee, ankle angles and, the vertical position of the barbell. Indeed, it was supposed that since we were trying to simulate a dangerous exercise (heavy load), the trajectory during lifting could not be free. Therefore, the movement was constraint in these terms: the maximal load accepted by the simulation must minimize the differences between angles at hip, knee and ankle during standing position and, the barbell must reached the same height it has in standing position. These considerations were possible because it is evident that during this exercise no fly phase is possible. The 1RM prediction was performed by using the simulated annealing algorithm which had the same parameters used for optimized simulations (see previous sections). Inertial parameters varied according to the formula presented in Chapter 3 (Page 57). The 1RM estimated was 141kg, a long ramp time was found for each joint which is explained by the fact that the model needed much torque to lift an heavy load. However, differently from all other simulations it was not found a proximal-to-distal sequence. This should be investigated again to better understand the reasons. Table 7.2.2 shows the activation

7. Model optimization - predictions

	Ramp Time			Onset Time		
	hip joint (ms)	knee joint (ms)	ankle joint (ms)	hip joint (ms)	knee joint (ms)	ankle joint (ms)
1RM	118	171	226	0	16	10

pattern. Data from experimental test considered only the load, any kinematic or kinetic measurements were performed due to technical reasons. Therefore, it is difficult to discuss results since any key data of the actual performance is missed. Moreover, kinematic data are not presented since they showed the same issue in relation to the previous simulations: high angular velocity and short propulsive phase. However, Figure 7.11 shows vertical GRF during the simulated 1RM and the Figure 7.12 shows the activation profile time history. It can only be suggested that other simulations should be run to improve the method to predict the 1RM and an actual performance should be recorded for a comparison.

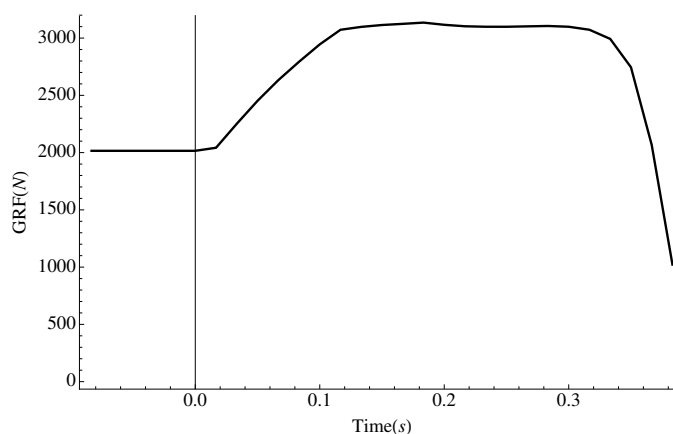


Figure 7.11: Vertical ground reaction force for the simulated half squat 1RM. The 0 in the abscissa axis represent the beginning of the propulsive phase.

7. Model optimization - predictions

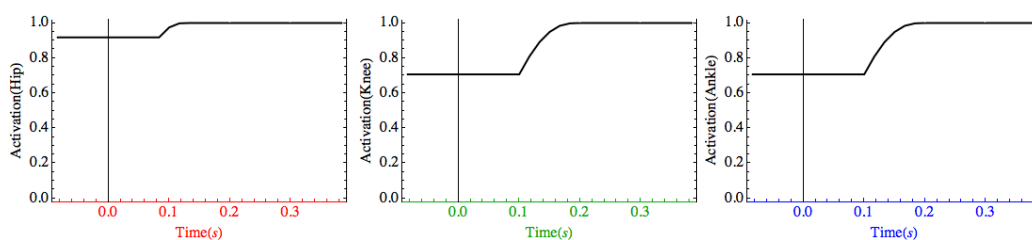


Figure 7.12: Activation profile time history of the simulated 1RM half squat.

7.3 Summary

In this chapter optimization procedures and results were presented. The method for optimisation of technique in the simulation model of squat jump was described. The components of the objective function were outlined and the penalties the model could incur were explained. The results of the optimisation process were discussed with reference to the differences in the kinetic features of the model between the matched and optimised simulations. The effects of increasing loads on jump height was investigated and a theoretical model was created. The 1RM for the back half squat was also predicted.

Chapter 8

Conclusions

8.1 General discussion

8.1.1 Simulated Performances

This research has shown the importance of using an accurate model-based torque which represent human muscle groups for vertical jumping with and without extra load purpose. A subject-specific monoarticular model was shown to produce insufficient torque at the ankle, to match the performance of the participant. At first, a torque correction for the ankle joint was required. Thus, an experiment allowed to make more accurate the representation of the ankle actuator. However, two models for each joint were created, the model based on the 5-parameter function implemented into simulations (run by the means of the brute-force algorithm), did not provide good agreement with the participant's squat jump. It failed to achieve the required displacement during flight. In the model based on 9-parameter function, implemented into simulations (run by the means of the simulated annealing algorithm), the simulator was able to exert more torque at hip and ankle joint than the previous model. Therefore, in the case of hip and knee extensors it could exert larger torques but in a shorter duration. Further, later activation of the ankle joint occurred showing that onset time have a crucial impact for height jump achievement. These data are in contrast with Lewis [49] who used a model based on monoarticularity assumption compared with a model which incorporated biarticular muscles. He found that if the biarticular muscles

are not incorporated then his model was not able to achieve half of the required displacement during flight. Other studies also showed the importance of biarticular muscles in jump height achievement [36; 82], they showed that mono- and biarticular muscles cooperation allows to transfer more power through the hip, knee and ankle in a proximal-to-distal sequence. Here, it seemed that a monoarticular representation was enough to approach the jump height recorded from experimental data. Probably, experiments performed at the dynamometer for the hip and the knee gave torque results very close to the maximal capacity of the participant. This allows to have a strong model. However, it has to be said that jump height for SJ and SJ+25kg was 3.8 cm and 1.4 cm less than actual performances for matching simulations. This is much better than results of other researches [49], but it is still not the jump height we were looking for. Actually, van Soest investigated the role of gastrocnemius (GAS) in vertical jumping found that jump height decreased by 10 mm when GAS was changed into a monoarticular muscle [82]. Therefore, it should be considered to incorporate biarticular muscles for future works.

Based on the model which better matched the actual performances, a prediction about the effect of extra load on jump height and a prediction of the 1RM gave interesting results. The first prediction was useful to create a model to establish at which load the model was not able to jump, whilst the second prediction gave a result very close to the actual performance. This suggested that we can take advantages from a model to obtain information without the necessity to perform many experiments with subjects. However, at first a subject-specific simulator must be create.

8.1.2 Electromechanical delay

An important thing to mention, is that torque generator activation ramp times in the results did not discuss the implications of electromechanical delay (EMD). This phenomena, is the delay which exists between the onset of electrical signal at the muscle measured through EMG and the measurement of tension [63]. Tillin et al. (2010) measured the EMD of strength trained athletes and control subjects and found delays of 6 ms to 15 ms, although the authors identified a

literature range of 50 ms to 250 ms. In the current model the activation of the torque generators and the torque associated with that level of activation in the contractile component have zero delay between them and therefore as for another work [49] the onset times calculated from the torque generator activation profiles would probably have been earlier in a human as opposed to the simulation model. In most cases this would have meant better agreement between torque generator activation profiles and the sEMG onsets measured for the participant. However, for the purpose of this thesis, the model demonstrated that the activation function provided sufficient complexity for these squat jump performances, although it is evident from sEMG time-histories that the muscle activations may not simply ramp up from a minimum level to a maximum level in one smooth ramp (Page 44).

8.1.3 Selection of cost function

The cost functions which were employed to obtain the system parameters, minimising the difference between the simulation model performance and the participant data, calculated a mean of all the performance measures assuming an even weighting. The results of the matching simulations demonstrated that the model was more effective at matching the kinematics than the vertical GRF time history. However, no GRF data were included in the cost function for SJ, SJ+25kg and SJ+50kg. If the goal is to match as close as possible the actual performance, it would may be suitable to include also the GRF in cost function. In addition, the time of the propulsive phase, the orientation of the whole body could be considered.

8.2 Research questions

A subject-specific 3-actuator torque forward driven model was developed to answer several questions about biomechanics and vertical squat jumping with and without extra load. Here, a brief recapitulation is reported:

1. **Is a subject-specific 3-actuator torque driven model based on a**

monoarticularity assumption able to match human vertical jumping performances?

The matching simulations disclosed that if a suitable correction for the ankle joint torque is considered (3.58 strength factor), then a vertical squat jump can be accurately reproduced by a model based on monoarticularity assumption. It has to be said that joint torque models must be accurate with respect to experimental data. Indeed, at first two model were created (Model A and Model B) to see how close they were to the actual performance. The Model A was based on 5-parameter function (data fitted using the trust region algorithm), and the brute force algorithm as search method during simulations. The Model B was based on 9-parameter function (fitted using simulated annealing algorithm (SA)), and the SA as search method for running simulations. The Model B showed more accuracy than the Model A. Good matching was found for jump height and joint displacements. This was true for all three squat jump conditions (SJ, SJ+25kg, SJ+50kg). GRF is not close to the actual performance and a model more accurate could give better outcomes in relation to power parameters. In addition, optimized simulations showed that the participant was slightly operating sub-optimally for the SJ+25kg and SJ+50kg. In fact, for each squat jump condition, the jump height increased. However, the SJ model was optimized and compared only against the matching SJ since the jump height of the matching simulation was almost 3 cm less than the actual SJ. SJ+25kg and SJ+50kg were optimized and compared against the actual performance and the matching simulation.

2. How accurately can the model reproduce the actual performance in squat jumps with and without extra load?

The SJ model, was able to jump 20.1 cm vs. 23.9 cm of the actual performance. The difference was 3.8 cm. Kinematic patterns were well matched over the whole phase of the jump and at the instant of the toe-off. However, some issues was found for angular velocities at each joint and for the vertical GRF. Angular velocities were up to 2 time greater than that measured in experimental conditions. Peak GRF was 1631.8 N in matching

simulation and 1450 N was the actual peak GRF in squat jump. Simulations of SJ+25kg and SJ+50kg showed that the model is accurate as the extra load increased. This is true especially considering the jump height. For the SJ+25kg the jump height was 16.1 cm (actual performance = 16.3 cm), whilst the SJ+50kg jumped 10.8 cm (actual performance = 10.4 cm). At toe-off joint angles matched well all conditions, but angular velocities in simulations were always greater than that measured. GRF was always overestimated and the propulsive phase was shorter than the actual performance for all conditions.

3. Is the model able to estimate the maximal load that a subject is able to lift in a half squat exercise?

In actual performance the participant was tested to obtain the 1RM for the back half squat exercise. The result was a range between 145kg and 155kg (barbell + plates). In fact, the subject at his strength capacity limit was able to lift 145kg, but the following attempt to lift 155kg failed. This means that the 1RM of the participant was very close to 145kg and, in any case it would not have been more than 155kg. The simulation gave a prediction of 141kg which is very close to the actual 1RM. However, a cost function was used to obtain this result, instead to let the model extend the segments unconstrained. The cost function included joint angles at standing up position and the vertical position of barbell which was on the shoulders. For predicting 1RM, the model was constrained to avoid that the model generated improbable trajectories. This, it was thought with respect to the hypothetical load that the back could safely sustain. Actually, the model was based on the assumption of multi-linked rigid segments. Thus, no attention was given to the impact of the maximal load that 1RM could provoke on the back.

However, it does not seem too ambitious that a simple model based on monoarticularity assumption can predict a strength performance of a specific subject. However, further development are required to understand better this prediction, since the mass lift was the only data recorded in actual performance.

4. What is the impact of adding extra load during squat jump on jump height and power output?

At that time, nobody used modelling to make predictions in strength and conditioning training. Sport techniques have been studied in biomechanics. In addition, mechanical features of the human movement are still the current focus of scientists. However, any research considered to investigate the effect of extra loads in squat jumping on jump height achievement. Optimized simulations revealed that, as expected, there is a linear relationship between the jump height and extra load. For each 5kg extra load the model jumped about 1 cm lower than the previous condition (e.g. 20kg = 17.2 cm, 25kg = 16.1 cm). The model was then able to predict which would be the extra load that would not allow the model to jump. This extra load was found at 109.7kg.

Global power output for each conditions was also investigated. However, further improvements and comparisons are necessary to obtain more accurate results about power output.

Finally, considering to model serie elastic components, improving the compliance of the model at the foot, should help to obtain more accuracy in future works to better investigate power output.

8.3 Simulation model strength

The maximum isometric (T0) torque parameter had to be increased for the simulation models (Model A and B) to achieve agreement with the squat jump performance of the participant. The magnitude of the increase seemed very large. A factor of 3.58 was used to scale the ankle joint model considering two experimental data that were compared to each other. However, neither the hip, nor the knee joints needed a strength factor. Lewis [49] for his model had to increase the T0 parameter for all three joints (hip, knee, ankle). For example the knee extensors and plantar flexors had strength increased by a factor of 1.6. It was concluded that the participant did not exert maximal torques during the dynamometer tri-

als, despite some experience of strength testing. Differently from Lewis, a simple model (Model B) based on monoarticularity assumption can jump as a specific subject does. Only one joint required a correction (ankle joint = plantar flexors). Despite a good result in terms of jump height, extremely familiarization with the use of the dynamometer is strongly recommended in order to obtain a strong model for each joint for implementing it into simulations. However, it is also recommended to test the strength of the ankle joint using different methods or machines that are different from the dynamometer.

In conclusion, if the goal is to predict performances about jump height with extra load, then the model was enough complex to answer this question.

8.4 Simulation model weakness

When comparing kinematic (angular velocities) the model showed to be not enough complex to match actual performances. Here, it was decided to take a calling trying to simplify the model as much as possible. Consequently only the contractile component was considered. Moreover, antagonist muscles were not included. The hypothesis now is that a poor matching performance was obtained for kinematic purposes and power output because the model needs to be developed in the future for improving kinematic and kinetic outcomes.

A software graphic simulation package was chosen to make easy the creation of this model. However, a big computational cost was required to complete matching simulations and optimization. This issue probably had an impact on the time available to analysis data and explore different conditions and situations. Probably, a symbolic-numeric software could make simulations faster and more accurate. This could allow to focus more on the application and not on the development of the model.

8.5 Future developments

This project wanted to be the first part of a work based on an original way to conduct research in strength and conditioning training. The model needed to

be developed and evaluate. At first, the simpler the better for understanding macroscopic features of vertical jumping. However, in the future, the model must be developed in the following areas:

- introduction of serie elastic components
- modeling of antagonist muscles
- development of the foot ground interface

In pure concentric movements, elastic features of the muscle-complex tendon could be less important than in other explosive exercises. However, it seems necessary to include the elastic component. Indeed, simulations showed a propulsive phase shorter than in actual performance. Therefore, it was supposed that tendons, could delay the transmission of the force improving the accuracy of GRF in relation to the duration of the jump.

Antagonist muscles should help to accurately match experimental kinematic data. Probably, with the intervention of these muscles, angular velocities would be more close to the actual performance.

The model was based on rigid segments, but humans have not this characteristics, wobbling masses could be considered [4; 58]. Moreover, it is supposed that an improvement of the foot-ground interface could help the model to match better GRF.

The immediate continuation of this project will be to use the model to simulate counter movement jumps including elastic components.

More generally, the model showed to accurately simulate human motion in the sagittal plane with respect to the actual jump height. Consequently it can be used in future to answer this kind of questions:

- What is the contribution of serie elastic components to concentric vertical jumping performance and counter movement jump?
- How sensitive is vertical jumping performance to variations in initial conditions?
- How is vertical jumping performance (with and without extra load) affected by variations in strength parameters at individual joints?

-
- How sensitive is vertical jumping performance (with and without extra load) to variations in muscle activation timings?
 - How do altered anthropometric and mass/inertia characteristics affect vertical jumping performance?
 - What are the limitations of 1RM half squat exercise?

8.6 Conclusion

With respect to the purposes of this study outlined at the beginning of this thesis, a subject-specific torque-driven model of vertical jumping was successfully developed, evaluated and optimised. Anthropometric, strength, and performance data were obtained from an healthy subject, ensuring subject-specificity. A torque-driven model was then evaluated against performance data and it showed a close match for some characteristics of the squat jump with and without extra load. This indicated that it is a good representation of the system it was simulating. The components of optimum technique were described, quantified, and discussed. In conclusion, it does not seem too ambitious to use experimental data combined with modeling and simulations to better understand strength training exercises. Finally, an interesting way to conduct research which is inspired from a paper of Yeadon [93] is suggested and recommended again: initially, a scientific investigation will probably take the form of a descriptive study which provides a record of what happens. The data may suggest a possible theory. Such a theory may be used to predict the outcome in a given situation. An experiment can then be conducted to determine the actual outcome. A comparison of theoretical and experimental outcomes can then establish the accuracy with which the theory models the activity. This will indicate the level of confidence that can be given to theoretical predictions and may suggest how the theory can be modified. The cycle of theory-prediction-experiment theory is shown in Figure 8.1.

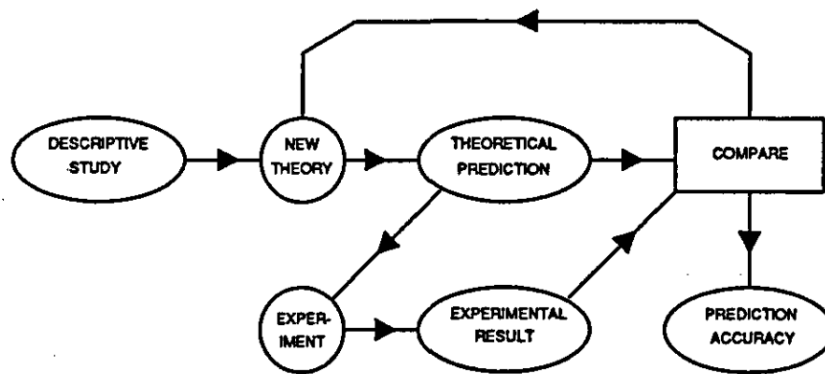


Figure 8.1: The cycle of theory-prediction-experiment theory, from Yeadon [93].

References

- [1] M. Gazzoni A. Rainoldi. *Strength and Conditioning*. Wiley-Blackwell, 2011. [5](#)
- [2] P. Aagaard, J. L. Andersen, P. Dyhre-Poulsen, A. M. Leffers, A. Wagner, S. P. Magnusson, J. Halkjaer-Kristensen, and E. B. Simonsen. A mechanism for increased contractile strength of human pennate muscle in response to strength training: changes in muscle architecture. *J Physiol*, 534(Pt. 2):613–623, Jul 2001. [3](#)
- [3] R Mcneill Alexander. Simple models of walking and jumping. *Human Movement Science*, 11(1-2):3–9, 1992. [2](#)
- [4] S. J. Allen, M. A. King, and M. R. Yeadon. Models incorporating pin joints are suitable for simulating performance but unsuitable for simulating internal loading. *J Biomech*, Mar 2012. [79](#), [96](#), [151](#)
- [5] Samuel James Allen. *Optimisation of performance in the triple jump using computer simulation*. PhD thesis, Loughborough University, Gymnastic Research Centre, UK, 2009. [2](#), [7](#), [12](#), [17](#)
- [6] Dennis E. Anderson, Michael L. Madigan, and Maury A. Nussbaum. Maximum voluntary joint torque as a function of joint angle and angular velocity: model development and application to the lower limb. *J Biomech*, 40(14):3105–3113, 2007. [11](#)
- [7] F. C. Anderson and M. G. Pandy. Storage and utilization of elastic strain energy during jumping. *J Biomech*, 26(12):1413–1427, Dec 1993. [7](#)

REFERENCES

- [8] Blake M. Ashby and Scott L. Delp. Optimal control simulations reveal mechanisms by which arm movement improves standing long jump performance. *J Biomech*, 39(9):1726–1734, 2006. [9](#)
- [9] A. E. Atwater. Biomechanics of overarm throwing movements and of throwing injuries. *Exerc Sport Sci Rev*, 7:43–85, 1979. [89](#)
- [10] V. Baltzopoulos and D. A. Brodie. Isokinetic dynamometry. applications and limitations. *Sports Med*, 8(2):101–116, Aug 1989. [11](#), [12](#), [29](#), [30](#)
- [11] Best C.H. Taylor N.B. West J.B. Best, C.H. *Best and Taylor's Physiological basis of medical practice, 12th edition*. Williams and Wilkins, Baltimore: London., 1990. [5](#)
- [12] M. F. Bobbert, K. G. Gerritsen, M. C. Litjens, and A. J. Van Soest. Why is countermovement jump height greater than squat jump height? *Med Sci Sports Exerc*, 28(11):1402–1412, Nov 1996. [13](#), [17](#), [139](#)
- [13] M. F. Bobbert, P. A. Huijing, and G. J. Van Ingen Schenau. A model of the human triceps surae muscle-tendon complex applied to jumping. *J Biomech*, 19(11):887–898, 1986. [7](#)
- [14] M. F. Bobbert and G. J. Van Ingen Schenau. Coordination in vertical jumping. *J Biomech*, 21(3):249–262, 1988. [5](#), [13](#), [17](#), [89](#), [93](#), [105](#), [136](#), [140](#)
- [15] M. F. Bobbert and A. J. Van Soest. Effects of muscle strengthening on vertical jump height: a simulation study. *Med Sci Sports Exerc*, 26(8):1012–1020, Aug 1994. [13](#)
- [16] Maarten F. Bobbert and Jan Peter van Zandwijk. Sensitivity of vertical jumping performance to changes in muscle stimulation onset times: a simulation study. *Biological Cybernetics*, 81:101–108, 1999. [13](#), [17](#), [105](#), [128](#), [140](#)
- [17] M. Brzycki. Strength testing-predicting a one-rep max from reps-to-fatigue. *JOperd*, 68:88–90, 1993. [141](#)

REFERENCES

- [18] F. Buchthal and H. Schmalbruch. Contraction times and fibre types in intact human muscle. *Acta Physiol Scand*, 79(4):435–452, Aug 1970. [5](#), [80](#), [81](#), [126](#)
- [19] Harald Bhm, Gerald K. Cole, Gert-Peter Brggemann, and Hanns Ruder. Contribution of muscle series elasticity to maximum performance in drop jumping. *J Appl Biomech*, 22(1):3–13, Feb 2006. [7](#)
- [20] R F Chandler, C E Clauser, J T McConville, H M Reynolds, and J W Young. Investigation of inertial properties of the human body. Technical report, Aerospace medical research laboratory, U.S. department of transportation national highway traffic safety administration Washington, D.C. 20590., March 1975. [xv](#), [xxvi](#), [19](#), [52](#), [54](#), [56](#), [121](#)
- [21] A. E. Chapman. The mechanical properties of human muscle. *Exerc Sport Sci Rev*, 13:443–501, 1985. [7](#)
- [22] A. Corana, M. Marchesi, C. Martini, and S. Ridella. Minimizing multimodal functions of continuous variables with the simulated annealing algorithm corrigenda for this article is available here. *ACM Trans. Math. Softw.*, 13(3):262–280, September 1987. [16](#), [17](#), [81](#)
- [23] J.T. Davies. *The Scientific Approach*. London: Academic Press., 1973. [15](#)
- [24] K A Edman. Double-hyperbolic force-velocity relation in frog muscle fibres. *J Physiol*, 404:301–321, 1988. [10](#)
- [25] Z. Erim, C. J. De Luca, K. Mineo, and T. Aoki. Rank-ordered regulation of motor units. *Muscle Nerve*, 19(5):563–573, May 1996. [4](#)
- [26] B. Feinstein, B. Lindegard, E. Nyman, and G. Wohlfart. Morphologic studies of motor units in normal human muscles. *Acta Anat (Basel)*, 23(2):127–142, 1955. [4](#)
- [27] W. O. Fenn and B. S. Marsh. Muscular force at different speeds of shortening. *J Physiol*, 85(3):277–297, Nov 1935. [9](#)
- [28] S. E. Forrester, M. R. Yeadon, M. A. King, and M T G. Pain. Comparing different approaches for determining joint torque parameters from isovelocity

REFERENCES

- dynamometer measurements. *J Biomech*, 44(5):955–961, Mar 2011. [2](#), [11](#), [12](#)
- [29] A. R. Fugl-Meyer. Maximum isokinetic ankle plantar and dorsal flexion torques in trained subjects. *Eur J Appl Physiol Occup Physiol*, 47(4):393–404, 1981. [36](#)
- [30] A. R. Fugl-Meyer, L. Gustafsson, and Y. Burstedt. Isokinetic and static plantar flexion characteristics. *Eur J Appl Physiol Occup Physiol*, 45(2-3):221–234, 1980. [36](#)
- [31] S. Fukashiro, P. V. Komi, M. Jrvinen, and M. Miyashita. In vivo achilles tendon loading during jumping in humans. *Eur J Appl Physiol Occup Physiol*, 71(5):453–458, 1995. [7](#)
- [32] M. Pain J. Van Hoecke G. Alberti N. Babault F. Yeadon. G. Cimadoro, A.E. Minetti. Comparison between squat jump vs. weighted squat jump: Simulation study. In *Proceedings of the 36th Annual Meeting of the American Society of Biomechanics.*, 2012. [12](#), [13](#)
- [33] Stuart Geman and Donald Geman. Stochastic relaxation, gibbs distributions and the bayesian restoration of images. *IEEE Transactions on Pattern Analysis and Machine Intelligence*, 6(6):721–741, November 1984. [16](#)
- [34] A. M. Gordon, A. F. Huxley, and F. J. Julian. The variation in isometric tension with sarcomere length in vertebrate muscle fibres. *J Physiol*, 184(1):170–192, May 1966. [xv](#), [6](#), [8](#)
- [35] L. Gregoire, H. E. Veeger, P. A. Huijing, and G. J. Van Ingen Schenau. Role of mono- and biarticular muscles in explosive movements. *Int J Sports Med*, 5(6):301–305, Dec 1984. [91](#)
- [36] L. Gregoire, H. E. Veeger, P. A. Huijing, and G. J. Van Ingen Schenau. Role of mono- and biarticular muscles in explosive movements. *Int J Sports Med*, 5(6):301–305, Dec 1984. [145](#)

REFERENCES

- [37] W. Herzog. The relation between the resultant moments at a joint and the moments measured by an isokinetic dynamometer. *J Biomech*, 21(1):5–12, 1988. [11](#), [12](#)
- [38] A V Hill. The heat of shortening and the dynamic constants of muscle. *Proceedings of the Royal Society of London. Series B, Biological Sciences*, 126(843):136–195, 1938. [xv](#), [6](#), [9](#), [10](#), [11](#), [59](#), [112](#), [127](#)
- [39] A. V. Hill. The series elastic component of muscle. *Proc R Soc Lond B Biol Sci*, 137(887):273–280, Jul 1950. [6](#)
- [40] A F Huxley. Muscle structure and theories of contraction. *Prog Biophys Biophys Chem*, 7:255–318, 1957. [3](#), [60](#)
- [41] A.F. Huxley. *Cross-bridge Action: Present Views, Prospects, and Unknowns, in Skeletal Muscle Mechanics: From Mechanisms to Function*. John Wiley & Sons, Ltd, Chichester., 2000. [3](#), [6](#)
- [42] M.I. Jackson. *The mechanics of the table contact phase of gymnastics vaulting*. PhD thesis, Loughborough University, Gymnastic Research Centre, UK, 2010. [17](#)
- [43] Leighton H. Johnson. Limitations of the descriptive method. *The Phi Delta Kappan.*, 34(6):241–242, 245, 1953. [14](#)
- [44] Chow J.W. Isokinetic exercise and knee joint forces during isokinetic knee extensions. In *Proceedings of the 25th Annual Meeting of the American Society of Biomechanics.*, pages 127–128, 2001. [12](#)
- [45] B Katz. The relation between force and speed in muscular contraction. *J Physiol*, 96(1):45–64, Jun 1939. [62](#)
- [46] E. Kellis and V. Baltzopoulos. Gravitational moment correction in isokinetic dynamometry using anthropometric data. *Med Sci Sports Exerc*, 28(7):900–907, Jul 1996. [12](#)

REFERENCES

- [47] Mark A. King, Pui W. Kong, and Maurice R. Yeadon. Determining effective subject-specific strength levels for forward dives using computer simulations of recorded performances. *J Biomech*, 42(16):2672–2677, Dec 2009. [17](#), [110](#)
- [48] Mark A. King, Cassie Wilson, and Maurice R. Yeadon. Evaluation of a torque-driven model of jumping for height. *J Appl Biomech*, 22(4):264–274, Nov 2006. [2](#), [7](#), [60](#), [79](#), [112](#), [113](#)
- [49] Martin Gary Charles Lewis. *Are Torque-Driven Simulation Models Limited by an Assumption of Monoarticularity?* PhD thesis, Loughborough University, Gymnastic Research Centre, UK, October 2011. [5](#), [6](#), [7](#), [9](#), [12](#), [13](#), [17](#), [62](#), [67](#), [82](#), [84](#), [116](#), [144](#), [145](#), [146](#), [149](#)
- [50] N. P. Linthorne. Analysis of standing vertical jumps using a force platform. *American Journal of Physics*, 69:1198–1204+, 2001. [128](#)
- [51] H Lund, K Sndergaard, T Zachariassen, R Christensen, P Blow, M Henriksen, E M Bartels, B Danneskiold-Samse, and H Bliddal. Learning effect of isokinetic measurements in healthy subjects, and reliability and comparability of biodex and lido dynamometers. *Clinical Physiology and Functional Imaging*, 25(2):75–82, 2005. [22](#)
- [52] Bobbert M.A. The effect of coordination on vertical jumping performance. In *International Society of Biomechanics in Sports*, 2002. [128](#)
- [53] Huub Maas and Peter A. Huijing. Effects of tendon and muscle belly dissection on muscular force transmission following tendon transfer in the rat. *J Biomech*, 45(2):289–296, Jan 2012. [84](#)
- [54] O R Madsen. Torque, total work, power, torque acceleration energy and acceleration time assessed on a dynamometer: reliability of knee and elbow extensor and flexor strength measurements. *European Journal Of Applied Physiology And Occupational Physiology*, 74(3):206–210, 1996. [22](#)
- [55] O R Madsen and U B Lauridsen. Knee extensor and flexor strength in elderly women after recent hip fracture: assessment by the cybex 6000 dynamometer

REFERENCES

- of intra-rater inter-test reliability. *Scandinavian Journal of Rehabilitation Medicine*, 27(4):219–226, 1995. [22](#)
- [56] Roberto Merletti, Matteo Avenaggiato, Alberto Botter, Ales Holobar, Hamid Marateb, and Taian M M. Vieira. Advances in surface emg: recent progress in detection and processing techniques. *Crit Rev Biomed Eng*, 38(4):305–345, 2010. [112](#)
- [57] Nicholas Metropolis, Arianna W. Rosenbluth, Marshall N. Rosenbluth, Augusta H. Teller, and Edward Teller. Equation of state calculations by fast computing machines. *The Journal of Chemical Physics*, 21(6):1087–1092, 1953. [16](#)
- [58] A. E. Minetti and G. Belli. A model for the estimation of visceral mass displacement in periodic movements. *J Biomech*, 27(1):97–101, Jan 1994. [151](#)
- [59] R. J. Monti, R. R. Roy, J. A. Hodgson, and V. R. Edgerton. Transmission of forces within mammalian skeletal muscles. *J Biomech*, 32(4):371–380, Apr 1999. [84](#)
- [60] M. V. Narici, L. Landoni, and A. E. Minetti. Assessment of human knee extensor muscles stress from in vivo physiological cross-sectional area and strength measurements. *Eur J Appl Physiol Occup Physiol*, 65(5):438–444, 1992. [3](#), [11](#)
- [61] M. V. Narici, M. D. Sirtori, S. Mastore, and P. Mognoni. The effect of range of motion and isometric pre-activation on isokinetic torques. *Eur J Appl Physiol Occup Physiol*, 62(3):216–220, 1991. [11](#), [22](#)
- [62] R. R. Neptune. Optimization algorithm performance in determining optimal controls in human movement analyses. *J Biomech Eng*, 121(2):249–252, Apr 1999. [15](#)
- [63] R. W. Norman and P. V. Komi. Electromechanical delay in skeletal muscle under normal movement conditions. *Acta Physiol Scand*, 106(3):241–248, Jul 1979. [145](#)

REFERENCES

- [64] L. R. Osternig. Isokinetic dynamometry: implications for muscle testing and rehabilitation. *Exerc Sport Sci Rev*, 14:45–80, 1986. [11](#), [30](#)
- [65] Sawhill J.A. Bates B.T. Osternig, L.R. and J. Hamill. Method for rapid collection and processing of isokinetic data. *Research Quarterly for Exercise and Sport*, 53(3):252 – 256, 1982. [12](#)
- [66] Heat O.V.S. *Investigation by Experiment*. London: Edward Arnold., 1970. [15](#)
- [67] M. G. Pandy. Computer modeling and simulation of human movement. *Annu Rev Biomed Eng*, 3:245–273, 2001. [13](#)
- [68] M. G. Pandy and F. E. Zajac. Optimal muscular coordination strategies for jumping. *J Biomech*, 24(1):1–10, 1991. [5](#), [13](#), [17](#), [89](#), [105](#), [110](#), [114](#), [116](#), [118](#), [120](#), [122](#), [140](#)
- [69] T. J. Patel and R. L. Lieber. Force transmission in skeletal muscle: from actomyosin to external tendons. *Exerc Sport Sci Rev*, 25:321–363, 1997. [83](#), [84](#), [101](#)
- [70] M. J. Pavol and M. D. Grabiner. Knee strength variability between individuals across ranges of motion and hip angles. *Med Sci Sports Exerc*, 32(5):985–992, May 2000. [30](#)
- [71] D. Pette and R. S. Staron. Myosin isoforms, muscle fiber types, and transitions. *Microsc Res Tech*, 50(6):500–509, Sep 2000. [3](#)
- [72] Street S.F. Ramsey, R.W. The isometric length-tension diagram of isolated skeletal muscle fibers of the frog. *Journal of Cellular and Comparative Physiology*. 15, 11-34., 15(1):11–34, 1940. [7](#), [8](#)
- [73] A. Sandow. Excitation-contraction coupling in muscular response. *Yale J Biol Med*, 25(3):176–201, Dec 1952. [3](#)
- [74] A.A. Sapega, J.A. Nicholas, D. Sokolow, and A. Saraniti. The nature of torque "overshoot" in cybex isokinetic dynamometry. *Med Sci Sports Exerc*, 14(5):368–75, 1982. [12](#)

REFERENCES

- [75] Beck S.D. *The simplicity of science*. London: Lutterworth Press., 1960. [15](#)
- [76] W. S. Selbie and G. E. Caldwell. A simulation study of vertical jumping from different starting postures. *J Biomech*, 29(9):1137–1146, Sep 1996. [9](#), [13](#), [17](#), [139](#)
- [77] A. Seyfarth. *Elastically operating legs strategies and construction principles*. PhD thesis, Jena University, Germany., 2000. [96](#)
- [78] V. Smerdu, I. Karsch-Mizrachi, M. Campione, L. Leinwand, and S. Schiaffino. Type iix myosin heavy chain transcripts are expressed in type iib fibers of human skeletal muscle. *Am J Physiol*, 267(6 Pt 1):C1723–C1728, Dec 1994. [3](#)
- [79] Peter C Terry and Costas I Karageorghis. Psychophysical effects of music in sport and exercise : An update on theory , research and application. *Society*, pages 415–419, 2006. [22](#)
- [80] Dimitrios E. Tsaopoulos, Vasilios Baltzopoulos, Paula J. Richards, and Constantinos N. Maganaris. Mechanical correction of dynamometer moment for the effects of segment motion during isometric knee-extension tests. *J Appl Physiol*, 111(1):68–74, Jul 2011. [29](#), [112](#)
- [81] G. J. Van Ingen Schenau, M. F. Bobbert, P. A. Huijing, and R. D. Woittiez. The instantaneous torque-angular velocity relation in plantar flexion during jumping. *Med Sci Sports Exerc*, 17(4):422–426, Aug 1985. [17](#), [36](#)
- [82] G. J. Van Ingen Schenau, M. F. Bobbert, and R. H. Rozendal. The unique action of bi-articular muscles in complex movements. *J Anat*, 155:1–5, Dec 1987. [145](#)
- [83] A. J. Van Soest and M. F. Bobbert. The contribution of muscle properties in the control of explosive movements. *Biol Cybern*, 69(3):195–204, 1993. [13](#)
- [84] A. J. Van Soest, M. F. Bobbert, and G. J. Van Ingen Schenau. A control strategy for the execution of explosive movements from varying starting positions. *J Neurophysiol*, 71(4):1390–1402, Apr 1994. [13](#)

REFERENCES

- [85] A. J. Van Soest, A. L. Schwab, M. F. Bobbert, and G. J. Van Ingen Schenau. Spacar: a software subroutine package for simulation of the behavior of biomechanical systems. *J Biomech*, 25(10):1219–1226, Oct 1992. [13](#)
- [86] A. J. Van Soest, A. L. Schwab, M. F. Bobbert, and G. J. Van Ingen Schenau. The influence of the biarticularity of the gastrocnemius muscle on vertical-jumping achievement. *J Biomech*, 26(1):1–8, Jan 1993. [13](#), [87](#)
- [87] A. M. Wani and S. K. Guha. A model for gradation of tension-recruitment and rate coding. *Med Biol Eng*, 13(6):870–875, Nov 1975. [4](#), [5](#)
- [88] S. Webber and D. Kriellaars. Neuromuscular factors contributing to in vivo eccentric moment generation. *J Appl Physiol*, 83(1):40–45, Jul 1997. [46](#)
- [89] S H Westing, J Y Seger, E Karlson, and B Ekblom. Eccentric and concentric torque-velocity characteristics of the quadriceps femoris in man. *Eur J Appl Physiol Occup Physiol*, 58(1-2):100–104, 1988. [62](#)
- [90] Cassie Wilson, Maurice R. Yeadon, and Mark A. King. Considerations that affect optimised simulation in a running jump for height. *J Biomech*, 40(14):3155–3161, 2007. [2](#), [79](#)
- [91] D.A. Winter. *Biomechanics and Motor Control of Human Movement*. Wiley, 2009. [7](#), [112](#)
- [92] N.N. Yanenko. *Computational algorithm*. Encyclopedia of Mathematics. Springer. [15](#)
- [93] M. R. Yeadon and J. H. Challis. The future of performance-related sports biomechanics research. *J Sports Sci*, 12(1):3–32, Feb 1994. [xxiv](#), [14](#), [152](#), [153](#)
- [94] Maurice R Yeadon. *The mechanics of twisting somersaults*. PhD thesis, Loughborough University, UK, 1984. [5](#), [72](#)
- [95] Maurice R Yeadon, Mark A King, and Cassie Wilson. Modelling the maximum voluntary joint torque/angular velocity relationship in human movement. *J Biomech*, 39(3):476–482, 2006. [xix](#), [5](#), [11](#), [12](#), [59](#), [60](#), [61](#), [113](#), [122](#)

REFERENCES

- [96] Jerzy Zawadzki, Tadeusz Bober, and Adam Siemieński. Validity analysis of the biodex system 3 dynamometer under static and isokinetic conditions. *Acta Bioeng Biomech*, 12(4):25–32, 2010. [11](#)

Appendix A

Working Model 2D specifications:

Version 5.2. For Windows©95/98/ME/2000/XP/NT©4.0 and later.

System Requirements:

Copyright ©2005-2012 Design Simulation Technologies, Inc.

Windows System Requirements:

1. *Windows 95/98/Me/2000/XP or Windows NT™ 4.0 (or later)*
2. *64MB of RAM*
3. *60 MB of hard disk space for a full installation*
4. *CD-ROM drive (for installation)*
5. *Sound card (for audio effects)*

Four rigid-link segments WM2D scripting codes:

WM VBasic script (Brute-force search Model A)

```
,-----  
Sub Main()  
  
Dim Doc as WMDocument  
Dim Hip as WMConstraint  
Dim Knee as WMConstraint  
Dim Ankle as WMConstraint  
Dim Motor1 as WMConstraint  
Dim Motor2 as WMConstraint  
Dim Motor3 as WMConstraint  
Dim Activation as WMOutput  
Dim Meter as WMOutput  
Dim Max1 as Single, FName as String  
Dim ForceRise as WMOutput  
Dim ActivationDelay as WMOutput  
  
FName = SaveFileName$("FileName")  
If FName = Empty then Exit Sub  
  
Set Doc = WM.ActiveDocument  
Set Hip = WM.ActiveDocument.Constraint("Hip")  
Set Knee = WM.ActiveDocument.Constraint("Knee")  
Set Ankle = WM.ActiveDocument.Constraint("Ankle")  
Set Motor1 = WM.ActiveDocument.Constraint("Motor1")  
Set Motor2 = WM.ActiveDocument.Constraint("Motor2")  
Set Motor3 = WM.ActiveDocument.Constraint("Motor3")  
Set Activation = WM.ActiveDocument.Output("Neuromuscular Activations")  
Set ForceRise = WM.ActiveDocument.Output("Force rise time")  
Set ActivationDelay = WM.ActiveDocument.Output("Activation delay")  
  
Set Meter = Doc.Output("Score")  
Doc.EraseMeterValues  
Doc.RetainMeterValues = False  
Doc.SelectAll False  
Doc.Select Meter, True
```

Open FName for Output as #1

```
h1="if(t<"
h2=", (0+((t-0)/"
h3=")^3)*((6*((t-0)/"
h4=")^2)-15*((t-0)/"
h5=")+10), 1)"
h6="*("
h7="*2*(1-(7.813e-05*(-(Body[7].p.r-Body[15].p.r)+180-95)^2))*((37430.81/
(214.5+abs(Constraint[31].dv.r)))-16.9026))"
```

```
k1="if(t<"
k2="+"
k3=", (0+((t-"
k4=")/"
k5=")^3)*((6*((t-"
k6=")/"
k7=")^2)-15*((t-"
k8=")/"
k9=")+10), 1)"
k10="*(-2*"
k11="*(1-(.0002791*(-(Body[7].p.r-Body[5].p.r)+180-125)^2))*((156099.08/
(475.6+abs(Constraint[34].dv.r)))-98.02))"
```

'ankle joint was corrected after functional isometric test (29th February 2012)

```
a1="if(t<"
a2="+"
a3=", (0+((t-"
a4=")/"
a5=" )^3)*((6*((t-"
a6=" )/)"
a7=" )^2)-15*((t-"
a8=" )/)"
a9=" )+10), 1)"
a10="*("
a11="*7.1596*((1-(.0003469*(Constraint[37].dp.r-41.753)^2))*((11947.85/
```

```

(163.8+abs(Constraint[37].dv.r))-5.52))"

'equations for equilibrium position before jumping
'all is managed by Motor 1 Motor 2 Motor 3

m1="if(t>"
m2=",0,(Body[15].cofm.p.x-Point[16].p.x)*-constraintforce(10002, 15).y)"
m3="if(t>"
m4=",0,((Body[15].cofm.p.x-Point[9].p.x)*-constraintforce(10002, 15).y)
+((Body[7].cofm.p.x-Point[9].p.x)
*-constraintforce(10002, 7).y))"
m5="if(t>"
m6=",0,((Body[15].cofm.p.x-Point[23].p.x)*-constraintforce(10002, 15).y)
+((Body[7].cofm.p.x-Point[23].p.x)*-constraintforce(10002, 7).y)
-((Point[23].p.x-Body[5].cofm.p.x)*-constraintforce(10002, 5).y))"

'-----
Parameter to change in order to variate the end of the equilibrium position

Ms=0.075 'end of the equilibrium condition for all three joints

'-----
Actuators (Rotational Motor) which allow to keep the equilibrium condition before the beginning
of the push-off phase of the jump
'-----

Motor1.MotorType = "Torque"
Motor1.Field.Formula= m1+str$(Ms)+m2
Motor2.MotorType = "Torque"
Motor2.Field.Formula= m3+str$(Ms)+m4
Motor3.MotorType = "Torque"
Motor3.Field.Formula= m5+str$(Ms)+m6

'-----
Fa=1
For Hr=.183 to .186 step .001
  For Kr=.268 to .271 step .001

```

```

For Kt=.003 to .008 step .001
  For Ar=.246 to .249 step .001
For At=.003 to .011 step .001
  For Fh= 1 to 1.5 step .1
For Fk= 1 to 1.5 step .1
Doc.Reset

Hip.MotorType = "Torque"
Hip.Field.Formula = h1+str(Hr)+h2+str(Hr)+h3+str(Hr)+h4+str(Hr)
+h5+h6+str(Fh)+h7
Hip.ActiveWhen.Formula= "t">+str(Ms)
Knee.MotorType = "Torque"
Knee.Field.Formula = k1+str(Kr)+k2+str(Kt)+k3+str(Kt)+k4
+str(Kr)+k5+str(Kt)+k6+str(Kr)+k7+str(Kt)+k8+str(Kr)+k9+k10+str(Fk)+k11
Knee.ActiveWhen.Formula= "t">+str(Ms)
Ankle.MotorType = "Torque"
  Ankle.Field.Formula = a1+str(Ar)+a2+str(At)+a3+str(At)+a4
+str(Ar)+a5+str(At)+a6+str(Ar)+a7+str(At)+a8+str(Ar)+a9+a10+str(Fa)+a11
Ankle.ActiveWhen.Formula= "t">+str(Ms)

',-----
Neuromuscular activation (quintic function by Yeadon)
',-----

Activation.Column(1).Cell.Formula = h1+str(Hr)+h2+str(Hr)+h3+str(Hr)+h4+str(Hr)+h5
Activation.Column(2).Cell.Formula = k1+str(Kr)+k2+str(Kt)+k3+str(Kt)+k4+str(Kr)+k5
+str(Kt)+k6+str(Kr)+k7+str(Kt)+k8+str(Kr)+k9
Activation.Column(3).Cell.Formula = a1+str(Ar)+a2+str(At)+a3+str(At)+a4+str(Ar)+a5
+str(At)+a6+str(Ar)+a7+str(At)+a8+str(Ar)+a9

',-----
Parameters to vary
',-----

ForceRise.Column(1).Cell.Formula = str(Hr)
ForceRise.Column(2).Cell.Formula = str(Kr)
ForceRise.Column(3).Cell.Formula = str(Ar)

```

```
ActivationDelay.Column(1).Cell.Formula = str(Kt)
```

```
ActivationDelay.Column(2).Cell.Formula = str(At)
```

```
Doc.Run 80
```

```
    Max1 = Meter.Column(1).Cell.Value
```

```
Max2 = Meter.Column(2).Cell.Value
```

```
Max3 = Meter.Column(3).Cell.Value
```

```
Max4 = Meter.Column(4).Cell.Value
```

```
if Max4>=0.21151 then
```

```
    Print #1, "HipR"; Hr; "KneeR"; Kr; "AnkleR"; Ar; "KneeDel"; Kt; "AnkleDel";
```

```
    At; "ScoreGRFangleVel"; Max1; "ScoreAngleVel"; Max2; "ScoreAngle";
```

```
    Max3; "HeightJump"; Max4; "StrengthFactor"; Fh; Fk; Fa
```

```
end if
```

```
    Next Fk
```

```
Next Fh
```

```
Next At
```

```
    Next Ar
```

```
Next Kt
```

```
Next Kr
```

```
Next Hr
```

```
Close #1
```

```
Doc.Reset
```

```
End Sub
```

```
,-----
```

WM VBasic script (Simulated annealing search Model B)

```
'-----  
Dim isTableHeader As Integer  
'-----  
  
Sub Main()  
    Dim deltaAcceptanceThreshold As Double  
    Dim initialTemperature As Double  
    Dim temperatureCoolingRate As Double  
  
    Begin Dialog UserDialog , ,238,70,"Simulated Annealing Solver"  
        CancelButton 188,40,40,14  
        PushButton 188,16,40,14,"Run".RunSimulatedAnnealing  
        Text 12,9,96,8,"Delta Acceptance Threshold",.deltaAcceptanceThresholdText  
        Text 12,31,100,8,"Initial Temperature",.initialTemperatureText  
        Text 12,54,112,8,"Temperature Cooling Rate (%)",.temperatureCoolingRateText  
        TextBox 128,8,36,12,.deltaAcceptanceThreshold  
        TextBox 128,29,36,12,.initialTemperature  
        TextBox 128,51,36,12,.temperatureCoolingRate  
    End Dialog  
  
    Dim SimulatedAnnealingDialog As UserDialog  
  
    'open the dialog panel for selecting the file  
    fileName = SaveFileName\$("File name")  
    If fileName = Empty then Exit Sub  
    Open fileName for Output as #1  
  
    'open the dialog box to input the initial parameters  
    Dialog SimulatedAnnealingDialog  
  
    deltaAcceptanceThreshold = SimulatedAnnealingDialog.deltaAcceptanceThreshold  
    initialTemperature = SimulatedAnnealingDialog.initialTemperature  
    temperatureCoolingRate = SimulatedAnnealingDialog.temperatureCoolingRate  
  
    isTableHeader = 0  
  
    call StartAnnealing(deltaAcceptanceThreshold, initialTemperature, temperatureCoolingRate)
```

```

Close #1
End Sub

'-----
'Main call for executing the simulated annealing
'-----

Sub StartAnnealing(deltaAcceptanceThreshold As Double, temperature As Double,
temperatureCoolingRate As Double)
'this parameter determines the number of parameters
    'and, as consequence, the number of lower and upper
    'boundaries to be initiated
Dim parameters_number As Integer

'this need to be changed with respect the number of parameters
'and MUST also be updated the lower and upper bound array in
'the subroutine 'generateParameters'
parameters_number = 6

Dim currentParameters(parameters_number) As Double
Dim nextParameters(parameters_number) As Double
Dim bestParameters(parameters_number) As Double

Dim iteration as Integer
'the probability
'Dim temperatureCoolingRate as Double
'Dim temperature as Double
Dim minTemperature as Double
Dim temperatureIterations As Integer
'Dim deltaAcceptanceThreshold as Double
Dim delta as Double

Dim currentCost As Double
Dim bestCost As Double
Dim nextCost As Double

Dim currentHighJump As Double

```

```

Dim nextHighJump As Double
Dim bestHighJump As Double

    Dim proba as Double

        temperatureCoolingRate = 1-temperatureCoolingRate/100
        'temperature = 400.0
        minTemperature = 0.001
        'deltaAcceptanceThreshold = 0.05
        maxIterations = parameters_number*50

        'MsgBox temperatureCoolingRate & " " & temperature & " " & deltaAcceptanceThreshold

        'init the currentParameters
        call generateParameters(currentParameters, parameters_number)

        'init the torque formula, this must be called before
        'invoking computeCostFunction
        call initTorqueFormulas(currentParameters)

        'init the cost function result
        call computeCostFunction(currentCost, currentHighJump)

        'init the best cost and high jump
        bestCost = currentCost
        bestHighJump = currentHighJump
        call copyArray(currentParameters, bestParameters, parameters_number)

    temperatureIterations = 1

        'while the temperature did not reach minTemperature
        While temperature > minTemperature

            'This show a meter named "Algorithm" which allow to control
            'what the simulated annealing is doing in real time
            Dim Algorithm as WMOutput
            Set Algorithm = WM.ActiveDocument.Output("Simulated Annealing Control Panel")

```

```

Dim startDate As Date
startDate = Now

iteration = maxIterations

'Show in the Algorithm meter current temperature and
'temperatureIterations
Algorithm.Column(2).Cell.Value = temperature
Algorithm.Column(3).Cell.Value = temperatureiterations

While iteration > 0
'Show in the Algorithm meter current iteration
Algorithm.Column(1).Cell.Value = iteration

'get the next random permutation of distances
call generateParameters(nextParameters, parameters_number)
call initTorqueFormulas(nextParameters)
call computeCostFunction(nextCost, nextHighJump)

'compute the delta between the current and next cost
delta = currentCost - nextCost
'msgbox delta
'if the new cost is better accept it and assign it

If delta < 0 Then
currentCost = nextCost
currentHighJump = nextHighJump
call copyArray(nextParameters, currentParameters, parameters_number)

If nextCost > bestCost Then
bestCost = nextCost

Algorithm.Column(4).Cell.Value = bestCost

```

```

bestHighJump = nextHighJump
call copyArray(nextParameters, bestParameters, parameters_number)
End If
Else
'generates a random number between 0 and 1
proba = Rnd

'if the new cost is worse accept
'it but with a probability level
'if the probability is less than
'E to the power -delta/temperature.
'otherwise the old value is kept
If proba < exp(-delta/temperature) Then
currentCost = nextCost
currentHighJump = nextHighJump
call copyArray(nextParameters, currentParameters, parameters_number)
End If
End If

'decrement the number of remaining iterations
iteration = iteration -1
Wend 'end iterations

Dim endDate as Date
endDate = Now

call printToResultsFile(bestParameters, bestCost, bestHighJump,
temperatureIterations, startDate, endDate)

'if (currentCost - bestCost) < deltaAcceptanceThreshold Then
'MsgBox "Best cost is " & bestCost & ", high jump is " & bestHighJump
,
''the control returns to the Main subroutine
''as the optimal value was found
'Exit Sub
'End If

```

```

'cooling process
temperature = temperature * temperatureCoolingRate

temperatureIterations = temperatureIterations + 1

currentCost = bestCost
currentHighJump = bestHighJump
call copyArray(bestParameters, currentParameters, parameters_number)

Wend 'end temperature
End Sub

'-----
'Computes the next random parameters
'-----

Sub generateParameters(parameters() As Double, parameters_number as Integer)
'Note: the parameters array assumes the following parameters
'order: Hr, Ht, Kr, Kt, Ar, At

precision = 1000
'parameters_number = ArrayDims(parameters)

Dim boundaries(parameters_number*2) As Double

'init boundaries array
boundaries(1) = 0.16 'Hr_low
boundaries(2) = 0.185 'Hr_up
boundaries(3) = 0.0 'Ht_low
boundaries(4) = 0.01 'Ht_up
boundaries(5) = 0.17 'Kr_low
boundaries(6) = 0.195 'Kr_up
boundaries(7) = 0.01 'Kt_low
boundaries(8) = 0.03 'Kt_up
boundaries(9) = 0.25 'Ar_low
boundaries(10) = 0.35 'Ar_up
boundaries(11) = 0.02 'At_low

```

```

boundaries(12) = 0.05 'At_up

Randomize

parameter_index = 1
For i=1 To parameters_number*2 Step 2
'compute a random value between boundaries
value = Random(boundaries(i)*precision, boundaries(i+1)*precision) / precision
'assign the computed value to
parameters(parameter_index) = value

'MsgBox parameters(parameter_index)

parameter_index = parameter_index + 1
Next i

'This show a meter named "Force Rise Time" and "Activation Delay"
'which allow to control what the simulated annealing is doing in real time
Dim RampTime as WMOutput
Dim OnsetTime as WMOutput
Set RampTime = WM.ActiveDocument.Output("Force Rise Time")
Set OnsetTime = WM.ActiveDocument.Output("Activation Delay")

'Show in the Data meter current parameters
RampTime.Column(1).Cell.Value = parameters(1)
RampTime.Column(2).Cell.Value = parameters(3)
RampTime.Column(3).Cell.Value = parameters(5)
OnsetTime.Column(1).Cell.Value = parameters(2)
OnsetTime.Column(2).Cell.Value = parameters(4)
OnsetTime.Column(3).Cell.Value = parameters(6)

End Sub

'-----
'Initialise the file where to save the simulaton results
'-----

Sub initResultsFile()

```

```

fileName = SaveFileName$("File name")
If fileName = Empty then Exit Sub
Open fileName for Output as #1
End Sub

',-----
'Print results to results file
',-----

Sub printToResultsFile(parameters() As Double, cost As Double, highJump as Double,
iteration As Integer, startDate As Date, endDate As Date)
Hr = parameters(1)
Ht = parameters(2)
Kr = parameters(3)
Kt = parameters(4)
Ar = parameters(5)
At = parameters(6)

If isTableHeader = 0 Then
Print #1, "iteration \$"; "start_date \$"; "end_date \$"; "cost \$"; "high_jump
 \$"; "hr \$"; "kr \$"; "ar \$"; "ht \$"; "kt \$"; "at"
Print #1, iteration; "\$"; startDate; "\$"; endDate; "\$"; cost; "\$"; highJump; "\$";
Hr; "\$"; Kr; "\$"; Ar; "\$"; Ht; "\$"; Kt; "\$"; At
Else
Print #1, iteration; "\$"; startDate; "\$"; endDate; "\$"; cost; "\$"; highJump; "\$";
Hr; "\$"; Kr; "\$"; Ar; "\$"; Ht; "\$"; Kt; "\$"; At
End If

isTableHeader = 1
End Sub

',-----
'Utility function to print an array
',-----

Sub printArray(array() As Double, size As Integer)
For i=1 To size
MsgBox array(i)
Next

```

End Sub

'-----
'Utility function to print the solution
'-----

Sub printSolution(parameters() As Double, parameters_number As Integer,
cost As Double, highJump As Double)

Dim message As String

For i=1 To parameters_number

message = message + "Parameter " + str(i) + ": " + str(parameters(i)) + " "

Next

MsgBox Message + " Cost: " + str(cost) + ", high jump: " + str(highJump)

End Sub

'-----
'Utility function to copy a source array into a destination array
'-----

Sub copyArray(srcArray() As Double, destArray() As Double, size As Integer)

For i=1 To size

destArray(i) = srcArray(i)

Next

End Sub

'-----
'Subroutine for creating the TORQUE JOINT FORMULAS (hip, knee, ankle)
'Note: formulas includes activation, torque-angle, torque-velocity functions
'and, joint equilibrium positions function
'-----

Sub initTorqueFormulas(parameters() As Double)

Dim Doc as WMDocument

Set Doc = WM.ActiveDocument

Dim torqueLength as string

Dim Theta as string

Dim UpperBody as WMBody

```

Set UpperBody = WM.ActiveDocument.Body("UpperBody")
Dim Thighs as WMBody
Set Thighs = WM.ActiveDocument.Body("Thighs")
Dim Shanks as WMBody
Set Shanks = WM.ActiveDocument.Body("Shanks")
Dim Foot as WMBody
Set Foot = WM.ActiveDocument.Body("Foot")
Dim Hip as WMConstraint
Dim Knee as WMConstraint
Dim Ankle as WMConstraint
Set Hip = WM.ActiveDocument.Constraint("Hip")
Set Knee = WM.ActiveDocument.Constraint("Knee")
Set Ankle = WM.ActiveDocument.Constraint("Ankle")

```

```

'-----
'Neuromuscular Activation (PARAMETERS)
'-----

Hr = parameters(1)
Ht = parameters(2)
Kr = parameters(3)
Kt = parameters(4)
Ar = parameters(5)
At = parameters(6)

h1="if(t<"
h2="+"
h3=", (0+((t-"
h4=")"/"
h5=")^3)*(6*((t-"
h6=")"/"
h7=")^2)-15*((t-"
h8=")"/"
h9=")+10),1)"

k1="if(t<"
k2="+"
k3=", (0+((t-"

```

```

k4=")"/"
k5=")^3)*((6*((t-"
k6=")"/"
k7=")^2)-15*((t-"
k8=")"/"
k9=")+10),1)"

```

```
'ankle joint was corrected after functional isometric test (29th February 2012).
```

```

a1= "if(t<"
a2= "+"
a3=",(0+((t-"
a4=")"/"
a5= ")^3)*((6*((t-"
a6= ")"/"
a7= ")^2)-15*((t-"
a8= ")"/"
a9= ") +10),1)"

```

```
'Here HipActivation, KneeActivation and AnkleActivation functions with parameters
```

```
' (modified by the algorithm)
```

```
'-----
```

```

HipActivation=h1+str(Hr)+h2+str(Ht)+h3+str(Ht)+h4+str(Hr)+h5+
str(Ht)+h6+str(Hr)+h7+str(Ht)+h8+str(Hr)+h9
'Msgbox HipActivation,, "hip"
KneeActivation = k1+str(Kr)+k2+str(Kt)+k3+str(Kt)+k4+str(Kr)+k5
+str(Kt)+k6+str(Kr)+k7+str(Kt)+k8+str(Kr)+k9
'MsgBox KneeActivation,, "knee"
AnkleActivation =a1+str(Ar)+a2+str(At)+a3+str(At)+a4+str(Ar)+
a5+str(At)+a6+str(Ar)+a7+str(At)+a8+str(Ar)+a9
'MsgBox AnkleActivation,, "ankle"

```

```
Dim Activations as WMOutput
```

```
Set Activations = WM.ActiveDocument.Output("Neuromuscular Activations")
```

```
Activations.Column(1).Cell.Formula = HipActivation
```

```

Activations.Column(2).Cell.Formula = KneeActivation
Activations.Column(3).Cell.Formula = AnkleActivation

Doc.Reset
End Sub
'-----
'Executes the simulation and return the cost function value.
'Note: initTorqueFormulas MUST be executed prior to this function.
'-----

Sub computeCostFunction(costFunctionResult As Double, highJump As Double)
Dim Doc as WMDocument
Dim Meter as WMOOutput

Set Doc = WM.ActiveDocument
Set Meter = Doc.Output("Score")

Doc.EraseMeterValues
Doc.RetainMeterValues = False
Doc.SelectAll False
Doc.Select Meter, True

'execute the simulation
Doc.Run 40

'set the cost function value and the high jump
costFunctionResult = Meter.Column(4).Cell.Value
highJump = Meter.Column(4).Cell.Value

Doc.Reset
End Sub
'-----

```

WM VBasic script (One Jump)

```
'-----  
Sub Main()  
  
Dim Doc as WMDocument  
Dim Hip as WMConstraint  
Dim Knee as WMConstraint  
Dim Ankle as WMConstraint  
Dim Motor1 as WMConstraint  
Dim Motor2 as WMConstraint  
Dim Motor3 as WMConstraint  
Dim Activation as WMOutput  
Dim Meter as WMOutput  
Dim Max1 as Single, FName as String  
Dim ForceRise as WMOutput  
Dim ActivationDelay as WMOutput  
  
Set Doc = WM.ActiveDocument  
Set Hip = WM.ActiveDocument.Constraint("Hip")  
Set Knee = WM.ActiveDocument.Constraint("Knee")  
Set Ankle = WM.ActiveDocument.Constraint("Ankle")  
Set Motor1 = WM.ActiveDocument.Constraint("Motor1")  
Set Motor2 = WM.ActiveDocument.Constraint("Motor2")  
Set Motor3 = WM.ActiveDocument.Constraint("Motor3")  
Set Activation = WM.ActiveDocument.Output("Neuromuscular Activations")  
Set ForceRise = WM.ActiveDocument.Output("Force rise time")  
Set ActivationDelay = WM.ActiveDocument.Output("Activation delay")  
  
'-----  
h1="if(t<"  
h2="+"  
h3=", (0+((t-"  
h4=")"/"  
h5=")^3)*((6*((t-"  
h6=")"/"  
h7=")^2)-15*((t-"  
h8=")"/"
```

h9=")+10),1)"

k1="if(t<"

k2="+"

k3=",(0+((t-"

k4=")"/"

k5=")^3)*((6*((t-"

k6=")"/"

k7=")^2)-15*((t-"

k8=")"/"

k9=")+10),1)"

'ankle joint was corrected after functional isometric test (29th February 2012)

a1= "if(t<"

a2= "+"

a3=",(0+((t-"

a4=")"/"

a5= ")^3)*((6*((t-"

a6=)"/"

a7= ")^2)-15*((t-"

a8=)"/"

a9= ") +10),1)"

'-----

Hr=.167 'hip ramp time

Kr=.187 'knee ramp time

Ar=.192 'ankle ramp time

ht=.003 'hip onset

kt=.028 'knee onset

at=.054 'ankle onset

Doc.Reset

'-----

Neuromuscular activation (quintic function by Yeadon)

'-----

```
Activation.Column(1).Cell.Formula = h1+str(Hr)+h2+str(Ht)+h3+str(Ht)+h4+str(Hr)
+h5+str(Ht)+h6+str(Hr)+h7+str(Ht)+h8+str(Hr)+k9
Activation.Column(2).Cell.Formula = k1+str(Kr)+k2+str(Kt)+k3+str(Kt)+k4+str(Kr)+
k5+str(Kt)+k6+str(Kr)+k7+str(Kt)+k8+str(Kr)+k9
Activation.Column(3).Cell.Formula = a1+str(Ar)+a2+str(At)+a3+str(At)+a4+str(Ar)+
a5+str(At)+a6+str(Ar)+a7+str(At)+a8+str(Ar)+a9
```

Doc.Run 80

Doc.Reset

End Sub

,-----

WM VBasic script (Model details)

Information Export Utility version 1.0.2

Date: 07-12-2012

Time: 00:35:02

Simulation File: SJ.wm2d

Section: Unit System

Distance: meters Energy: joules Force: newtons
Mass: kilograms Power: watts Time: seconds
Frequency: Hz

Section: Integration Settings

	Variable/	Animation	Overlap	Assembly	
Integrator	Fixed	Step	Error	Error	Gravity

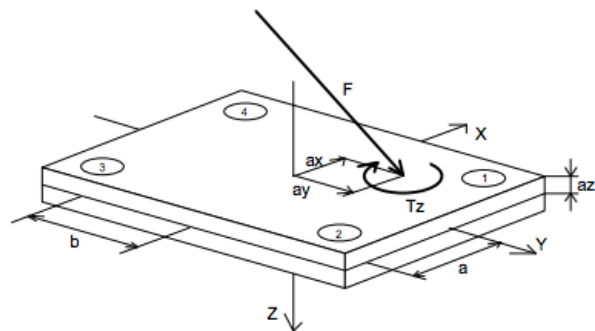
,-----
kutta_merson Variable 0.017 0.000 0.000 Linear

,-----
Gravity Constant 9.807
,-----

Appendix B

Kistler specifications

Kistler Force Plate Formulae

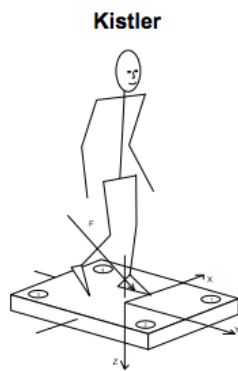


Force plate output signals

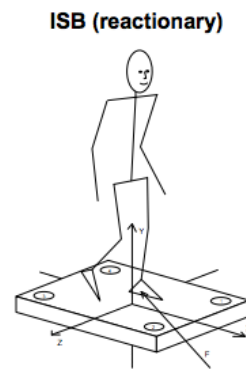
Output signal	Channel	Description
fx12	1	Force in X-direction measured by sensor 1 + sensor 2
fx34	2	Force in X-direction measured by sensor 3 + sensor 4
fy14	3	Force in Y-direction measured by sensor 1 + sensor 4
fy23	4	Force in Y-direction measured by sensor 2 + sensor 3
fz1 ... fz4	5 ... 8	Force in Z direction measured by sensor 1 ... 4

Figure 2: Kistler force plate output schema.

Coordinate systems



$$\begin{aligned}
 -F_y &= F_x \\
 F_z &= F_y \\
 -M_y &= M_x \\
 M_z &= M_y \\
 M_x &= M_z \\
 -M_y' &= M_x' \\
 M_x &= M_z' \\
 a_y &= a_x \\
 -a_x &= a_z \\
 T_z &= T_y
 \end{aligned}$$



Different coordinate system of one force plate

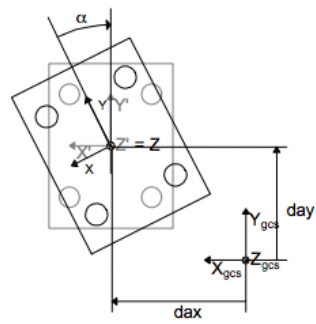


Figure 3: Kistler force plate coordinates.

Parameter	Calculation
Fx_{gcs}	$(Fx * \cos \alpha) + (Fy * \sin \alpha)$
Fy_{gcs}	$(Fy * \cos \alpha) - (Fx * \sin \alpha)$
Fz_{gcs}	Fz
Mx_{gcs}	$ay_{gcs} * Fz_{gcs}$
My_{gcs}	$-ax_{gcs} * Fz_{gcs}$
Mz_{gcs}	$(ax_{gcs} * Fy_{gcs}) - (ay_{gcs} * Fx_{gcs})$
Mx'_{gcs}	$Mx_{gcs} + (az0 * Fy_{gcs})$
My'_{gcs}	$My_{gcs} - (az0 * Fx_{gcs})$
ax_{gcs}	$dax + (ax * \cos \alpha) + (ay * \sin \alpha)$
ay_{gcs}	$day + (ay * \cos \alpha) - (ax * \sin \alpha)$
Tz_{gcs}	Tz

Figure 4: Calculations.

Biodex specifications

Biodex S4 Biodex System 4 Specifications



Specifications S4 PRO

S4 PRO Patient Positioning System with motorized seat height, fully assisted Dynamometer height adjustment, front-to-back and side-to-side chair adjustment.

- **S4 PRO features:**
 - 17" Flat Panel LCD Touch Screen Monitor
 - Multi-Mode operation: Isokinetic, Isometric, Isotonic, Reactive Eccentric and Passive
 - Concentric speed up to 500 deg/sec
 - Eccentric speed up to 300 deg/sec
 - Concentric torque up to 500 ft-lb (680 Nm)
 - Eccentric torque up to 400 ft-lb (544 Nm)
 - Passive speed as low as .25 deg/sec
 - Passive torque as low as .5 ft-lb
 - Isotonic torque as low as .5 ft-lb
- **Clinical Data Station:**
 - 2.8 GHz Pentium 4 CPU
 - 80 GB Hard Drive
 - 512 MB RAM
 - 48x CDRW
 - Windows™ XP Operating System
 - Biodex Advantage Software
 - LCD Flat Panel Touch Screen Color Monitor with integrated speakers
 - Color Printer
- Attachments for Ankle, Knee, Shoulder, Elbow, Wrist and Hip
- Attachment Cart
- Calibration Kit
- Manuals and Wall Chart
- 64 square feet operating space (6 square meters)
- 220 VAC
- Certification: ETL and cETL listed to UL 60601-1, CAN/CSA C22.2 No.: 601-1-M90 and EN60601-1. CE conformity to M.D.D. 93/42/EEC



Specifications S4 QUICK-SET

S4 Quick-Set Patient Positioning System with fixed seat height, fully assisted Dynamometer height adjustment, front-to-back chair adjustment.

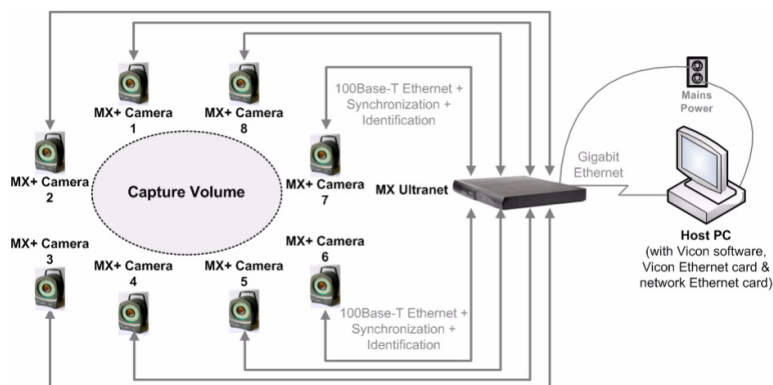
- **S4 Quick-Set features:**
 - 17" Flat Panel LCD Touch Screen Monitor
 - Multi-Mode operation: Isokinetic, Isometric, Isotonic, Reactive Eccentric and Passive
 - Concentric speed up to 500 deg/sec
 - Eccentric speed up to 300 deg/sec
 - Concentric torque up to 500 ft-lb (680 Nm)
 - Eccentric torque up to 400 ft-lb (544 Nm)
 - Passive speed as low as .25 deg/sec
 - Passive torque as low as .5 ft-lb
 - Isotonic torque as low as .5 ft-lb
- **Clinical Data Station:**
 - 2.8 GHz Pentium 4 CPU
 - 80 GB Hard Drive
 - 512 MB RAM
 - 48x CDRW
 - Windows™ XP Operating System
 - Biodex Advantage Software
 - LCD Flat Panel Touch Screen Color Monitor with integrated speakers
 - Color Printer
- Attachments for Ankle, Knee, Shoulder, Elbow, Wrist
- Attachment Cart
- Calibration Kit
- Manuals and Wall Chart
- 32 square feet operating space (3 square meters)
- 220 VAC
- Certification: ETL and cETL listed to UL 60601-1, CAN/CSA C22.2 No.: 601-1-M90 and EN60601-1. CE conformity to M.D.D. 93/42/EEC



Figure 5: Biodex specification.

Vicon specifications: basic motion capture architecture.

Vicon MX architecture consists of from one-eight MX cameras, an MX Ultraret, and the host PC. This basic architecture is illustrated in the following Figure.



Performance	Frame Rate (fps)	
	59.94	119.88
Resolution (pixels)	1012 H x 987 V	947 H x 881 V
Aspect Ratio	1:1	1:1
Usable sensor size (mm)	10.12 h x 9.87 v	9.47 h x 8.81 v
Shuttered	No	No
Sensor Type	CMOS	CMOS

Figure 6: Vicon specification.
